Design of Organic Rankine Cycles for Conversion of Waste Heat in a Polygeneration Plant

by

Kevin J. DiGenova

B.S., Mechanical Engineering
Massachusetts Institute of Technology, 2007

Submitted to the Department of Mechanical Engineering
in partial fulfillment of the requirements for the degree of

Master of Science in Mechanical Engineering
at the
Massachusetts Institute of Technology
September, 2011

Signature of Author: _____
Department of Mechanical Engineering
August 19, 2011

Certified by: _____
John G. Brisson
Professor of Mechanical Engineering
Thesis Supervisor

Accepted by: _____
David E. Hardt
Chair, Committee on Graduate Students

Design of Organic Rankine Cycles for Conversion of Waste Heat in a Polygeneration Plant

by

Kevin J. DiGenova

Submitted to the Department of Mechanical Engineering on August 19, 2011 in partial fulfillment of the requirements for the degree of Master of Science in Mechanical Engineering

ABSTRACT

Organic Rankine cycles provide an alternative to traditional steam Rankine cycles for the conversion of low grade heat sources, where steam cycles are known to be less efficient and more expensive. This work examines organic Rankine cycles for use in a polygeneration plant that converts coal feedstock into hydrocarbon products and electricity. Since a Fischer Tropsch reactor is the largest source of low grade heat in the polygeneration plant, rejecting heat at a constant temperature of 240°C, the analysis in this work focuses on utilizing the waste heat from this process.

Organic Rankine cycles (ORC's) are modeled in MATLAB using pure substance data available from Refprop 8.0. Various working fluids are considered, with a particular focus on hexane, heptane, octane, nonane, and decane. Hexane is the best option for the Fischer Tropsch heat source and the working fluids considered here. A set of ORC design concepts (building blocks) is developed to allow a cycle to be matched to a generic heat source, and is demonstrated using the Fischer Tropsch heat source profile. The low pressure steam Rankine cycle achieves a 20.6% conversion, while a baseline hexane organic Rankine cycle achieves a 26.2% conversion efficiency for the same Fischer Tropsch heat source. If the ORC building blocks are combined into a cycle targeted to match the temperature-enthalpy profile of the heat source, this customized hexane cycle achieves 28.5% conversion efficiency.

For a polygeneration plant with a 25,000 ton per day input of coal, the conversion efficiency is improved by 0.3 to 0.5 points. Moreover, by combining the ORC building blocks identified in this work into new configurations, cycle designers can create customized organic Rankine cycles that target any heat source temperature-enthalpy profile to achieve improved conversion efficiencies.

Thesis Supervisor: John G. Brisson
Title: Professor of Mechanical Engineering

Acknowledgements

I would first like to thank Professor Brisson for his guidance in writing this thesis, his support in my development as an engineer, and his frequent in-depth analysis of the geography and ecosystems of coastal Maine. The work presented herein results from the efforts of many members of the conversion research project. Barbara Botros, my fellow researcher in the heat integration group, was an invaluable resource throughout the whole process. The guidance and feedback of Randy Field was indispensible, as was the technical support of Robert Brasington and Srinivas Seethamraju.

I would also like to thank the members of the Cryogenics Engineering Laboratory, particularly Doris Elsemiller who makes everything run smoothly, and always seems to know the right buttons to push and the right strings to pull. And to my fellow labmates: Teresa Peters, Barbara Botros, Wayne Staats, Martin Segado, Jake Hogan, and of course Francisco Alonso Dominguez Espinosa: thank you for all of the collaboration on late night problem sets, the light-hearted discussions of thermodynamics and heat transfer and the weighty dialogues on the merits of the Simpsons. The Cryolab has truly been a wonderful place to work for the last two years, with Friday *Ignition Remix* dance parties and lunchtime games of chess, and I will miss you all.

I would be remiss to not mention my family. Thanks to my parents, who are always available with moral support, whether over the phone or by making the drive up from Connecticut. Thanks to all of my siblings, who are always willing to share their dry sense of humor and help me keep my life in perspective.

Thanks are most due to my lovely fiancée, Cristi, who has promised to marry me in two weeks as long as my thesis is signed. Cristi, you have provided loving support in the way of words, deeds, and food, and you have been my motivation to finish this thesis on time. Thank you.

Table of Contents

List of Figures

List of Tables

Table 38: Temperature vs. Change in Enthalpy per Time data for "Stream Preheat" as it heats from 81°C down to 240°C. The composition of "Stream Preheat" is, by mole fraction: 0.308 CO; 0.028 CO_2; 0.619 H_2; 0.001 H_2O; 0.038 N_2; 0.007 Ar; and trace amounts of O_2, HCl, CH_4. ----- - 134 -

1 Introduction

This thesis investigates the use of organic Rankine cycles as an alternative to traditional steam Rankine cycles for converting low grade waste heat into shaft work. Steam cycles are known to be inefficient at converting heat sources below 300°C due to the inherent requirement that steam be superheated before expansion. Many organic fluids do not require superheat when used as working fluids in Rankine cycles, allowing them to achieve better efficiency than steam at low temperatures. The heat source considered in this work is a Fischer Tropsch (FT) reactor, along with associated processes, that converts synthetic gas comprised primarily of CO and H_2 into longer chain hydrocarbons. The Fischer Tropsch reaction is highly exothermic, and must be maintained at a constant 240°C temperature, making it a prime candidate as a heat source for an organic Rankine cycle. The FT reactor considered in this work is assumed part of a larger chemical plant that converts a coal feedstock into multiple products, including methanol, liquid fuels, and electricity.

The production of multiple energy end products from a single plant, referred to as polygeneration, and has been shown to improve the efficiency of resource conversion (Serra, Lozano, Ramos, Ensinas, & Silvia, 2009). Current global trends in energy supply and demand are causing an increased emphasis on the efficient utilization of natural resources. In the last thirty years, total energy demand has increased by over 75% worldwide, a rate of 2% increase per year, and it is anticipated to continue increasing at similar rates (International Energy Agency, 2010). If current growth trends continue, demand will outpace the availability of natural resources in the foreseeable future (Serra, Lozano, Ramos, Ensinas, & Silvia, 2009). More efficient use of natural resources is a necessary component of meeting this challenge.

1.1 Polygeneration

The MIT-BP Conversion Research Program has undertaken a project to study a polygeneration plant that converts high-carbon, low-value feedstock into high value energy

products. In this interest, A polygeneration simulation model was created using Aspen Plus® modeling software from Aspentech. This polygeneration plant model provides the context for this thesis, so a brief overview is provided here.

The MIT-BP polygeneration model is primarily based upon a National Energy Technology Laboratory (NETL) report: "Baseline Technical and Economic Assessment of a Commercial Scale Fischer-Tropsch Liquids Facility" (Van Bibber, Shuster, Haslbeck, Rutkowski, Olson, & Kramer, 2007). This model, referred to in this thesis as the BP Polygeneration Plant Model, provides baseline values for the mass and energy balances in a polygeneration plant. Figure 1.1 is a representation of the overall mass and energy flows of feedstock and products for the BP Polygeneration Plant Model. The plant feedstock is Illinois No. 6 bituminous coal at a rate of 25,000 tons per day (TPD) with a higher heating value (HHV) flow rate of 8014 MW. The plant output consists of 1880 MW of electricity, 1950 TPD of liquid fuels (HHV flow rate of 1040 MW), and 4300 TPD of methanol (HHV flow rate of 1029 MW).

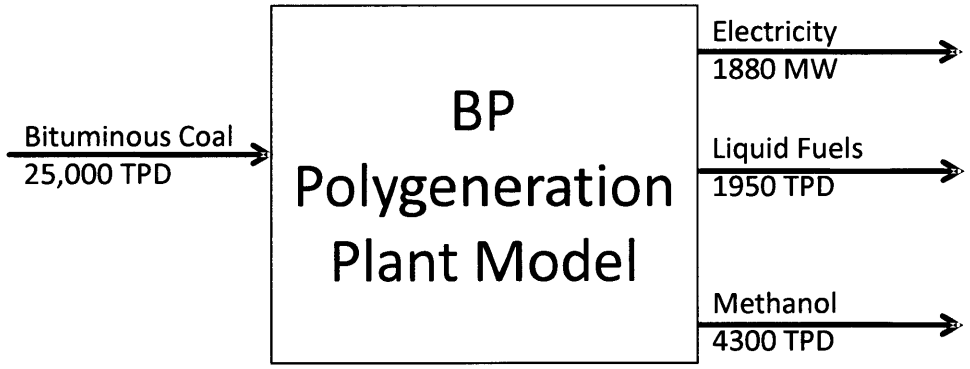

Figure 1.1: BP Polygeneration Plant Model feedstock and product flows. The plant takes a coal input at an HHV flow rate of 8014 MW, and puts out hydrocarbon products at an HHV flow rate of 2069 MW and electricity at a power output of 1880 MW.

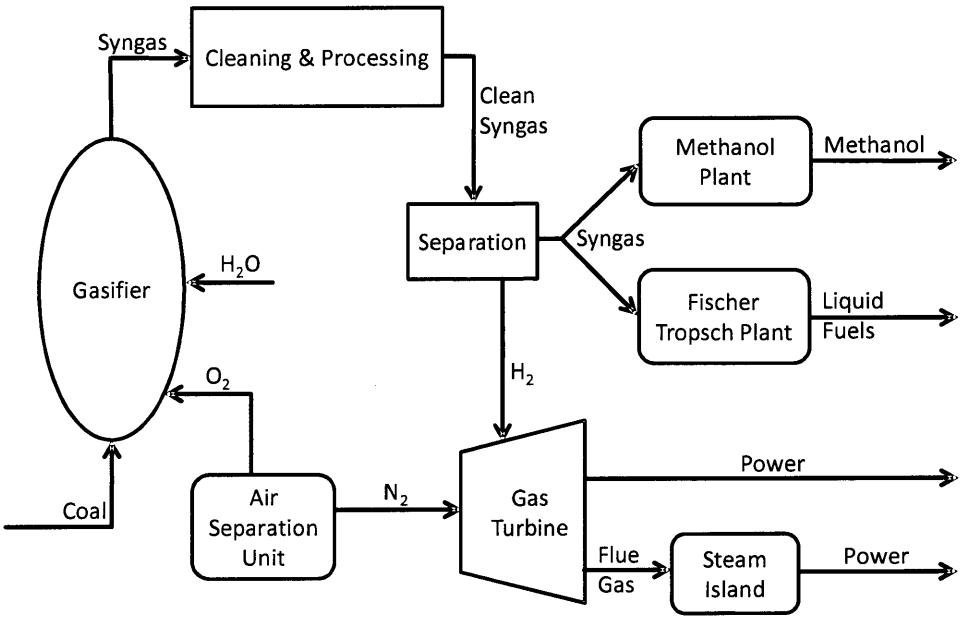

Figure 1.2: Schematic diagram of the BP Polygeneration Plant Model. The BP Polygeneration Plant Model calculates mass and energy balances for a polygeneration plant that converts coal into useful products, including methanol, liquid fuels, and electricity.

Figure 1.2 is a schematic diagram of the polygeneration plant, with major subsystems labeled. Coal feedstock entering the plant is passed through the gasifier, where it is reacted at high temperature (1370°C) with oxygen from an air separation unit (ASU) and steam, thereby creating synthetic gas (syngas), which is primarily a mixture of CO and H_2. The syngas stream leaving the gasifier passes through a series of cleaning and processing steps. A scrubber removes chlorides and particulates, and a water-gas shift reactor converts most of the CO to CO_2 by means of the water-gas shift reaction:

$$CO + H_2O \Leftrightarrow CO_2 + H_2 \quad . \tag{1}$$

This reaction controls the ratio of CO to H_2 in the syngas to meet the feed stream requirements of the methanol and FT reactors which are further downstream. Following the water-gas shift,

hydrogen sulfide (H_2S) and carbon dioxide (CO_2) are removed by physical absorption from the stream in a Selexol unit. The H_2S is separated into H_2 and S_2 in a sulfur recovery unit.

Finally, the clean syngas stream undergoes a membrane separation where it is split into three streams: syngas is sent to the methanol and Fischer Tropsch plants for conversion into hydrocarbon products, and some hydrogen is removed and sent to the gas turbine. The hydrogen stream is mixed with nitrogen from the ASU, and combusted in the gas turbine to generate power. Further, the flue gas from the gas turbine is used to generate steam for a steam island, where it may be used for power or for process heating.

The steam island plays an important role in facilitating heat integration in the polygeneration plant. Many of the processes in the polygeneration plant require cooling or heating, and steam is used as a heat transfer medium to move heat around the plant and meet the needs of the various processes. Any heat which is not needed to meet process requirements is available for use in a steam Rankine cycle, where it is used to generate power. The steam island produces 801 MW of power in baseline operation, accounting for 42.6% of the overall polygeneration plant electricity output. Thus, improvements to the plant heat integration, as realized through changes to the steam island, will have a significant effect in overall plant conversion efficiency.

Steam is known to be an inefficient and expensive means of converting low grade heat into work, so low temperature heat sources in the polygeneration plant provide opportunity for improved conversion efficiency and power output. The Fischer Tropsch reactor is by far the single largest source of low temperature heat in the polygeneration plant. The FT reaction is exothermic and isothermal, providing 309 MW of heat – 3.8% of the overall heating value flow rate input to the plant – at a constant temperature of 240°C. Thus, heat from the Fischer Tropsch reactor is a primary focus of this thesis, and the FT reaction is considered here in greater detail.

1.2 Fischer Tropsch Synthesis

Fischer Tropsch synthesis is a catalyzed process for converting synthesis gas containing hydrogen and carbon monoxide into longer chain hydrocarbon products. Fischer Tropsch synthesis was developed in Germany during the 1920s by Franz Fischer and Hans Tropsch as a method of producing fuels and chemicals from coal derived gas [Steynberg & Dry]. Since its invention, this process and variations on it have been commonly used in coal to liquids and gas to liquids operations.

Fischer Tropsch synthesis is used to generate paraffinic products, olefinic products, and oxygenated hydrocarbons such as alcohols. Light gases, such as methane, can be produced more efficiently by other means, so they are undesirable in an FT reaction. The yield from a Fischer Tropsch reactor is temperature dependent, and there are two temperature ranges in which FT reactors operate: Low Temperature Fischer Tropsch (LTFT), and High Temperature Fischer Tropsch (HTFT).

HTFT units react gas phase hydrocarbons in the temperature range 320°C-350°C, thereby increasing the selectivity of small chain hydrocarbons in the product stream, including undesirable byproducts in the (C_1-C_4) size range. A high reactor temperature causes high rates of reaction, so HTFT reactors have greater throughput than LTFT reactors. Low Temperature Fischer Tropsch (LTFT) units react liquid phase hydrocarbons in the temperature range 220°C-250°C. Operating the reaction at lower temperatures increases the selectivity of long chain hydrocarbons including waxes (C_{20}-C_{70}), and decreases the output of undesirable gaseous byproducts.

The BP Polygeneration Plant Model employs a Low Temperature Fischer Tropsch reactor as a paraffin source. Paraffins, or alkanes, are hydrocarbons of the form "C_nH_{2n+2}", which are particularly valuable as liquid fuels and liquid fuel components. A fixed bed Fischer Tropsch reactor is used with a cobalt catalyst (which is highly selective for alkanes), and a constant reaction temperature of 240°C. The reactor has a shell and tube configuration with cobalt

catalysts inside the tubes and cooling water on the shell side to remove the heat of reaction. As depicted in Figure 1.3, syngas flows into the top of the reactor and through the tube bundle where the Fischer Tropsch synthesis occurs. This fixed catalyst geometry makes catalyst regeneration very difficult, so catalyst poisoning is a serious concern. Therefore, the syngas cleaning processes have high purity requirements when removing contaminants such as sulfur which could poison the cobalt catalyst.

Boiling steam is an effective means of controlling the reaction temperature, but an expensive and inefficient means of generating power from the FT heat of reaction. Therefore, there is great value in finding alternative working fluids to absorb heat from the FT reactor. Organic fluids have been shown to be more effective than steam at low temperatures.

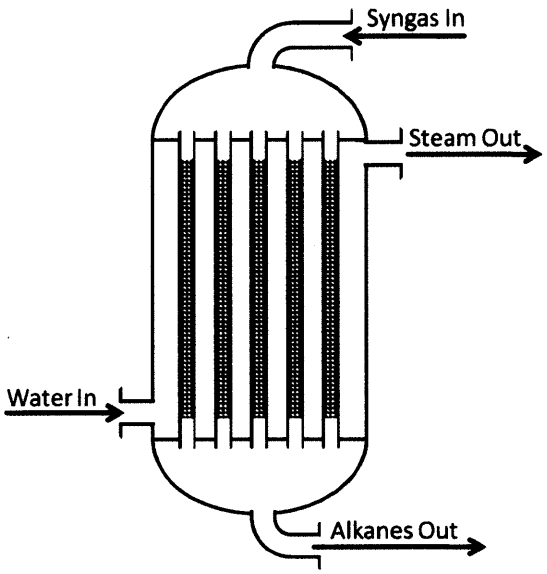

Figure 1.3: Diagram of fixed bed Fischer Tropsch reactor. Basic shell and tube configuration for a Fischer Tropsch reactor with cobalt catalysts. The exothermic FT reaction is maintained at a constant temperature of 240°C by boiling water outside the catalyst lined tubes where the reaction occurs.

1.3 Organic Rankine Cycles

A traditional steam Rankine cycle is a heat engine that operates between a heat source and a heat sink. Water is pumped to high pressure, preheated, boiled, and superheated by heat transfer from the heat source, and then the steam is expanded to generate power. The low pressure steam is condensed by heat transfer to the heat sink, and the cycle starts over. At low temperatures (< 300°C), steam Rankine cycles are both inefficient and expensive. Organic fluids, or fluids with carbon in their molecular structure, often provide a cost effective and efficient alternative to steam for converting low temperature heat sources into electricity. The concept of using organic working fluids in a Rankine cycle, known as an organic Rankine cycle (ORC), dates back at least as far as 1962, when Tabor et. al. patented vapor turbines capable of extracting power from organic working fluids (Tabor & Bronicki, 1962).

Today, multiple companies offer ORC systems capable of generating power from heat sources which range from less than 100°C all the way up to 400°C (Quoilin & Lemort, 2009). These systems target low temperature heat sources, including geothermal, waste heat recovery, solar thermal, and combined heat and power applications. Currently, there are over forty ORC plants in operation worldwide, with a total installed capacity of over 750 MW, and individual units that may range in size from thousands of Watts up to tens of Megawatts (Bronicki & Schochet, 2005). Organic Rankine cycles are a maturing technology with the potential to generate electricity from low-grade heat sources which are often underutilized. In this thesis, organic Rankine cycles are shown to be an effective means of converting low grade heat provided by a Fischer Tropsch reactor in a polygeneration plant into useful shaft work.

1.4 Overview

Chapter 2 presents analysis of organic Rankine cycles based on a pure substance model, and compares cycles using various organic working fluids and steam. The FT reactor is modeled as a constant temperature heat source at 240°C. The thermodynamic characteristics of

organics are discussed, and the advantage of organics over steam is demonstrated. Then, fluid selection criteria are presented for choosing an organic working fluid to fit a particular application. Alkanes show great potential as working fluids for converting heat from the Fischer Tropsch reactor.

Chapter 3 relaxes the self-imposed constraint of a constant temperature heat source. Pinch analysis, a widely used method for heat integration of complex systems, is introduced and applied to the Fischer Tropsch plant – including the reactor and associated processes – so that an organic Rankine cycle can be constructed to use all of the available heat source. A set ORC building blocks are analyzed, each one affecting the cycle heating profile. The building blocks are then combined to create a customized organic Rankine cycle specifically targeted towards converting the Fischer Tropsch heat source. The customized cycle significantly improves the conversion efficiency of the system.

Chapter 4 presents practical considerations for implementing organic Rankine cycles within the BP Polygeneration plant. A basic cost model is created to compare the equipment costs for organic Rankine cycles using various working fluids. Hexane is shown to be the clear choice for an ORC that targets the Fischer Tropsch plant heat source. The cost model is further used to show the cost of a customized hexane ORC which specifically targets the FT heat source, and the customized cycle is shown to compare favorably with a baseline ORC using hexane. A more advanced cost model that accounts for the actual heat exchanger network necessary to operate the customized hexane ORC is suggested as future work.

Finally, the complimentary nature of the organic Rankine cycle and the Fischer Tropsch reaction is discussed. Hexane, which is the working fluid shown to be best suited for an ORC using the FT heat source, is one of the products of the Fischer Tropsch reaction. The advantages of using a Fischer Tropsch liquid as the working fluid in an integrated FT-ORC system are discussed, and one possible design for such a system is proposed.

2 Organic Rankine Cycles

2.1 Context

The BP Polygeneration Plant Model has been created to study strategies for maximizing resource efficiency by simultaneously producing liquid fuels, chemicals, and power from a coal gasification process. A survey of plant heat flows indicated an abundance of heat available at low temperatures (<250°C) where steam Rankine cycles are known to be inefficient. The single largest source of low temperature heat in the BP Polygeneration Plant is the Fischer Tropsch (FT) reactor, which converts syngas into useful liquids and waxes. This exothermic reaction rejects a significant heat load, but must be held at a temperature of 240°C in order to produce the desired products. This chapter discusses the use of organic working fluids in a Rankine cycle as a more efficient option than steam for converting the heat from the Fischer Tropsch reactor into shaft work.

2.2 Rankine Cycle Modeling

For this work, fluids were modeled as pure substances using the thermodynamic database compiled by the National Institute of Standards and Technology (NIST) in Refprop 8.0 (Lemmon, Huber, & McLinden, 2007). Two Rankine cycle configurations were studied: one configuration for wet fluids such as steam, and one configuration for dry fluids such as hexane and other organics. The Rankine cycle was idealized to consist of an isentropic compression, isobaric heating at high pressure (P_{high}), isentropic expansion, and isobaric cooling at low pressure (P_{low}). The effects of pump and expander inefficiencies were then accounted for by assuming an isentropic efficiency for those components. The pressure drop in the heat exchangers was assumed to be small, and was not accounted for when calculating cycle states.

2.2.1 Wet Fluids

Each Rankine cycle operates between a heat source at high temperature, T_{source}, and a heat sink at low temperature, T_{sink}. In order to assure that heat transfer can occur across a finite heat transfer area, there is a minimum temperature drop ΔT_{min} from the heat source to the working fluid. For the purpose of this analysis, the same ΔT_{min} is maintained from the working fluid to the heat sink. Therefore, the fluid can reach a maximum temperature of $T_{max} = T_{source} - \Delta T_{min}$, and a minimum temperature of $T_{min} = T_{sink} + \Delta T_{min}$. Figure 2.1 is a schematic for the fluid path through a steam Rankine cycle along with the related fluid states on a Temperature vs. Specific Entropy (T-s) diagram. The specific work transfer rates, $\dot{w}$, and the specific heat transfer rates, $\dot{q}$, are represented in the schematic. The steam vapor dome, which delineates the boundary of the two-phase region, is represented by a black line on the Temperature vs. Specific Entropy diagram.

For a steam Rankine cycle, the fluid begins at State 1 as a saturated liquid at low pressure, P_{low}, before being pumped up to high pressure, P_{high}, at State 2. The high pressure liquid is then preheated by heat transfer from the heat source to a saturated liquid at State 3. The fluid boils at constant temperature, passing through the two-phase region and reaches a saturated vapor at State 4. From this saturated vapor state, the fluid is superheated to the maximum cycle temperature, T_{max}, at State 5. Then the steam is expanded to the low pressure as work is extracted in the expander. During this expansion, the steam passes back under the vapor dome, resulting in some condensation and a two-phase fluid at low pressure, P_{min}, and low temperature, T_{min}, at State 6. The low pressure fluid is condensed at constant pressure by transferring heat to the heat sink until it returns to the original, saturated liquid at State 1.

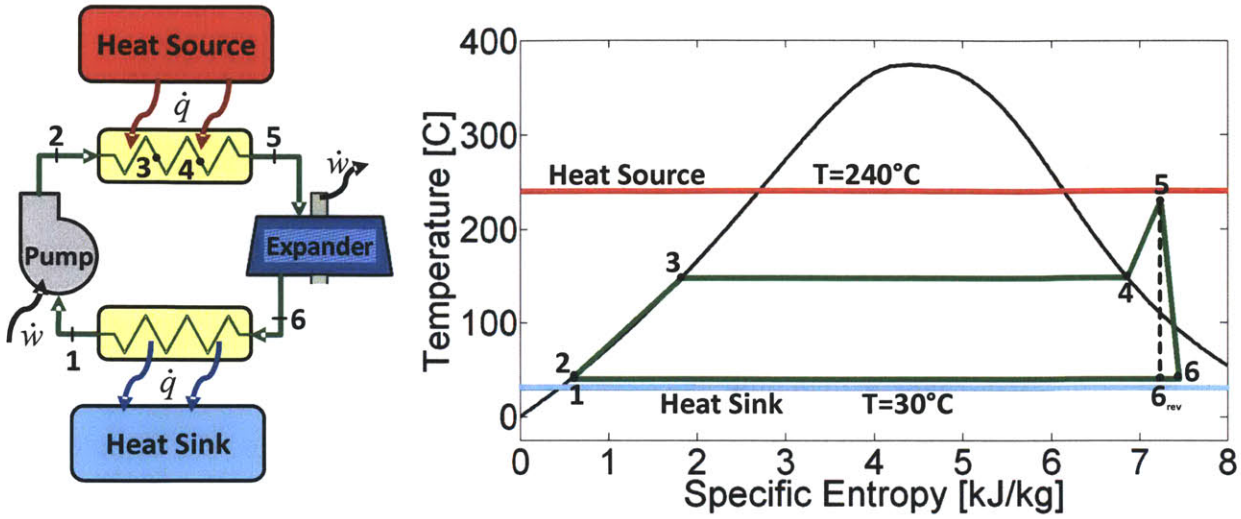

Figure 2.1: Schematic diagram and *T-s* plot of a steam Rankine cycle. In a steam Rankine cycle, a heat source at high temperature and a heat sink at low temperature provide the necessary potential to operate the heat engine. Steam is a wet fluid, meaning the saturated vapor curve has a negative slope $(dT/ds)_{sat}$. Thus, superheating from State 4 to State 5 is necessary to avoid excessive condensation in the expander, which operates between State 5 and State 6.

In the pure substance model, each single phase fluid state can be defined by any two thermodynamic properties. Because fluids boil at constant temperature along an isobar, two-phase states cannot be identified by temperature and pressure; another property such as quality or average specific volume must be specified. Table 1 contains the variables that are used to represent the thermodynamic properties of the fluid. Numbered subscripts refer to the fluid state.

Table 1: Variables used to represent thermodynamic properties

h	specific enthalpy
s	specific entropy
T	temperature
P	pressure
Q	quality

State 1 is fully defined as a saturated liquid at the minimum cycle temperature. In order to determine State 2, we first locate State 2_{rev}, which assumes that the fluid is pumped from P_1 to P_2 at constant entropy. State 2_{rev}, then, is defined by pressure $P_2 = P_{high}$ and specific entropy $s_{2,rev} = s_1$. Liquid pumps are not reversible, however, so an isentropic pump efficiency of η_{pump} is used to calculate the specific enthalpy of State 2:

$$h_2 = \left(\frac{h_{2,rev} - h_1}{\eta_{pump}} \right) + h_1 \quad . \tag{2}$$

State 2 is then fully defined by its pressure, P_2, and specific enthalpy, h_2.

The maximum cycle pressure, P_{high}, can be chosen from experience, such as using the low pressure steam value from the BP Polygeneration Plant Model. Alternatively, P_{high} can be chosen to guarantee a particular condensation limit at the expander exit. States 3 through 5 are also at the maximum cycle pressure of P_{high}. State 3 is saturated liquid, State 4 is saturated vapor, and State 5 is superheated steam at the maximum cycle temperature such that $T_5 = T_{max}$. From State 5 to State 6 the fluid is expanded back to low pressure and work is extracted. By first assuming an adiabatic and isentropic expansion, we determine a reversible turbine exit state 6_{rev}, as plotted in Figure 2.1. The expander isentropic efficiency, η_{exp}, is then used to find the specific enthalpy of state 6:

$$h_6 = h_5 - (h_5 - h_{6,rev}) \cdot \eta_{exp} \quad . \tag{3}$$

State 6 is then fully defined by pressure and specific enthalpy.

Table 2 contains the state information for a steam Rankine cycle as described above. The heat source is assumed to be waste heat from a plant process in the BP Polygeneration Plant. This heat source, which will be described in greater detail in Chapter 3, is an exothermic chemical reaction which converts syngas from a coal gasifier into useful liquids and waxes. This reaction emits a substantial heat load, and must be constantly cooled to maintain a

Table 2: Steam Rankine cycle states with a high pressure of 450 kPa, a heat source at 240°C, and a heat sink at 30°C. Pump and expander efficiencies are assumed to be 0.9.

	specific enthalpy	specific entropy	Temperature	Pressure	Quality
State	h [kJ/kg]	s [kJ/kg-K]	T [°C]	P [kPa]	Q [kg/kg]
1	167.5	0.572	40	7.39	0
2rev	168.0	0.572	40.01	450	subcooled
2	168.0	0.573	40.03	450	subcooled
3	623.1	1.821	147.9	450	0
4	2743.4	6.856	147.9	450	1
5	2921.3	7.243	230	450	superheated
6rev	2256.4	7.243	40	7.39	0.868
6	2322.8	7.455	40	7.39	0.896

temperature of 240°C to assure the desirable product mix. It is the single largest source of low temperature heat in the BP Polygeneration Plant. The heat sink is assumed to be cooling water at 30°C. The cooling water has a large mass flow such that it does not experience measurable change in temperature during heat transfer from the cycle.

To assure heat transfer from the hot stream to the cold stream of a heat exchanger, a temperature potential, ΔT, must be maintained at all locations. The smallest temperature potential in the heat exchanger, ΔT_{min}, must be small enough to limit the entropy generation caused by heat transfer across large temperature gradients but large enough to limit the heat transfer area. Cycles considered here use a minimum temperature potential of $\Delta T_{\min} = 10°C$. This value is based on "experience values" of ΔT_{min} suggested by Linnhoff et. al of 5°C for a refrigeration system and 20°C for a heavy chemical process (Linnhoff, et al., 1994). Therefore, the working fluid has maximum temperature of 230°C and minimum temperature of 40°C.

Pump and expander efficiencies are set at $\eta_{pump} = \eta_{exp} = 0.9$. The BP Polygeneration Aspen Model uses low grade heat sources to generate steam at a pressure of 450 kPa, a

pressure level based on the NETL report on fossil energy plants (Woods, et al., Revision 2, 2010). Therefore, this cycle evaluation uses $P_{high} = 450\,\text{kPa}$.

The cycle state data can be used to calculate important cycle characteristics. Conservation of energy applied to the expander shows that the specific work output is equal to the change in specific enthalpy across the expander:

$$w_{exp,dry} = (h_5 - h_6) \quad . \tag{4}$$

This expander specific work output, $w_{exp,dry}$, has the subscript "dry" because the actual expander work output needs to be adjusted for wetness in the expander. Wetness, Y, is defined as the percent of condensation in the fluid [kg/kg]. Wetness and quality, Q, sum to 1:

$$Y + Q = 1 \quad . \tag{5}$$

Liquid droplets increase the frictional loss on spinning blades which degrades the work output (Leyzerovich, 2005). This effect is non-linear and turbine design dependent, but it can be approximated empirically with the Baumann rule. The Baumann rule applies a correction factor to the calculated turbine work output such that 1% average wetness in the expander results in a 1% reduction of expander specific work output:

$$w_{exp} = w_{exp,dry} \cdot \left(1 - Y_{avg}\right) \quad . \tag{6}$$

In Equation (6), w_{exp} is the actual specific work output realized across the expander. The average wetness of the turbine, Y_{avg}, is defined as the average of the turbine inlet wetness, Y_{in}, and turbine exit wetness, Y_{out}:

$$Y_{avg} = \frac{\left(Y_{in} + Y_{out}\right)}{2} \quad . \tag{7}$$

The following cycle characteristics can be defined:

$$\text{Expander Specific Work} = w_{exp} = (h_5 - h_6)\cdot(1 - Y_{avg}) \tag{8}$$

$$\text{Pump Specific Work} = w_{pump} = h_1 - h_2 \tag{9}$$

$$\text{Cycle Net Specific Work} = w_{net} = w_{exp} + w_{pump} \tag{10}$$

$$\text{Specific Heat Transfer In} = q_{in} = h_5 - h_2 \tag{11}$$

$$\text{Cycle Efficiency} = \eta_{cyc} = \frac{w_{net}}{q_{in}} \quad . \tag{12}$$

The maximum possible efficiency for a reversible heat engine operating between a heat source at temperature T_{source} and a heat sink at temperature T_{sink} is the Carnot efficiency, η_{carnot}:

$$\eta_{carnot} = \frac{T_{source} - T_{sink}}{T_{source}} \quad . \tag{13}$$

The ratio of the cycle efficiency to the Carnot efficiency indicates the ability of this cycle to optimal convert heat input from the constant temperature heat source into shaft work output. This percent of optimal efficiency, also called the 2nd Law Efficiency, will be denoted as η_{opt}:

$$\eta_{opt} = \frac{\eta_{cyc}}{\eta_{carnot}} \quad . \tag{14}$$

Table 3 lists the values of these cycle characteristics for the steam cycle described above.

Table 3: Steam Rankine cycle characteristics for a cycle with a high pressure of 450 kPa and heat source and sink of 240°C and 30°C respectively.

Fluid	Y_{avg} [kg/kg]	w_{exp} [kJ/kg]	w_{pump} [kJ/kg]	w_{net} [kJ/kg]	q_{in} [kJ/kg]	η_{cyc}	η_{Carnot}	η_{opt}
Water	0.0521	567.3	-0.5	566.8	2753.3	20.6%	40.9%	50.3%

2.2.2 Dry Fluids

The organic Rankine cycle (ORC) model employed in this work for dry fluids also operates between a heat source at high temperature, T_{source}, and a heat sink at low temperature, T_{sink}. Figure 2.2 is a schematic for the fluid path through an organic Rankine cycle along with the related fluid states on a Temperature vs. Specific Entropy (T-s) diagram. Decane is used as the working fluid in this example. Again, the specific work transfer rate is $\dot{w}$, and the specific heat transfer rate is $\dot{q}$. The fluid saturated states which are the boundary of the two-phase region are represented by a black line on the T-s diagram. The cycle begins at State 1 as a saturated liquid at low pressure, P_{low}, and at the cycle minimum temperature, T_{min}. The fluid is pumped up to high pressure, P_{high}, at State 2. The high pressure liquid is then preheated from State 2 to State 4, and boiled from State 4 to State 5 by heat transfer from the heat source. (State 3 has

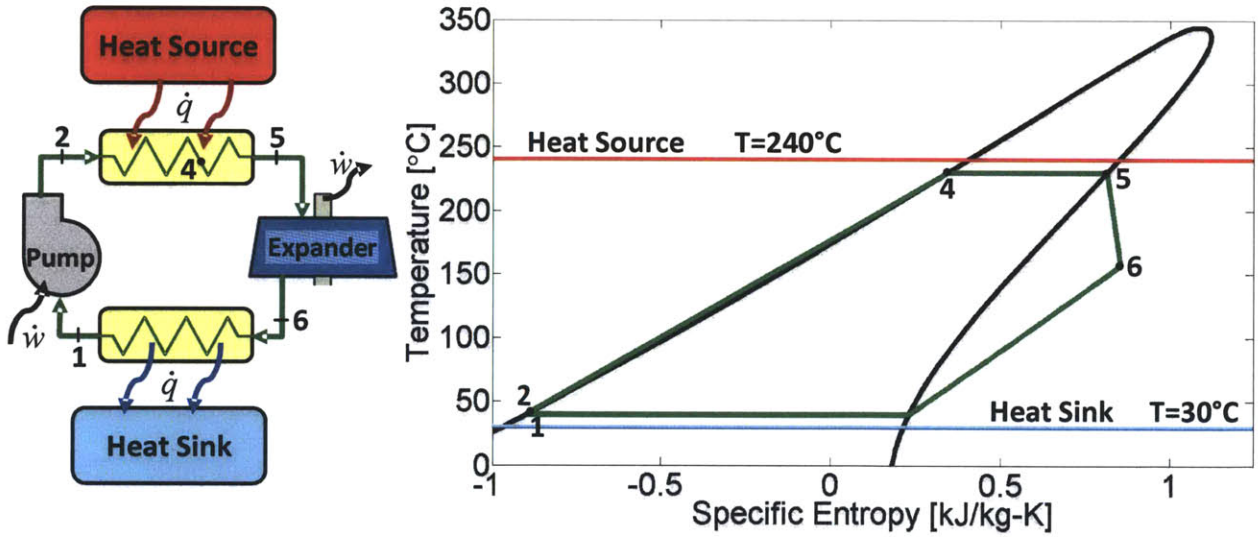

Figure 2.2: Schematic diagram and T-s plot of an organic Rankine cycle. In an organic Rankine cycle, a heat source at high temperature and a heat sink at low temperature provide the necessary potential to operate this heat engine. The working fluid is hexane, which is a dry fluid, meaning the saturated vapor curve has a positive slope $(dT/ds)_{sat}$. This causes the vapor dome to have an appearance of leaning over to the right, and it means that superheat is not necessary to prevent condensation in the expander.

been skipped here for reasons that will become clear shortly.) Due to its drying nature, the fluid can be expanded directly from a saturated vapor at State 5 to a superheated vapor state at low pressure at State 6. The low pressure vapor is then cooled and condensed back into a low pressure liquid at State 1.

One consequence of expanding a dry fluid is that the expander exit stream, State 6 in Figure 2.2, is a superheated vapor at elevated temperature such that $T_6 > T_{min}$. Therefore, there is an opportunity to transfer heat from the low pressure vapor stream into the high pressure liquid stream as part of the preheating process that occurs from State 2 to State 4. A recuperator is added to recover heat from the superheated expander exit stream, thereby

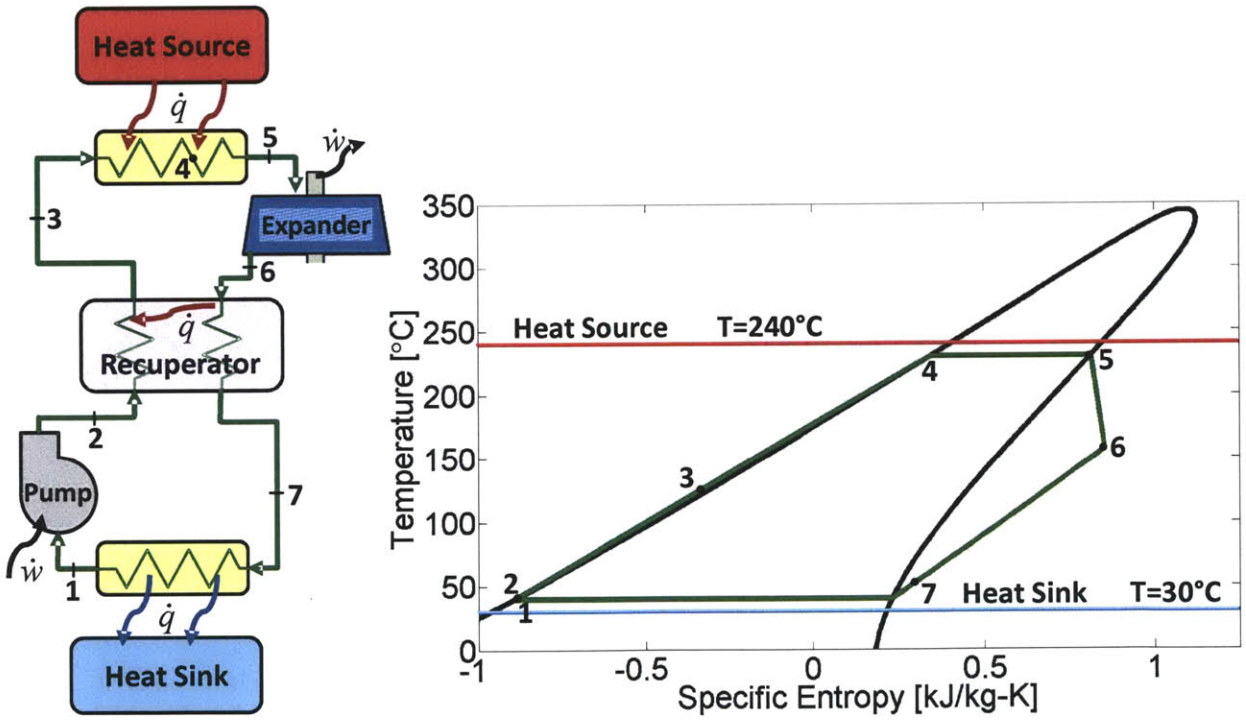

Figure 2.3: Schematic diagram and *T-s* plot of a baseline ORC with recuperator. The expander exit stream at State 6 passes through a recuperator where heat is transferred to the high pressure liquid leaving the pump at State 2. The hot vapor exits the recuperator at State 7 slightly above saturation temperature, while the cold liquid exits the recuperator at an intermediate temperature T_3, which falls between T_2 and T_4.

reducing the necessary heat input to operate the cycle. Figure 2.3 is the schematic of an organic Rankine cycle with a recuperator as described. The hot vapor enters the recuperator directly out of the expander at State 6, and exits the recuperator at low temperature at State 7. The cold stream enters the recuperator as high pressure liquid at State 2 and exits the recuperator at some elevated temperature at State 3.

For the dry fluid, cycle states are calculated in the same manner as for the wet fluid. State 1 is saturated liquid at a temperature slightly above the heat sink temperature to assure heat transfer such that $T_1 = T_{sink} + \Delta T_{min}$. State 1 determines the low pressure isobar for the organic Rankine cycle, $P_{low} = P_1$. The high pressure, P_{high}, is determined by the expander inlet condition at State 5. No superheating is required for the dry fluid, so State 5 is a saturated vapor with a temperature slightly below the heat source temperature such that $T_5 = T_{source} - \Delta T_{min}$. Consequently, the high pressure for the cycle is the saturation pressure for the fluid at temperature T_5 such that $P_{high} = P_5 = P_{sat}(T_5)$.

With the high and low pressures defined, the remaining state points can be determined. State 4 is a saturated liquid at high pressure, $P_4 = P_{high}$. State 2 is defined by first assuming the pump is reversible, yielding state 2_{rev} which corresponds to an isentropic pressurization from State 1 such that $P_{2,rev} = P_{high}$ and $s_{2,rev} = s_1$. Having defined state 2_{rev}, an isentropic pump efficiency, η_{pump}, is used in Equation (2) to find h_2, thus defining State 2. In the same manner, a reversible expander exit State 6_{rev} can be found where $P_{6,rev} = P_{low}$ and $s_{6,rev} = s_5$. The specific enthalpy of State 6 is then determined by assuming an isentropic expander efficiency, η_{exp}, and using Equation (3).

As seen in Figure 2.3, the organic Rankine cycle with a dry working fluid has State 3 and State 7 associated with the recuperator. The hot vapor stream in the recuperator (State 6 to State 7) has a smaller specific heat capacity than the cold liquid stream (State 2 to State 3). Therefore, the recuperator will pinch at the cold end such that $T_7 = T_2 + \Delta T_{min}$. State 7, which is

at pressure P_{low} and temperature T_7, is now fully defined. The enthalpy of State 3 is determined by evaluating the First Law of Thermodynamics on a control volume surrounding the recuperator:

$$h_3 = h_6 - h_7 + h_2 \quad . \tag{15}$$

The thermodynamics and heat transfer in the recuperator will be explored in greater detail in Chapter 3.

Table 4 contains the state information for an organic Rankine cycle as described above. The working fluid for this cycle is decane. Just as with the steam cycle example, the heat source is waste heat from a plant process at a constant temperature of 240°C, the heat sink is cooling water at a constant temperature of 30°C, and a minimum temperature potential of $\Delta T_{min} = 10°C$ is maintained between the working fluid and the source or sink for all states. Pump and expander efficiencies are set at $\eta_{pump} = \eta_{exp} = 0.9$.

Table 4: Organic Rankine cycle states for a decane cycle with heat source and sink of 240°C and 30°C respectively. The expander and pump have isentropic efficiencies of 0.9.

	specific enthalpy	specific entropy	Temperature	Pressure	Quality
State	h (kJ/kg)	s (kJ/kg-K)	T (°C)	P (kPa)	Q
1	-338.74	-0.894	40	0.4867	0
2rev	-338.26	-0.894	40.1	348.6	Subcooled
2	-338.19	-0.894	40.1	348.6	Subcooled
3	-124.85	-0.295	128.0	348.6	Subcooled
4	164.30	0.345	230	348.6	0
5	400.13	0.814	230	348.6	1
6rev	227.54	0.814	149.5	0.4867	Superheated
6	244.82	0.854	157.3	0.4867	Superheated
7	31.45	0.287	51.0	0.4867	Superheated

All of the fluid states for the organic Rankine cycle have been defined, and cycle characteristics can be considered. The Baumann rule for turbine wetness has no effect on this cycle, because there is no condensation when expanding a dry fluid. The expander specific work output, w_{exp}, from Equation (8), pump specific work input, w_{pump}, from Equation (9), and cycle net specific work output, w_{net}, from Equation (10) are calculated in the same manner as they were for the wet steam Rankine cycle. For the dry working fluid, the specific heat recovered in the recuperator, q_{rec}, must be considered:

$$q_{rec} = h_6 - h_7 \quad . \tag{16}$$

The specific heat input from external sources which is required to operate the organic Rankine cycle, q_{in}, is reduced accordingly:

$$q_{in} = h_5 - h_2 - q_{rec} \quad . \tag{17}$$

The cycle efficiency, Carnot efficiency, and optimal efficiency are defined in the same manner for a dry fluid as for a wet fluid, by Equations (12), (13), and (14) respectively.

Cycle characteristics for this organic Rankine cycle using decane are included in Table 5. The steam Rankine cycle characteristics which were previously reported in Table 3 are also included to facilitate a comparison between the two cycles.

Table 5 shows that the organic Rankine cycle achieves superior efficiency to the steam

Table 5: Organic Rankine cycle characteristics for a decane cycle with heat source and sink of 240°C and 30°C respectively. Steam Rankine cycle results for a comparable cycle are included. Expander and pump efficiencies are assumed to be 0.9.

Fluid	Y_{avg} [kg/kg]	w_{exp} [kJ/kg]	w_{pump} [kJ/kg]	w_{net} [kJ/kg]	q_{rec} [kJ/kg]	q_{in} [kJ/kg]	η_{cyc}	η_{Carnot}	η_{opt}
Water	0.0521	567.3	-0.5	566.8	N/A	2753.3	20.6%	40.9%	50.3%
Decane	N/A	155.3	-0.5	154.8	213.4	525.0	29.5%	40.9%	72.0%

Rankine cycle, which will be discussed shortly. The specific heat transfer into the cycle, q_{in}, and the specific work output from the cycle, w_{net}, are each much greater for water than for decane. This difference is caused by the substantially larger latent heat of water, which is about 20 times that of decane. Thus, for a given heat source, the decane cycle will require a much larger mass flow than the steam cycle to absorb heat at the same rate. Also, the pump work input for the organic cycle consumes 3.3% of expander work, whereas the pump work input for the steam cycle consumes less than 0.1% of expander output. This means that the decane Rankine cycle is more susceptible to pump inefficiencies than the steam Rankine cycle.

2.3 Fluid Selection

Choosing the correct fluid for an organic Rankine cycle is essential to achieving the best possible performance. The choice of fluid will not only affect the efficiency of the cycle, but also the reliability, safety, environmental impact, and cost of the cycle. Included here is a discussion of important factors to consider when screening fluids.

2.3.1 Thermodynamic Considerations

The primary consideration affecting fluid selection is efficiency. The purpose of the ORC is to convert heat into shaft work. Steam is more benign and has better availability, reliability, and environmental impact than any organic fluid choice, so any alternative to steam must output more work than a steam Rankine cycle.

The efficiency of a Rankine cycle depends on the working fluid properties and the heat source and heat sink available to the cycle. For this thesis, the heat source considered is an exothermic chemical reaction maintained at constant temperature of $T_{source} = 240\,°C$. The heat sink is cooling water with a mass flow great enough to maintain a constant temperature of $T_{sink} = 30\,°C$. Heat transfer across a temperature gradient is inherently inefficient. Therefore, given the constant temperature heat source and sink described, working fluid should absorb

heat as close to T_{source} as possible and reject heat as close to T_{sink} as possible. Fluid properties which help to achieve these heat transfer goals increase cycle efficiency. A minimum temperature difference, ΔT_{min}, is maintained between the working fluid and the heat source or heat sink to assure heat transfer.

Given the constraint on maximum cycle temperature, dry fluids achieve a higher temperature for heat transfer into the system than wet fluids. State points for a wet Rankine cycle and dry Rankine cycle are plotted on adjacent T-s diagrams in Figure 2.4. The loci of saturated states are represented by black lines on each diagram. The wet and dry Rankine cycles operate between the heat source and the heat sink described above, so that both the wet fluid and the dry fluid have the same maximum cycle temperature, $T_5 = T_{max} = T_{source} - \Delta T_{min}$, and minimum cycle temperature, $T_1 = T_{min} = T_{sink} + \Delta T_{min}$.

Dry fluids are defined by the positive slope $(dT/ds)_{sat}$ of the saturated vapor line on the T-s diagram. This gives the appearance that the vapor dome leans over to the right, as seen in Figure 2.4. Dry fluids do not condense when expanded isentropically from a saturated vapor state. Instead, this expansion results in a superheated vapor. In contrast, wet fluids have a negative slope $(dT/ds)_{sat}$ of the saturated vapor line on the T-s diagram. When a wet fluid is

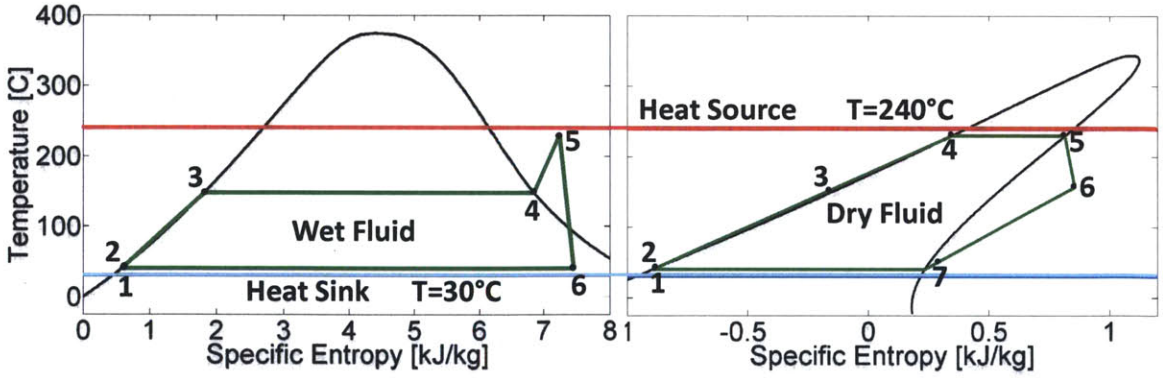

Figure 2.4: T-s diagrams for Rankine cycles using a wet working fluid (left) and a dry working fluid (right) operating between a heat source and a heat sink. The wet working fluid requires superheat, resulting in a lower boiling temperature than the dry fluid.

expanded from a saturated vapor state, it begins to condense.

Condensation in the expander raises two problems, as briefly discussed in Section 2.2.1. The liquid condensation droplets cause frictional losses in rotating machinery, so that the efficiency of an expander with internal condensation is lower than the efficiency of an expander with dry gas flowing through it. Also, condensation in an expander causes wear and reduces equipment usable life. For this reason, equipment usually has an allowable condensation limit, and fluid passing through the expander is kept above this limit by superheating before entering the expander.

The wet Rankine cycle on the left side of Figure 2.4 reaches is a saturated vapor at State 4, and is then superheated up to State 5. This superheating requirement forces the wet fluid to have a lower boiling temperature $T_3 < T_{max}$. In contrast, the dry fluid boils at the highest possible temperature, $T_4 = T_{max}$. Thus, the lack of superheating allows the dry fluid to absorb heat at higher temperature than the wet fluid.

On the cooling side of the cycle from State 6 to State 1, wet fluids reject all of their heat in the condenser at the minimum temperature $T_{min} = T_{sat}(P_{low})$. This is an advantage for wet fluids, because heat is rejected with little entropy generation. In contrast, dry fluids exit the expander as superheated vapor at elevated temperature, State 6 on the right side of Figure 2.4. Directly rejecting heat from State 6 to the cooling water at T_{sink} generates entropy, and could be a disadvantage for dry cycles. Fortunately, most of the heat from the superheated expander exit stream can be recovered in a recuperator from State 6 to State 7, and used to preheat the cold liquid exiting the pump from State 2 to State 3. The use of a recuperator negates the disadvantage of the elevated expander exit temperature for a dry fluid rejecting heat.

While the recuperator reduces entropy generation during heat rejection from the cycle, it also reduces entropy generation during heat absorption by the cycle. The coldest working fluid temperature at which heat is absorbed without the recuperator is T_2, but with the recuperator included the coldest temperature at which heat is absorbed is raised to T_3. Thus,

the heat transfer from the source into the wet fluid occurs from State 2 up to State 5 across a large temperature gradient. The heat transfer from the heat source into the recuperated dry cycle occurs only from State 3 up to State 5, across a much smaller temperature gradient. The recuperator greatly improves the cycle efficiency for a cycle operating between a constant temperature heat source and a constant temperature heat sink.

The advantage of dry fluids over wet fluids is illustrated by Figure 2.5, which shows efficiencies for Rankine cycles using several fluids. The wet fluids are analyzed as described Section 2.2.1, and the dry fluids are analyzed as described in Section 0. Phigh for water is 450 kPa to match the low pressure steam level from the BP Polygeneration Plant Model. Phigh for ethanol is 4698.8 kPa to assure a maximum wetness of 10% at the expander exit. All of the cycles have a

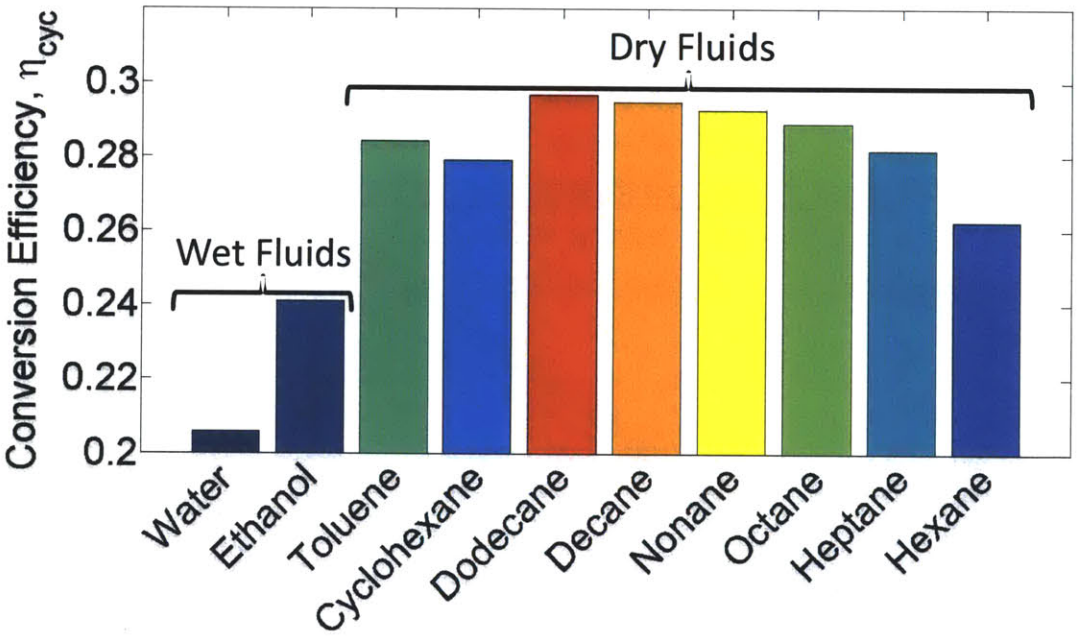

Figure 2.5: Cycle efficiencies for a heat engine operating between a maximum temperature of 230°C and a minimum temperature of 40°C using various working fluids. The efficiencies range from a low of 20.6% for water to a high of 29.7% for dodecane. The Carnot efficiency for a cycle operating at these temperatures is 37.8%. The dry fluids exhibit higher efficiencies than the wet fluids. Working fluid states and cycle characteristics for this chart are included in Appendix I.

ΔT_{min} of 10°C resulting in a maximum cycle temperature of $T_{max} = 230°C$ and a minimum temperature of $T_{min} = 40°C$. Isentropic pump and expander efficiencies of $\eta_{pump} = \eta_{exp} = 0.9$. The Baumann rule (see Section 2.2.1) is in effect for wet fluids.

Dry fluids exhibit a clear efficiency advantage over wet fluids in Figure 2.5. Dry fluids can be further characterized to narrow the field of potential working fluid choices. Figure 2.6 is a plot of the cycle heating profiles for alkanes varying in size from hexane (C_6H_{14}) up to decane ($C_{10}H_{22}$). The heat source at $T_{source} = 240\,°C$ is plotted in red. The effects of the recuperator are neglected here to isolate other properties which improve efficiency. Each dry fluid absorbs heat from the source beginning at the pump exit temperature (State 2 in Figure 2.4) and ending at the expander inlet (State 5 in Figure 2.4).

As the size of the working fluid hydrocarbon chain increases from hexane to decane, the temperature at which heat is absorbed into the cycle also increases. Thus, the longer chain

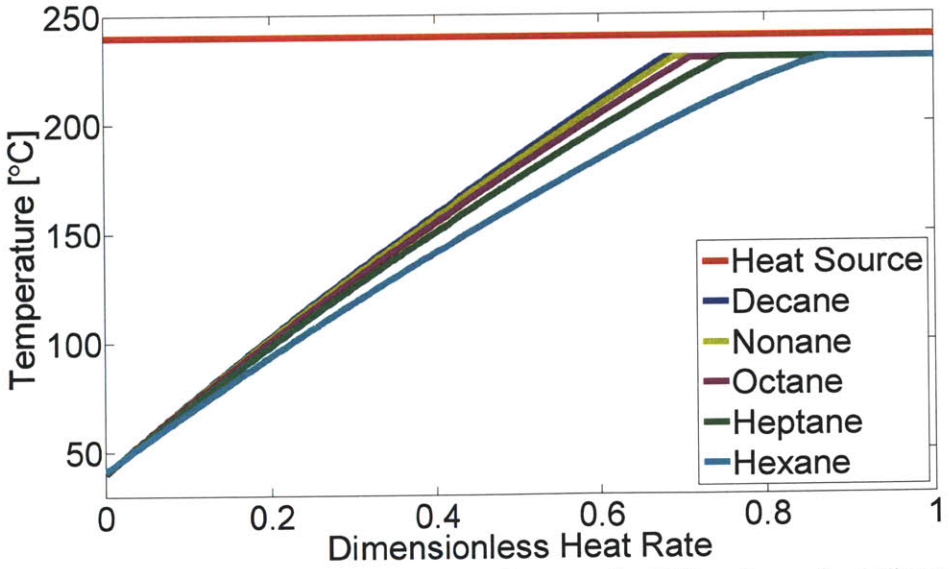

Figure 2.6: Temperature profile of the heat requirements for ORC's using various alkanes as the working fluid. The heat rate absorbed by each cycle has been normalized to the total heat rate of the heat source. The heavier working fluids have larger latent heats, thus absorbing heat at temperatures closer to the heat source than the lighter working fluids.

hydrocarbons have better conversion efficiency for this heat source. The increased temperature at which heat is absorbed is a direct result of the latent heat input as a percentage of the overall heat input. In Figure 2.6, the total heat rate for the cycle has been normalized to a value of 1. The heat rate that is absorbed as latent heat is represented by the constant temperature plateau for each working fluid at $T_{max} = 230\,°C$. Only the final 12% of heat rate absorbed by hexane as the working fluid occurs as latent heat at T_{max}, while for decane 32% of heat rate absorbed by the working fluid occurs as latent heat at T_{max}.

The increased fraction of latent heat for heavier hydrocarbons is a direct result of their higher critical temperature. The loci of saturated states for hexane, octane, and decane are plotted in Figure 2.7. The critical temperature for each fluid is located at the apex of the vapor dome, where the saturated liquid curve meets the saturated vapor curve. The minimum cycle temperature and maximum cycle temperature are identified by black dashed lines. Each

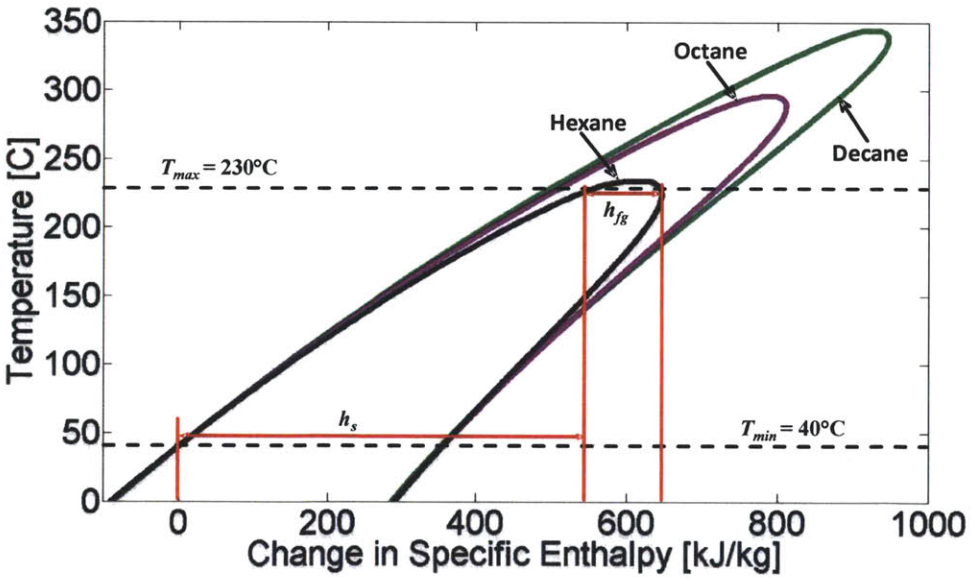

Figure 2.7: Loci of saturated states for hexane, octane, and decane on a Temperature vs. Specific Enthalpy diagram. At the maximum cycle temperature, T_{max}, the width of the vapor dome is larger with increasing critical temperature of the working fluid, such that latent heat at T_{max} is larger with increasing T_{crit}.

working fluid absorbs heat along a high pressure isobar which closely follows the saturated liquid curve for the fluid from T_{min} to T_{max} (sensible heat). Each working fluid is then boiled at constant temperature from the saturated liquid state to a saturated vapor state at T_{max} (latent heat). The magnitudes of the sensible heat, h_s, and the latent heat, h_{fg}, for hexane are indicated by red arrows.

Octane and hexane boil at the same temperature, T_{max}, but octane has a higher critical temperature. Therefore, boiling occurs closer to the critical temperature for hexane than for octane, and as a result the latent heat is much smaller for hexane than for octane. The same argument can be extended to decane. Additionally, Figure 2.7 makes evident that the sensible heat required to preheat each working fluid from T_{min} to T_{max} at high pressure decreases as the critical temperature increases. These two trends result in the increase of latent heat as a percentage of overall heat absorption into the cycle.

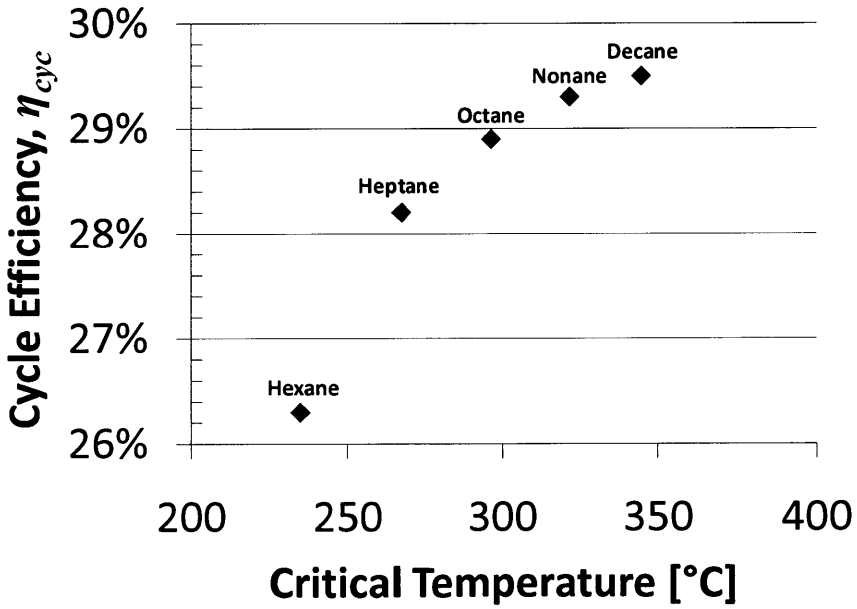

Figure 2.8: ORC efficiency for various alkanes with different critical temperatures using a constant temperature heat source of 240°C. Efficiency increases with working fluid critical temperature. The heat sink is cooling water at 30°C, ΔT_{min} is 10°C.

Table 6: Critical temperatures for select organics and water.

Fluid	T_{crit} [°C]
Water	373.95
Toluene	318.6
Cyclohexane	280.49
Dodecane	384.95
Decane	344.55
Nonane	321.4
Octane	296.17
Heptane	266.98
Hexane	234.67

The increased latent heat associated with increasing critical temperature, T_{crit}, is amplified by the affect of the recuperator. Baseline ORC efficiency is plotted against working fluid critical temperature in Figure 2.8. The efficiencies plotted here are based on the previously stated assumption of a constant temperature heat source at 240°C, and the recuperator is included. The critical temperatures for some organics and water are included in Table 6 above.

2.3.2 Reliability

There are a number of important fluid considerations which may not change the thermodynamic efficiency of an organic Rankine cycle, but affect the reliability and safety of the cycle. A brief discussion of triple point temperature, chemical stability, and safety follows.

The triple point of a fluid is the temperature and pressure at which the solid, liquid, and gas phases coexist. Any ORC working fluid should have a low triple point temperature such that $T_{tp} < T_{min}$. If the cycle approaches the triple point temperature, there is a risk that the fluid will solidify and cause equipment failures. Triple point temperatures for fluids considered in this work are listed in Table 7. As a general rule, it is desirable to have a triple point temperature lower than that of water.

Table 7: Triple point temperatures and normal boiling points of select fluids.

Fluid	T_{tp} [°C]	T_{boil} [°C]
Water	0.01	99.98
Toluene	-95.15	110.6
Cyclohexane	6.32	80.74
Dodecane	-9.55	216.15
Decane	-29.65	174.12
Nonane	-53.45	150.76
Octane	-56.78	125.62
Heptane	-90.6	98.38
Hexane	-95.32	68.71

Any compound chosen as a working fluid must be chemically stable within the temperature and pressure ranges of the cycle. Degradation of a working fluid can change its thermodynamic properties rendering the cycle unpredictable and ineffective. Some products of organic decomposition may cause coking and block equipment passages if not removed. Dehydrogenation can be a particularly challenging issue for hydrocarbons as temperatures increase (Doty & Siddarth, 2009). Hydrogen gas becomes trapped in the condenser, where it interferes with heat transfer and takes up volume. Consequently, the pressure and the temperature in the condenser increase, resulting in a decreased pressure ratio across the expander and a degradation of work output.

Thermal stability of organic compounds is greatly reduced by the presence of oxygen, such that air and water leakages into an ORC are undesirable. If the cycle is maintained at a pressure greater than or equal to its environment, all system leakages will be outward. The normal boiling point temperature, T_{boil}, helps to quickly identify fluids which will maintain pressures higher than atmospheric pressure as they condense. The normal boiling point is the saturation temperature of a fluid at atmospheric pressure, and therefore it is the lowest possible condensation temperature, T_{min}, which can be used if the cycle is to remain above atmospheric pressure.

The thermal stability limitations of many fluids have been studied for organic Rankine cycle applications, including various refrigerants (Calderazzi & di Paliano, 1997), (Morgan, Mills, Zakak, Reinhold, & Carr, 1982), pentanes (Andersen & Bruno, 2005) and other hydrocarbons and hydrofluorocarbons (Jain, Demirgian, Krazinski, Bushby, & Mattes, 1984). These papers generally conclude that thermal stability of working fluids for ORC applications is fluid specific, with allowable temperature limits ranging from 90°C up to 396°C. Degradation often results in the build up of non-condensable gases in the condenser. Methods for reducing known degradation rates have also been studied (Doty & Siddarth, 2009). Doty goes so far as to claim that organic working fluids can be used at temperatures as high as 527°C (800K) if proper precautions are taken. The allowable rate of decomposition for a working fluid depends on the frequency with which the fluid will be refreshed for a given application. A review of major ORC technologies lists acceptable heat source temperatures ranging from 80°C up to 400°C, with most units targeted at heat sources in the 100°C to 300°C range (Quoilin & Lemort, 2009).

2.3.3 Safety

Human safety considerations are also important for selecting a working fluid. One safety concern is the potential for a working fluid to combust or explode. It is desirable to choose a fluid with a high flash point, which is the temperature at which the liquid phase of a fluid gives off enough vapor to be ignited by an external source. The Occupational Safety and Health Administration (OSHA), a federal agency under the United States Department of Labor, classifies liquids by their flammability (for volatile liquids) or combustibility (for non-volatile liquids) using the classification system listed in Table 8, which starts with the most dangerous fluids and progresses towards the benign.

Another safety concern is the toxicity of a substance, which refers to direct harm that may be inflicted upon a person by exposure to the substance. The acceptable limits of toxicity for a working fluid in an organic Rankine cycle are dependent on the application. For instance, introducing a toxic substance into an otherwise benign system may be a poor choice, but using

Table 8: OSHA classification system for flammable and combustible liquids (National Institute for Occupational Safety and Health, 2005). Classifications in this table are listed from most dangerous (Class IA) to least dangerous (Class IIIB).

Classification	Definition
Class IA flammable liquid	Flash Point below 73°F and Boiling Point below 100°F
Class IB flammable liquid	Flash Point below 73°F and Boiling Point at or above 100°F
Class IC flammable liquid	Flash Point at or above 73°F and below 100°F
Class II combustible liquid	Flash Point at or above 100°F and below 140°F
Class IIA combustible liquid	Flash Point at or above 140°F and below 200°F
Class IIIB combustible liquid	Flash Point at or above 200°F

a toxic substance in an industrial plant already equipped to handle dangerous materials may add little risk or cost. OSHA publishes Permissible Exposure Limit (PEL) standards for various chemicals. These limits regulate the amount of substance in the air on an 8 hour time weighted average, and are a good starting point for evaluating the toxicity of a substance. Select PEL's and flammable liquid classifications are included in Table 9. Toluene and cyclohexane, which are aromatic substances, are more toxic than alkanes. Nonane has a high enough normal boiling temperature that it is not considered an air contaminant and is not assigned a PEL.

It is also desirable to choose a fluid with a high Lower Explosive Limit (LEL), which is the concentration of the fluid vapor (% by volume) in air that will explode if ignited by an external

Table 9: Select fluid safety data for organic substances retrieved from the NIOSH Pocket Guide to Chemical Hazards.

Fluid	PEL (ppm)	Classification	LEL	UEL
Toluene	200	Class IB Flammable Liquid	1.1%	7.1%
Cyclohexane	300	Class IB Flammable Liquid	1.3%	8.0%
Nonane	N/A	Class IC Flammable Liquid	0.8%	2.9%
Octane	500	Class IB Flammable Liquid	1.0%	6.5%
Heptane	500	Class IB Flammable Liquid	1.1%	6.7%
Hexane	500	Class IB Flammable Liquid	1.1%	7.5%

source. The Upper Explosive Limit (UEL) is the concentration of a fluid at which it becomes too rich to ignite. Together, the LEL and the UEL define a range of concentrations over which the fluid vapor is explosive in air. LEL and UEL values for some organic fluids are listed in Table 9.

2.3.4 Environmental Impact

Working fluid environmental impact must be considered as well. The Intergovernmental Panel on Climate Change (IPCC) calculates values of the Global Warming Potential (GWP) of various gases. The GWP is a metric for comparing the amount of radiative energy absorbed by gases in the atmosphere over a given time period, referenced to 1 kg of CO_2 gas. Hydrocarbons larger than methane typically have low GWP's, but they may have indirect Global Warming Potential based on their tendency to affect other substances in the atmosphere (Forster, et al., 2007).

2.3.5 Cost

Any practical system design requires a consideration of the cost for implementation. Cost models are discussed in greater depth in Chapter 4, but there are some general rules which can help narrow down the options before undertaking more complex analyses. Fluids should be commercially available, so that the material cost of the working fluid itself is not prohibitive. Also, fluids with low volume flows allow for smaller equipment sizes. Low volume flow fluids can be identified by their high critical temperature, their high critical pressure, and their low boiling temperature.

Recall from Section 2.3.1 that for similar fluids, a higher critical temperature corresponds to a larger latent heat. Thus, a fluid with a high critical temperatures will typically require a smaller mass flow than a fluid with a lower critical temperature to achieve a given heat transfer rate into the fluid. Furthermore, a high critical pressure, P_{crit}, for a fluid corresponds to a high saturation pressure at the maximum temperature. Vapors at high pressure are more dense than vapors at low pressure, so the same mass flow requires a lower volume flow rate than for

a fluid at high pressure. If the pressure is too high, then wall thicknesses required for tubes and equipment will begin to drive costs up. The critical pressure of water, 22064 kPa, provides a reasonable ceiling for working fluid critical pressure, and the organics considered here all have lower critical pressures than water.

Finally, as discussed in the previous section, a low boiling temperature corresponds to a high pressure in the condenser, which increases the density of the fluid in the condenser and decreases the volume flow. Table 10 contains critical pressures for some organics as well as water. Critical temperature and normal boiling temperatures are also repeated here for comparison.

The alkanes ranging in size from hexane to decane, included in Table 9, have decreasing critical pressure with increasing size. These same alkanes have increasing normal boiling point with increasing size. Both of these trends make organic Rankine cycles using lighter alkanes such as hexane less expensive than ORC's using heavier alkanes such as decane. This cost will be explored in greater detail in Chapter 4 on Implementation.

Table 10: Critical pressures, critical temperatures, and normal boiling point temperatures for selected fluids.

Fluid	P_{crit} (kPa)	T_{crit} [°C]	T_{boil} [°C]
Water	22064.0	373.95	99.98
Toluene	4126.3	318.6	110.6
Cyclohexane	4075.0	280.49	80.74
Dodecane	1817.0	384.95	216.15
Decane	2103.0	344.55	174.12
Nonane	2281.0	321.4	150.76
Octane	2497.0	296.17	125.62
Heptane	2736.0	266.98	98.38
Hexane	3034.0	234.67	68.71

2.3.6 Fluid Selection Conclusions

A constant temperature heat source at 240°C is available for conversion into work by an organic Rankine cycle. Fluid selection criteria for cycle performance, reliability, safety, environmental impact, and cost have been considered. Thermodynamic performance is the primary consideration, and dry fluids exhibit a clear advantage over wet fluids for cycle conversion efficiencies. High critical temperature also correlates positively with ORC conversion efficiency, making longer chain hydrocarbons such as decane more efficient than smaller hydrocarbons such as hexane.

Fluid choice will also greatly affect the cost of ORC equipment, with high critical pressure and low normal boiling temperature being desirable qualities. Small chain hydrocarbons such as hexane will allow smaller equipment and less capital cost than longer chain hydrocarbons such as decane. This trend of smaller hydrocarbons being both less expensive and less efficient will be explored in more detail in Chapter 4 on implementation.

Table 11: Summary of fluid selection criteria for an ORC to convert a constant temperature heat source at 240°C into shaft work. Targets are listed in the first row.

Fluid	P_{crit} (kPa)	T_{crit} [°C]	T_{boil} [°C]	T_{tp} [°C]	Flammable Liquid Classification	LEL	UEL	PEL (ppm)
Target	high, less than water	high	low	<water	see Table 8	high	low	high
Water	22064.0	373.95	99.98	0.01	N/A	N/A	N/A	N/A
Toluene	4126.3	318.6	110.6	-95.15	IB	1.1%	7.1%	200
Cyclohexane	4075.0	280.49	80.74	6.32	IB	1.3%	8.0%	300
Dodecane	1817.0	384.95	216.15	-9.55	IIA	0.6%	N/A	N/A
Decane	2103.0	344.55	174.12	-29.65	II	0.8%	2.6%	N/A
Nonane	2281.0	321.4	150.76	-53.45	IC	0.8%	2.9%	N/A
Octane	2497.0	296.17	125.62	-56.78	IB	1.0%	6.5%	500
Heptane	2736.0	266.98	98.38	-90.6	IB	1.1%	6.7%	500
Hexane	3034.0	234.67	68.71	-95.32	IB	1.1%	7.5%	500

Safety and environmental factors must be considered for any fluid choice, and allowable limits for these factors depend on the context in which the cycle will be used. Table 11 summarizes the fluid selection criteria discussed in this chapter for water and some organic compounds. "Target" refers to the desired value for each fluid property.

3 Customizable Organic Rankine Cycles

In Chapter 2 the concept of an organic Rankine cycle (ORC) was introduced, and its utility for converting low temperature heat sources into shaft work was demonstrated by thermodynamic principle. The cycles considered in Chapter 2 assumed the availability of a constant temperature heat source. Often, heat sources have complex temperature profiles making it difficult to choose the best cycle for conversion of heat into work. In Chapter 3, modifications to the ORC are explored which improve the efficiency of the cycle. Each modification is a building block for the cycle designer, and taken together they can be configured into a cycle that meets the needs of any situation. These cycle building blocks will be demonstrated using heat sources derived from the BP Polygeneration Plant model.

3.1 Pinch Analysis Methods

A polygeneration plant contains many streams which flow between various processes within the plant as they are converted from feed stock into products and byproducts. Each process has temperature and heat requirements such that streams must be heated and cooled as they pass through the plant. To achieve these heat transfers, complex heat exchanger networks are designed between processes and streams. Utility streams, often steam, may be used as a medium for heat transfer around the plant. Utility streams are fluid flows in the polygeneration plant that transfer heat between processes and convert excess heat into electricity. Importantly, utility streams are defined by the plant designer, unlike process streams which are set by the process requirements. Pinch analysis was popularized in the 1970's as a method for setting design targets for heat exchanger networks in process plants. Since then it has been expanded to wider use as a design tool for integrated energy and process systems (Linnhoff, et al., 1994). A discussion of pinch analysis techniques used in this research is included here.

3.1.1 Utility Stream Profile

The thermal characteristics of a utility stream are defined by the temperature verse change in specific enthalpy (T-Δh) profile of the stream and by the mass flow of the stream. Utility streams for the purpose of this analysis are assumed to be at constant pressure, and do not undergo any work transfers, only heat transfers. Therefore, an energy balance on any utility stream will yield:

$$q = \Delta h \tag{18}$$

where q is the specific heat transfer into the stream, and Δh is the change in specific enthalpy of the stream. A change in specific enthalpy is related to a change in temperature by means of specific heat at constant pressure, c_p, of the fluid:

$$c_p = \left(\frac{dh}{dT} \right)_P \tag{19}$$

where dT is an incremental change in temperature, dh is an incremental change in specific enthalpy, and the subscript p denotes constant pressure. Specific heat at constant pressure is a function of temperature, though in certain situations it can be considered constant over moderate temperature ranges. Equations (18) and (19) can be combined to define the relationship of specific heat transfer to stream temperature at constant pressure:

$$dq = c_p \cdot dT \quad . \tag{20}$$

The thermodynamic profile of a hypothetical utility stream, labeled Stream 1, is plotted on a T-Δh graph in Figure 3.1. Stream 1 is water at a pressure of 4 MPa over a temperature range from 35°C to 85°C, and was chosen arbitrarily to illustrate the concept of a stream T-Δh profile. According to Equation (18), a change in specific enthalpy of the stream is due to a specific heat transfer into the stream. The T-Δh graph, then, indicates how much heat transfer per unit mass into or out of a stream is necessary to achieve a given temperature change. As

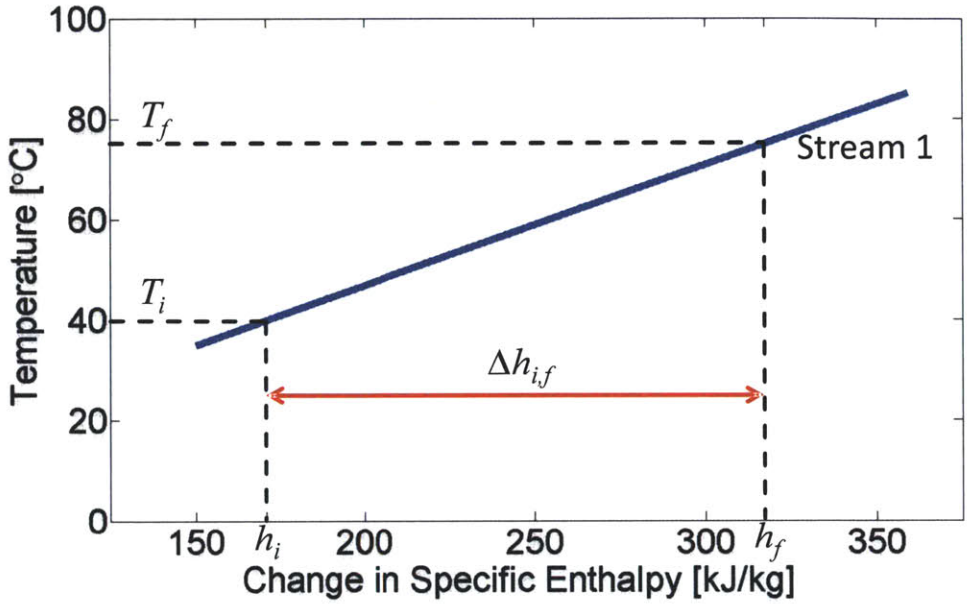

Figure 3.1: T-Δh profile of a hypothetical utility stream. A specific heat transfer $q = \Delta h_{i,f}$ is necessary to change the stream temperature from T_i to T_f.

plotted in Figure 3.1, a heat transfer into Stream 1 equal to $h_f - h_i = \Delta h_{i,f} = 146.2\,\text{kJ/kg}$ is required to heat the stream from $T_i = 40°C$ to $T_f = 75°C$. Similarly, to reduce the temperature from T_f to T_i, a heat transfer out of the system equal to $\Delta h_{i,f}$ is required.

The x-axis of Figure 3.1 is 'Change in Specific Enthalpy' rather than 'Specific Enthalpy'. This is an important distinction for pinch analysis, because the purpose of this graph is to determine the relationship between heat transfer and temperature, so the reference specific enthalpy value is unimportant. Consequently, a stream profile can be translated horizontally on the T-Δh graph. If the entire curve for Stream 1 translates horizontally, the value of $\Delta h_{i,f}$ will not change.

To completely define a utility stream it is necessary to identify the mass flow rate of the stream, $\dot{m}$. For a process plant operating at steady state, the mass flow rate of any given utility stream is constant with time. Therefore, mass flow rate can be included in the heat capacity of the system so that Equation (19) becomes:

$$\dot{m} \cdot c_p = \dot{m} \cdot \left(\frac{dh}{dT} \right)_P \tag{21}$$

where $\dot{m} \cdot c_p$ is a heat capacity rate. In the same way that specific heat capacity, c_p, determined the amount of specific heat transfer, q, necessary to change the stream temperature, the heat capacity rate, $\dot{m} \cdot c_p$, determines the total heat transfer rate, $\dot{Q}$, necessary to change the temperature of a constant pressure stream flowing through the system. Equation (20) can then be written on a flow rate basis:

$$d\dot{Q} = \dot{m} \cdot c_p \cdot dT \quad . \tag{22}$$

Furthermore, pinch analysis literature defines a variable H, called total enthalpy (Linnhoff, et al., 1994). This total enthalpy is defined in the pinch analysis literature as:

$$dH = \dot{m} \cdot dh \quad . \tag{23}$$

The variable H defined in Equation (23) has units of power (energy per time), so a time dependent notation, $\dot{H}$, will be used in this thesis. This variable is called "total enthalpy per unit time" or just "enthalpy per time" or "enthalpy flow rate." Equation (23) is rewritten as

$$d\dot{H} = \dot{m} \cdot dh \quad . \tag{24}$$

Including the flow rate considerations, Equation (18) can now be rewritten as

$$\dot{Q} = \Delta \dot{H} \tag{25}$$

where $\Delta \dot{H}$ is change in total enthalpy per unit time. A utility stream's temperature-enthalpy profile can be graphed on a Temperature vs. Change in Total Enthalpy per Time (T-$\Delta \dot{H}$) diagram. Just as with the T-Δh stream profile, the enthalpy reference state doesn't matter, and stream profiles can be translated horizontally on the graph. The T-$\Delta \dot{H}$ diagram for Stream 1

from the previous example (water at a constant pressure of 4 MPa over a temperature range of 35°C to 85°C) is plotted in Figure 3.2. The stream is now assigned a mass flow rate of $\dot{m}_1 = 1\,\text{kg/s}$. A second stream is plotted which has identical specific heat capacity, $c_p(T)$, to Stream 1, but has twice the mass flow rate such that $\dot{m}_2 = 2 \cdot \dot{m}_1 = 2\,\text{kg/s}$. The two streams have been shifted horizontally along the x-axis of the graph so that they intersect at temperature T_i. A change in temperature from T_i to T_f for Stream 1 requires a heat transfer rate of $\dot{Q}_1 = \Delta\dot{H}_1 = 146.2\,\text{kW}$, as seen in Figure 3.2. For Stream 2, a heat transfer rate of $\dot{Q}_2 = \Delta\dot{H}_2 = 2 \cdot \Delta\dot{H}_1$ is required to heat from T_i to T_f. Changing the mass flow stretches the stream profile horizontally by a proportional amount.

The individual utility streams in a plant can be combined into a composite curve that provides a thermodynamic profile of the utilities for the entire plant. To create this composite

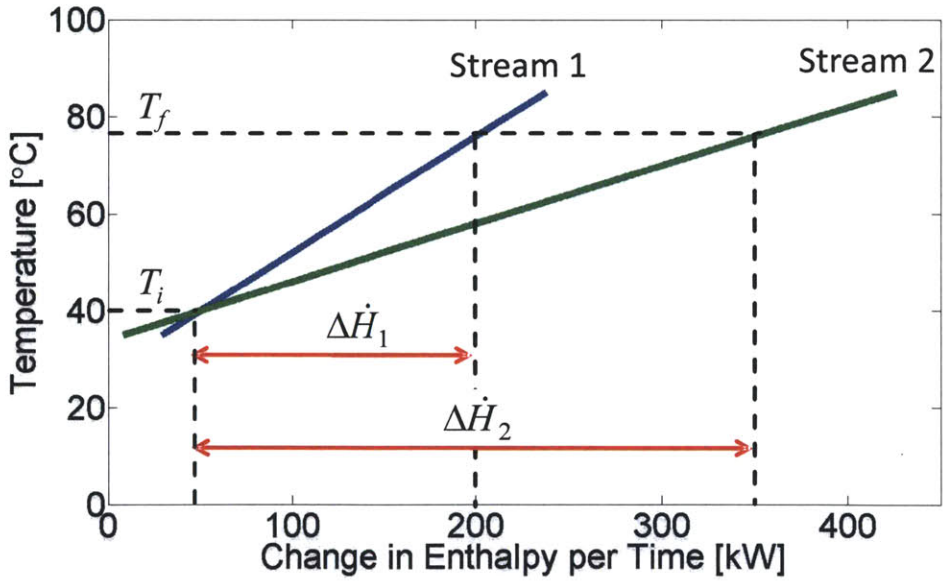

Figure 3.2: Temperature vs. Change in Enthalpy per Time profiles of two hypothetical utility streams. The streams have the same specific heat profile, $c_p(T)$, but Stream 2 has twice the mass flow of Stream 1. Thus, Stream 2 is stretched horizontally so that any change in temperature of Stream 2 requires twice the heat transfer rate that Stream 1 would require.

curve, the changes in enthalpy per time associated with each stream profile are summed at every temperature. Figure 3.3 demonstrates this concept on T-$\Delta\dot{H}$ graphs. On the left are two arbitrary utility stream profiles. To increase the temperature of Stream 1 from T_a to T_b, a change in total enthalpy per time of $\Delta\dot{H}_{ab,1}$ is required. Similarly, to increase the temperature of Stream 1 from T_b to T_c, a change in total enthalpy of is $\Delta\dot{H}_{bc,1}$ required. Stream 2 requires a change in total enthalpy per time of $\Delta\dot{H}_{ab,2}$ in order to increase in temperature from T_a to T_b. Stream 2 has a maximum temperature of T_b, so that heat transfer interactions with Stream 2 do not occur above this temperature.

On the right side of Figure 3.3 is the composite curve comprised of these two streams. The change in total enthalpy per time at any temperature on the composite curve is the sum or changes in total enthalpy per time at that temperature for Stream 1 and Stream 2. Therefore, to increase the temperature of the composite curve from T_a to T_b, a change in total enthalpy per time of $\Delta\dot{H}_{ab} = \Delta\dot{H}_{ab,1} + \Delta\dot{H}_{ab,2}$ is required. This is true for any arbitrary temperatures T_a

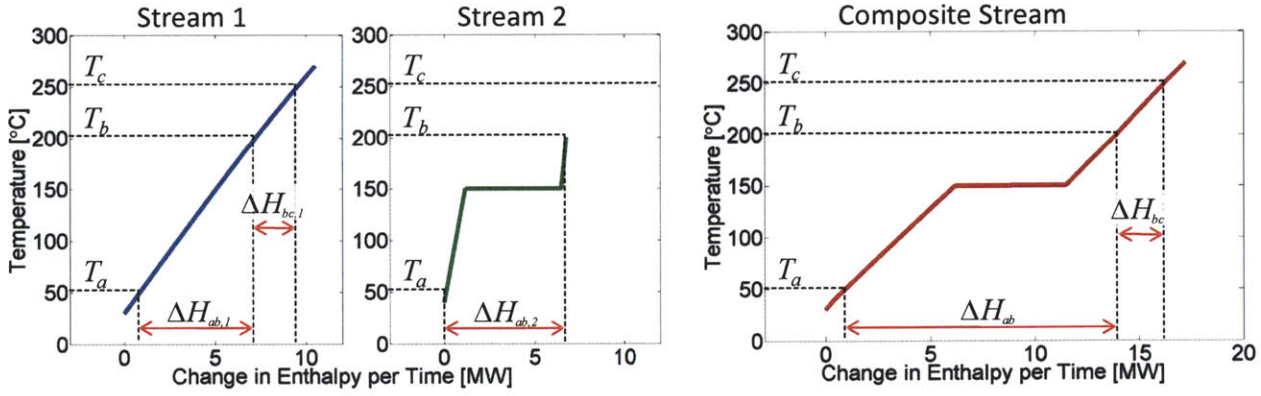

Figure 3.3: The T-$\Delta\dot{H}$ profiles of individual utility streams are combined to form a composite stream profile. Stream 1 and Stream 2 (left) are combined to form a composite curve (right) by summing the enthalpy flow rates of the streams at every temperature. There is a subtle kink in the composite curve at temperature T_b where Stream 2 ends.

and T_b. Also, in order to change the temperature of the composite stream from T_b to T_c, a change in total enthalpy per time of $\Delta\dot{H}_{bc} = \Delta\dot{H}_{bc,1}$ is required, because Stream 2 does not contribute any heat capacity rate above the temperature T_b.

Stream 2 in Figure 3.3 contains a constant temperature plateau at $T = 150\,°C$ where there is a change in the enthalpy flow rate but no change in temperature. That plateau is caused by the latent heat of the utility stream as boiling occurs at constant pressure. By choosing a different pressure, the temperature of that plateau can be adjusted to meet the needs of a particular plant. This concept will play an important role in selecting utilities.

3.1.2 Process Streams

Process streams in a polygeneration plant are fluid and heat flows which are necessary to process the raw feedstock into product streams. Each intermediate process between raw feedstock and product stream has its own temperature and heat transfer requirements that can be defined by a $T\text{-}\Delta\dot{H}$ curve, much in the same manner as utility streams. From a thermodynamic point of view, it is irrelevant what mass flows, pressures, and materials make up the process streams, as long as the heating profile is known. The process streams can be separated into two groups, heat sources and heat sinks. Heat sources are streams which require the removal of heat: condensing fluids, streams undergoing exothermic reactions, or streams which must be cooled from high temperature to low temperature. Heat sinks are streams which require additional heat: boiling fluids, streams undergoing endothermic reactions, or streams which must be heated from low temperature to high temperature. All of the heat transfer requirements of the process streams must be met, either by process to process heat transfer from a heat source to a heat sink, or by interactions with the utility streams. All of the heat sources can be combined into one composite heat source curve for the plant. Likewise, heat sinks can be combined into a composite heat sink curve.

3.1.3 Pinch Point

The composite heat source curve described above can be plotted on a T-$\Delta\dot{H}$ diagram along with a heat sink composite curve. A temperature potential must be maintained between the source and the sink at all locations to guarantee heat transfer from the heat source into the heat sink across a finite heat exchange area. The minimum allowable temperature potential is called the pinch temperature potential, or ΔT_{pinch}. The left side of Figure 3.4 shows a composite heat source curve and a composite heat sink curve plotted on the same T-$\Delta\dot{H}$ axes. The composite heat sink curve has been moved horizontally until the minimum temperature potential between the two curves is equal to the pinch temperature potential, $\Delta T_{min} = \Delta T_{pinch}$. This point of minimum temperature potential is called the pinch point. The pinch point for the heat source and heat sink curves shown in Figure 3.4 occurs at a heat source temperature of $T_{source} = 100\,°\text{C}$. The pinch point could be identified by the heat source temperature or the heat sink temperature at the pinch point. For this thesis, the pinch temperature, T_{pinch}, will always refer to the hot side of the pinch point, such that $T_{pinch} = T_{source}$ at the pinch point.

Once the heat sinks have been accommodated, any change in enthalpy flow rate

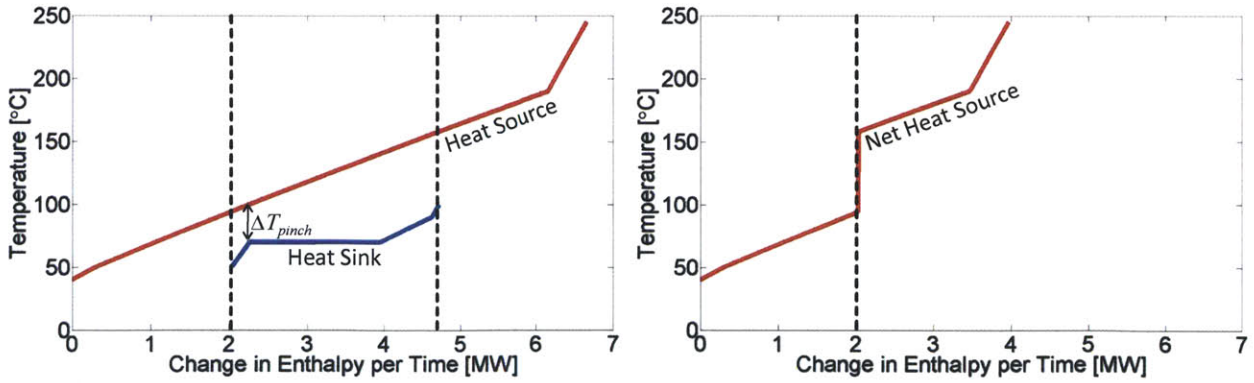

Figure 3.4: T-$\Delta\dot{H}$ diagram of composite heat source and composite heat sink pinch point. The curves are aligned such that the minimum temperature potential between the two curves is ΔT_{pinch}. The portion of the composite heat source curve which is not consumed by heat sinks is available for heating utilities.

remaining in the composite heat source curve must be absorbed by utilities. This net heat source remaining for utilities can be viewed graphically by removing the portion of the composite heat source curve which corresponds to the composite heat sink curve. In Figure 3.4, the section of the heat source curve between the dotted lines is removed, yielding the net heat source curve seen on the right side of the figure.

The BP Polygeneration Plant Model considered in this thesis has significant heat sources and very few heat sinks. Therefore, heat sinks are accounted for by allocating appropriate heat sources to them and removing those heat sources from the composite heat source curve.

3.1.4 Utility Pinch Point

Just as with the composite heat source and sink curves, there is a pinch point between the composite heat source curve and the utilities. The pinch point is defined by the minimum allowable temperature potential between the two curves, ΔT_{pinch}. The utilities are chosen to achieve the primary goal of assuring all of the necessary heat transfer for plant processes, and the secondary goal of converting heat from the composite heat source curve into shaft work. It is well established that high temperature heat can be converted into shaft work more efficiently than low temperature heat. Therefore, in the examples that follow, the utilities are designed to maximize the heat absorbed from high temperature sources before focusing on lower temperatures.

The following example illustrates the method used in this thesis for choosing the utilities. A composite heat source curve and utilities are plotted in Figure 3.5. The utilities are water at a pressure of 450 kPa. The utility curve is first moved horizontally so that the maximum change in enthalpy per time of the utility curve aligns with the maximum change in enthalpy per time of the heat source curve at $\dot{H}_{max} = 125.4\,\text{MW}$. The maximum utility temperature is then chosen so that there is a pinch point at this maximum change in enthalpy per time as indicated in the figure. This temperature constraint could be relaxed to allow

increased utilization of the heat source, but this adds complexity to the calculations and was not generally found to be advantageous for the heat sources considered in this thesis.

The black curve in Figure 3.5 represents a 1 kg/s mass flow, here denoted $\dot{m}_1$, of steam with the maximum point constrained as described above. Recall from Section 3.1.1 that increasing the mass flow of a utility stream causes the stream profile to stretch horizontally on the T-$\Delta\dot{H}$ axes. The utility mass flow is increased until either a second pinch point occurs, or the available heat source is exhausted. In this example, the second pinch point is located at the pinch point change in enthalpy per time of $\dot{H}_{pinch} = 77.9\,\text{MW}$. The mass flow of the water utility stream reaches $\dot{m}_2 = 21.2\,\text{kg/s}$. If the mass flow of the water were increased any more, the temperature potential between the heat source and the utility stream would drop below ΔT_{pinch}.

Any residual heat which is not absorbed by the utilities will be rejected to cooling water

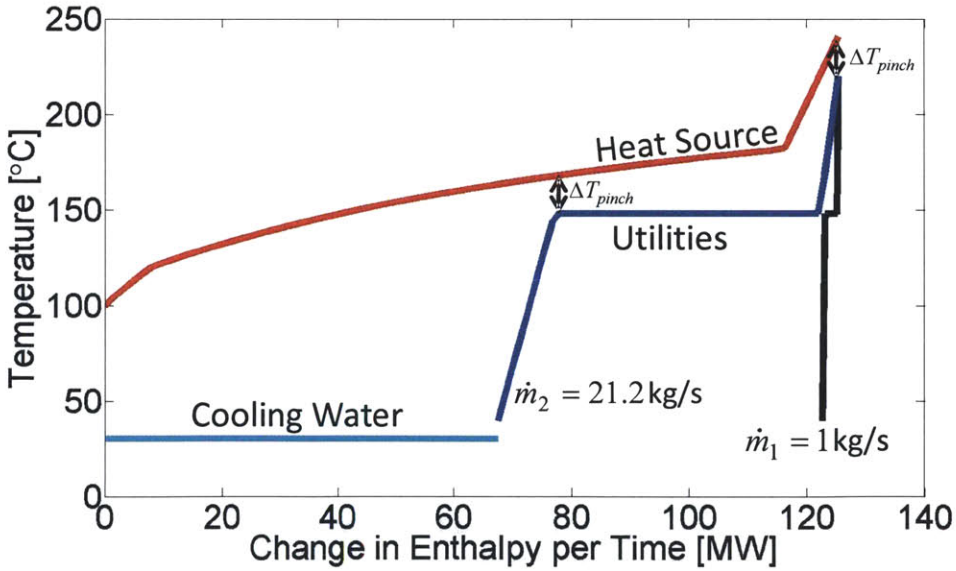

Figure 3.5: T-$\Delta\dot{H}$ plot of the pinch point for hypothetical heat source with utilities. Utilities are chosen to use high temperature heat first. The mass flow rate of the utility stream is increased until a pinch point occurs. Any left over heat rate in the heat source curve is rejected to cooling water.

and cannot be converted into shaft work. Referring to Figure 3.5, this means that 67.5 MW of the heat source for this example will not be used by the utility stream. This concept of heat source utilization will be discussed in greater depth in Section 3.4.

3.2 The Fischer Tropsch Plant as a Heat Source

In the BP polygeneration plant model, the greatest source of low grade heat is the Fischer Tropsch (FT) reactor, which produces over 300 MW of heat. Figure 3.6 is a schematic of the Fischer Tropsch plant from the BP Polygeneration Plant Model. A feed stream of synthetic gas (syngas) is preheated and then reacted in the Fischer Tropsch reactor. The FT reactor converts syngas, which is primarily CO and H_2, into longer chain hydrocarbons and light gases. The heavy hydrocarbons leaving the reactor are sent to the distillation side of the Fischer Tropsch plant for further processing into diesel and naphtha product streams. The light gases are recycled to increase the percentage of syngas that is converted into liquid fuels in the plant.

The most significant heat sources and sinks are on the reactor side of the Fischer Tropsch plant, shown in Figure 3.6, rather than on the distiller side. Three heat sources and one heat sink are considered for this analysis. The FT reactor itself produces 309 MW of heat at a

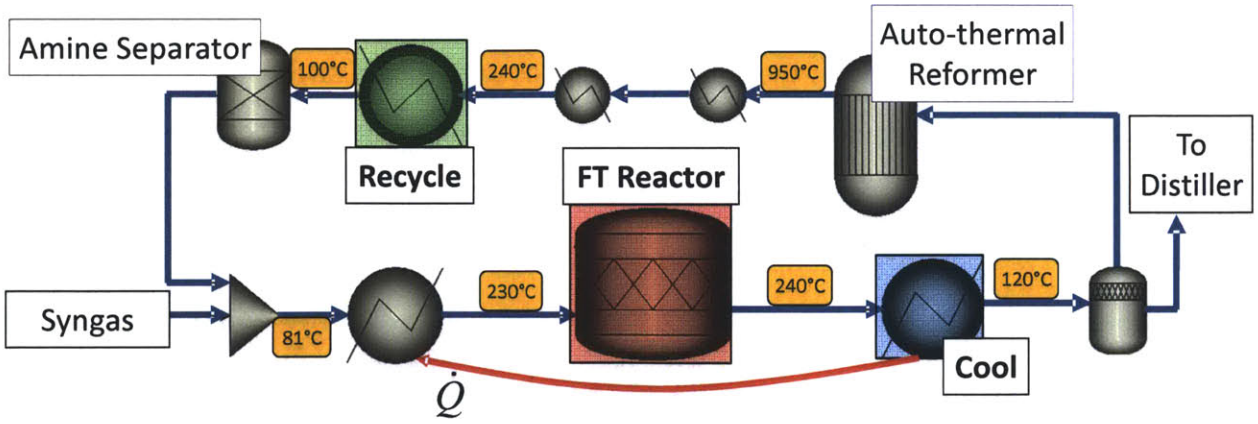

Figure 3.6: Fischer Tropsch plant schematic diagram showing three major sources of low grade heat. Blue arrows indicate the syngas and product flow path through the plant. The reactor product stream (Cool) is used to preheat the syngas entering the FT reactor.

constant temperature of 240°C. The reactor feed stream must be preheated from 81°C up to 240°C before entering the reactor, accounting for a 45 MW heat sink. The product stream exiting the reactor is cooled from 240°C down to 120°C to separate the light gases from the heavy long chain hydrocarbons. This cooling process provides 93 MW of heat. The recycle stream passes through an auto-thermal reformer, where some methane is oxidized to achieve a temperature of 950°C and break down the recycle stream into carbon monoxide, carbon dioxide, hydrogen, and steam. This recycle stream must then be cooled from 950°C down to 100°C before it passes through an amine separator that removes the carbon dioxide. As previously noted, steam Rankine cycles are inefficient at low temperatures. Therefore, the high temperature heat (>240°C) is used for steam generation, and the low temperature heat (<240°C) is available for an organic Rankine cycle. This is a convenient cut-off temperature because it matches the temperature in the FT reactor. The recycle stream cooling from 240°C down to 100°C provides an additional 71 MW of heat. Fluid states for all of these streams were calculated using the Peng-Robinson equation of state with the Boston-Mathias alpha function (PR-BM) in Aspen Plus®. The stream compositions and $T\text{-}\Delta\dot{H}$ data for these streams are listed in Appendix II.

The product stream cooling is used as a heat source to preheat the reactants entering the FT reactor. Figure 3.7 shows the $T\text{-}\Delta\dot{H}$ profiles for the product stream (red) and the feed stream (blue) with a corresponding schematic. The minimum pinch temperature potential is chosen to be $\Delta T_{pinch} = 10°C$, as previously explained in Section 2.2.1 . The hot product stream has a maximum temperature of 240°C at State 3 leaving the reactor, so it can only heat the feed stream to a temperature of $240°C - \Delta T_{pinch} = 230°C$ at State 2. The additional heat rate required to heat the feed stream from 230°C to 240°C is provided by the FT reactor.

The cold feed stream entering the reactor is superheated syngas vapor which must be preheated from 81°C at State 1 to 240°C at a constant pressure of 3.5 MPa. This feed stream has a nearly constant heat capacity rate. The hot product stream, however, contains longer

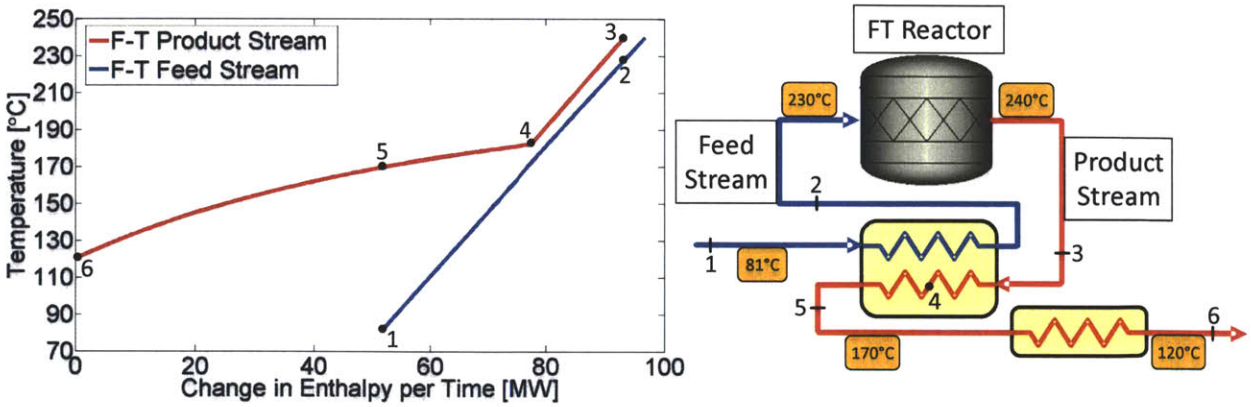

Figure 3.7: T-$\Delta\dot{H}$ plot of Fischer Tropsch reactant and product streams with schematic diagram of preheater. Before entering the FT reactor, the feed stream is preheated from State 1 to State 2 by heat transfer from the product stream as it cools from State 3 to State 5.

chain hydrocarbons and some water which begin to condense out when the stream cools below 182°C at State 4. As the heavier substances begin to condense, their latent heat is combined with the sensible heat of non-condensable gases, resulting in a greater heat capacity rate for the product stream as it cools from 182°C at State 4 down to 120°C at State 6. This effect is seen in Figure 3.7 as the slope of the product stream curve is more shallow below the temperature of 182°C than above it.

The change in heat capacity rate of the hot product stream causes this heat exchanger to be unbalanced on the cold end. Transferring heat across a large temperature gradient at low temperatures is inherently inefficient. The heat can be used more effectively if temperature drop from the product stream at State 5 to the feed stream at State 1 is reduced. This balance is achieved by reducing the mass flow rate of the hot product stream between State 4 and State 5, thereby reducing the heat capacity rate for that part of the stream.

The mass flow of the product stream can be split once the stream has been cooled to 182°C, so that below this temperature only part of the product stream mass flow is used to preheat the cold reactant stream. Figure 3.8 is a schematic of this split product stream

configuration with a corresponding T-$\Delta\dot{H}$ plot. As before, the hot product exits the reactor at State 3, with a mass flow rate of $\dot{m}_p = 117.4\,\text{kg/s}$, and passes through a heat exchanger where it preheats the cold feed stream. The product stream is cooled from State 3 to State 4, while heating the feed stream from an intermediate State 1b up to State 2. The hot product stream then splits so that only part of the hot stream mass flow rate, $\dot{m}_0$, is used to preheat the feed stream from the inlet State 1 to the intermediate State 1b. The remaining product stream mass flow rate, $\dot{m}_p - \dot{m}_0$, is cooled from State 4b to State 6 as part of the heat source for the organic Rankine cycle.

The partial hot stream mass flow, $\dot{m}_0$, necessary to preheat the feed stream from State 1 to State 1b is found using:

$$\dot{m}_0 = \dot{m}_p \cdot \frac{\Delta\dot{H}_{1,1b}}{\Delta\dot{H}_{4,6}} \tag{26}$$

where $\Delta\dot{H}_{1,1b}$ is the required cold stream change in enthalpy per time from State 1 to State 1b, and $\Delta\dot{H}_{4,6}$ is the available hot stream change in enthalpy per time as the stream cools from State 4 to State 6. The values $\Delta\dot{H}_{1,1b} = 25.7\,\text{MW}$ and $\Delta\dot{H}_{4,6} = 77.3\,\text{MW}$ can be seen graphically in Figure 3.8. Equation (26) results in a necessary preheating mass flow of $\dot{m}_0 = 39.0\,\text{kg/s}$.

The T-$\Delta\dot{H}$ for the product stream without the split mass flow, which was originally presented in Figure 3.7, is also plotted in Figure 3.8 (red) so that the two configurations can be easily compared. In both configurations, the heat rate to the left of feed stream State 1 is not needed for preheating the feed stream, and is available for an organic Rankine cycle. The split stream configuration does not change magnitude of this heat rate that is available for the ORC, but it increases the temperature at which that heat rate is available. The split product stream, cooling from State 4b to State 6 in Figure 3.8, is at a higher temperature than the configuration with no split, plotted in red.

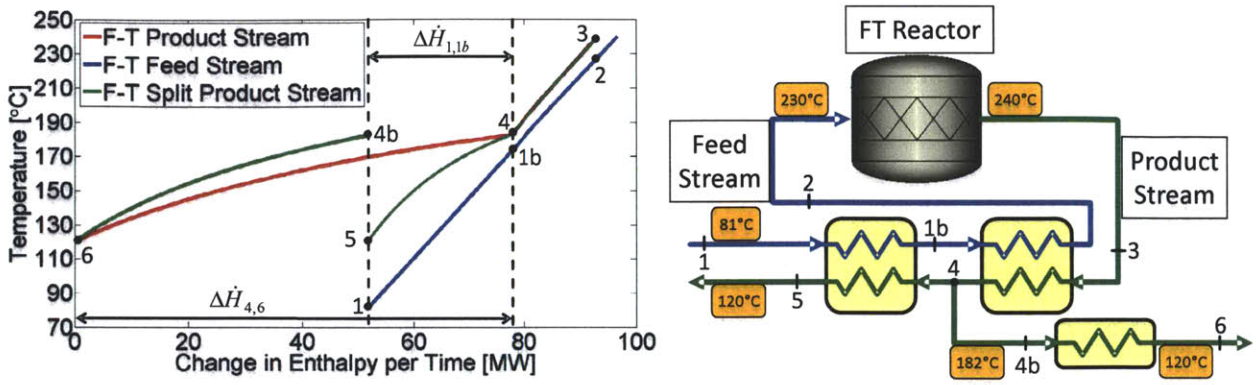

Figure 3.8: T-$\Delta\dot{H}$ plot of the FT reactor feed stream and split reactor product stream with schematic diagram of split preheater. The FT reactor product stream (green) is used to preheat the feed stream (blue). When the product stream cools to 182°C at State 4, some constituents begin to condense out, causing an increased heat capacity rate. Thus, product stream is split once it cools to 182°C, so that only a fraction of the mass flow is used for preheating at colder temperatures. This configuration increases the temperature of the extra heat rate which is available for use in an ORC as the stream is cooled from State 4b to State 6.

With the syngas preheating thus accounted for, the Fischer Tropsch plant heat source is composed of the three heat sources previously described: the FT Reactor, the split product

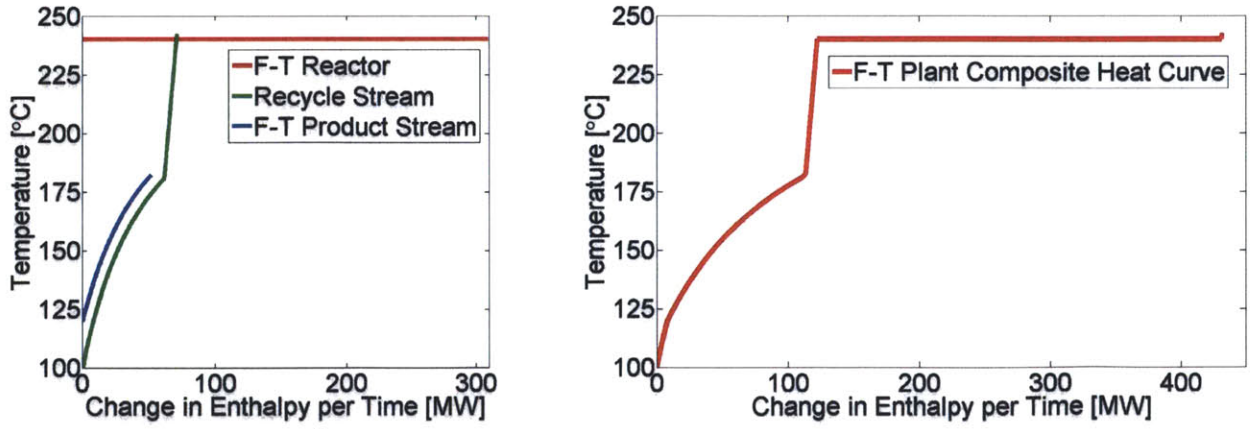

Figure 3.9: T-$\Delta\dot{H}$ plot of three heat streams in the Fischer Tropsch plant (left) that are combined into one composite heat curve (right). Change in enthalpy per time is summed at every temperature.

stream, and the recycle stream. The T-$\Delta\dot{H}$ curves for these three streams are plotted on the left side of Figure 3.9 below. The enthalpies of these three streams are combined, yielding the composite heat curve plotted right side of Figure 3.9. This composite heat curve for the Fischer Tropsch plant will be the targeted heating profile for customized organic Rankine cycles. The Fischer Tropsch composite heat source provides a total heat transfer rate of $\dot{Q}_{source} = 431.8\,\text{MW}$ over a temperature range from 100°C up to 240°C.

3.3 Heat Source Matching

The Fischer Tropsch plant composite heating curve is used as the heat source for a Rankine style heat engine. In the analysis that follows, the heat sink for this heat engine is assumed to be cooling water maintained at a constant temperature of $T_{sink} = 30°\text{C}$. Heat transfer across a temperature gradient generates entropy, thereby reducing the efficiency of the heat engine. Thus, an ideal cycle has a working fluid heat requirement identical to the heat source. A practical cycle, however, requires a temperature difference between the heat source and working fluid so that heat transfer occurs over a finite area. For this analysis, the minimum temperature potential in the Rankine cycle heat exchangers is $\Delta T_{pinch} = 10°\text{C}$. Given this pinch temperature constraint, the best possible cycle configuration has a working fluid heat requirement such that the temperature of the working fluid, T_{wf}, is 10°C colder than heat source temperature, T_{source}, along the entire T-$\Delta\dot{H}$ curve:

$$T_{wf} = T_{source} - \Delta T_{pinch} \quad . \tag{27}$$

Figure 3.10 shows the T-$\Delta\dot{H}$ profile of the FT heat source in red, as well as the cycle heat requirement for a low pressure (LP) steam Rankine cycle. This is the same baseline steam Rankine cycle defined in Section 2.2.1, and the state points for this cycle are included in Appendix I. A hypothetical "best cycle" is also plotted, which maintains a constant temperature

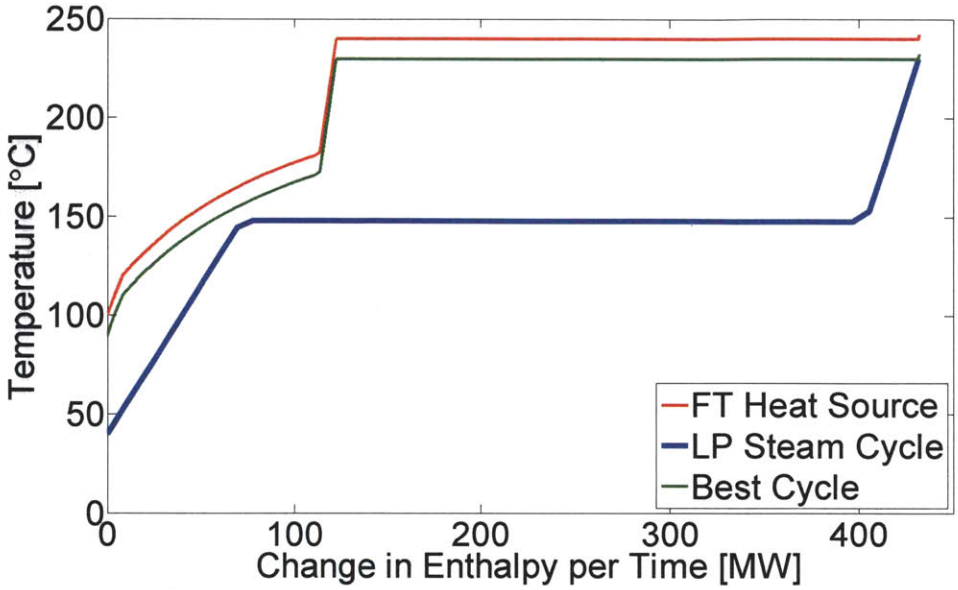

Figure 3.10: T-$\Delta\dot{H}$ plot of the Fischer Tropsch composite heating curve with two potential cycle heating profiles. A low pressure steam Rankine cycle heat curve with large ΔT resulting in significant entropy generation, and an "best cycle" heat curve with the smallest feasible ΔT thereby limiting entropy generation.

difference of ΔT_{pinch} between the heat source and the working fluid. There is significant room for improvement from the LP steam cycle to the best cycle.

3.4 ORC Building Blocks

There is an efficiency advantage to be gained by matching the heat requirement of a thermodynamic cycle with the available heat source. Therefore, a set of cycle manipulations which alter the heating profile of organic Rankine cycles have been investigated. A methodology is proposed for using these various cycle manipulations as building blocks to create an organic Rankine cycle with a working fluid heat requirement that matches any available heat source, thus maximizing the conversion efficiency of the ORC.

In Chapter 2, cycles were analyzed on a per unit mass basis. For this present analysis, a known heat source provides a total heat transfer rate, $\dot{Q}_{source}$, as an input to the

thermodynamic cycle. Therefore, the cycle must be analyzed on a flow rate basis. This requires multiplying specific properties and specific thermodynamic interactions by a working fluid mass flow rate, $\dot{m}_{wf}$. Equations (8) through (12) from Section 2.2.1, which define important cycle characteristics, are reproduced here:

$$\text{Expander Specific Work} = w_{exp} = (h_5 - h_6) * (1 - Y_{avg}) \tag{8}$$

$$\text{Pump Specific Work} = w_{pump} = h_1 - h_2 \tag{9}$$

$$\text{Cycle Net Specific Work} = w_{net} = w_{exp} + w_{pump} \tag{10}$$

$$\text{Specific Heat Transfer In} = q_{in} = h_5 - h_2 \tag{11}$$

$$\text{Cycle Efficiency} = \eta_{cyc} = \frac{w_{net}}{q_{in}} \quad . \tag{12}$$

The variables w and q are thermodynamic interactions, specific work and specific heat transfer, respectively. The average wetness, Y_{avg}, is zero for the dry fluids used for organic

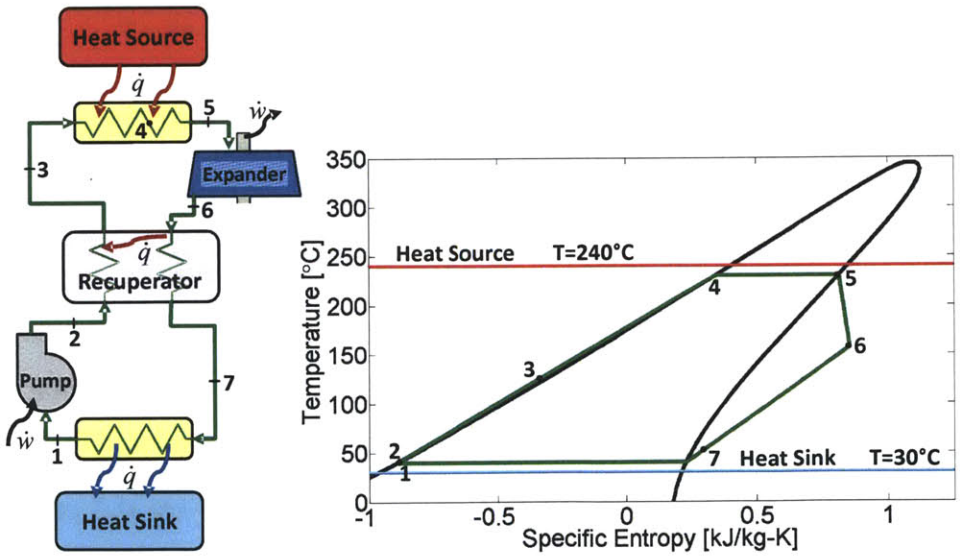

Figure 3.11: Duplicate of Figure 2.3. Schematic diagram and *T-s* plot of a baseline organic Rankine cycle with recuperator.

Rankine cycles. The variable h represents the fluid property specific enthalpy. The numbered subscripts refer to fluid cycle states, as shown in Figure 3.11. The cycle characteristics defined on a flow rate basis, then, become:

$$\text{Expander Work Output Rate} = \dot{W}_{exp} = \dot{m}_{wf} * w_{exp} \tag{28}$$

$$\text{Pump Work Input Rate} = \dot{W}_{pump} = \dot{m}_{wf} * w_{pump} \tag{29}$$

$$\text{Cycle Net Work Rate} = \dot{W}_{net} = \dot{W}_{exp} + \dot{W}_{pump} \tag{30}$$

$$\text{Heat Transfer Rate In} = \dot{Q}_{in} = \dot{m}_{wf} * q_{in} \tag{31}$$

$$\text{Cycle Efficiency } \eta_{cyc} = \frac{\dot{W}_{net}}{\dot{Q}_{in}} = \frac{w_{net}}{q_{in}} \quad . \tag{32}$$

The heat transfer rate into the cycle, $\dot{Q}_{in}$, will be less than the heat transfer rate available from the source, $\dot{Q}_{source}$, if the cycle is limited by a pinch point. A variable called heat source utilization, U_{cyc}, is defined here as the fraction of the available heat rate that is actually transferred into the cycle:

$$U_{cyc} = \frac{\dot{Q}_{in}}{\dot{Q}_{source}} \quad . \tag{33}$$

A second type of efficiency, called the thermodynamic conversion efficiency, η_{conv}, is now defined as the efficiency of the cycle in converting the heat rate available from the heat source into power:

$$\eta_{conv} = \frac{\dot{W}_{net}}{\dot{Q}_{source}} \quad . \tag{34}$$

Combining Equations (31) through (34), the relationship between cycle efficiency, conversion efficiency, and cycle heat utilization can be shown to be:

$$\eta_{conv} = \eta_{cyc} * U_{cyc} \quad . \tag{35}$$

The goal of designing a cycle is to maximize the work output which can be achieved from a given heat source, so the thermodynamic conversion efficiency, η_{conv}, is the primary metric for comparing cycle configurations. The Fischer Tropsch plant heat source described in Section 3.2 is used to demonstrate the effect of each cycle building block on conversion efficiency. For the FT plant, the total available heat rate is $\dot{Q}_{source} = 431.8$ MW .

Each cycle configuration is demonstrated by using the example of alkanes ranging in size from hexane to decane as the working fluid. Alkanes have the desirable physical qualities of organics described in Section 2.3.1, and fluid thermodynamic data for these alkanes is readily available in NIST Refprop 8.0 (Lemmon, Huber, & McLinden, 2007).

The conversion efficiency of the cycle shown in Figure 2.3 above can be determined using pinch analysis methods with the Fischer Tropsch plant as a heat source. Figure 3.12 shows the working fluid heat requirement for alkanes plotted on a T-$\Delta\dot{H}$ graph along with the FT heat source profile.

Due to the large heat supply at 240°C from the FT reactor, all of the ORC's are chosen such that the constant temperature boiling occurs at $T_{sat} = 240°C - \Delta T_{pinch}$. This creates a pinch point at the maximum heat source enthalpy, as described in Section 3.1.4. The mass flow of the cycle is then adjusted until a second pinch point occurs or the FT heat source is exhausted (100% heat source utilization).

Figure 3.12 shows competing trends as the working fluid progresses from lightest (hexane) to heaviest (decane). The heavier alkanes match the FT heat source profile more closely than the lighter alkanes. However, due to the pinch point, the heat source utilization decreases as the working fluid choice proceeds from light to heavy. The conversion efficiency is a product of these two effects, and turns out to be highest for nonane. The baseline steam cycle heat requirement curve is also included for comparison. The organic Rankine cycles

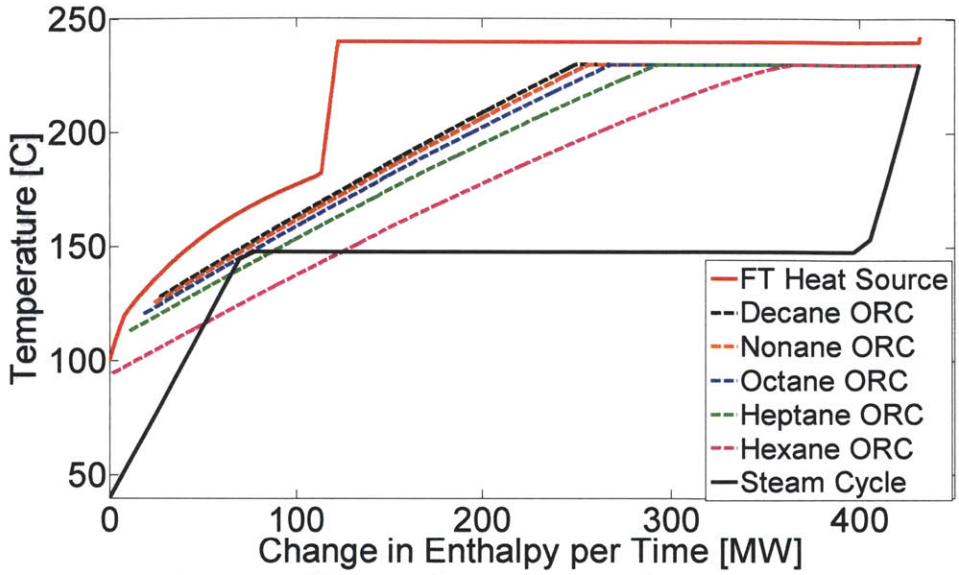

Figure 3.12: ORC heating profile using alkanes as working fluids, plotted with the FT heat source profile. The larger alkanes (such as decane) more closely match the heat source, but are limited by the pinch point to lower heat source utilization. The baseline steam Rankine cycle is also included, but it has poor heat source matching.

achieve much better heat source matching than the steam Rankine cycle.

The organic Rankine cycles plotted in Figure 3.12 use the simplest practical cycle configuration for an ORC using a dry working fluid. This cycle configuration consists of a pump, a heat source, an expander, a recuperator, and a condenser as described previously and shown

Table 12: Cycle characteristics for baseline cycles with alkane working fluids and steam.

Cycle	Baseline ORC	Baseline ORC	Baseline ORC	Baseline ORC	Baseline ORC	Baseline Rankine Cycle
Working Fluid	Hexane	Heptane	Octane	Nonane	Decane	Steam
T_{pinch} [°C]	104.0	122.9	130.6	135.3	137.9	N/A
$\dot{m}_{wf}$ [kg/s]	846.4	808.3	787.0	776.9	771.6	156.6
$\dot{W}_{net}$ [MW]	113.0	118.6	119.4	119.5	119.4	88.8
η_{cyc}	26.3%	28.2%	28.9%	29.3%	29.5%	20.6%
U_{cyc}	99.6%	97.5%	95.7%	94.5%	93.8%	100%
η_{conv}	26.2%	27.5%	27.7%	27.7%	27.7%	20.6%

above in Figure 3.11, and will be called the baseline cycle. Each cycle modification will be compared to this baseline cycle. Recall that T_{pinch} has been defined as the heat source temperature at the pinch point. Table 12 contains cycle characteristics for the baseline cycle with each alkane working fluid.

3.4.1 Recuperator

The concept of integrating a recuperator into an organic Rankine cycle was introduced when the ORC was still a fledgling technology (Tabor & Bronicki, 1962). The recuperator takes advantage of the elevated temperature at the expander exit and transfers heat from the superheated low pressure expander exit stream into the subcooled high pressure liquid stream on the other side of the cycle. The inclusion of a recuperator reduces the heating requirement for the cycle, as seen in Figure 3.13. The blue curve is the heat requirement per unit mass for a

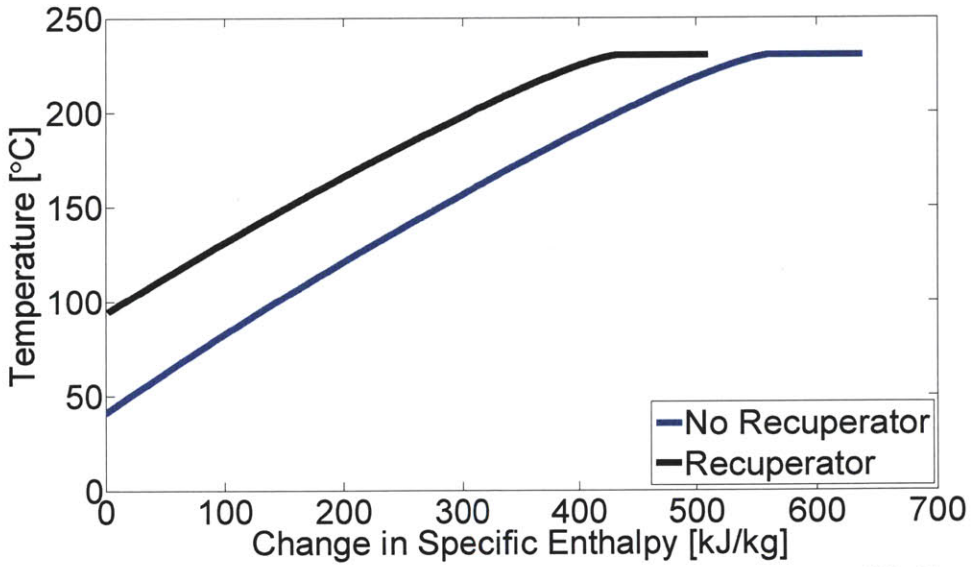

Figure 3.13: T-Δh plot of hexane ORC heat requirement with recuperator (black) and without recuperator (blue). Adding a recuperator reduces the heat requirement for this hexane ORC by 129.4 kJ/kg. All heat input below 94°C is supplied in the recuperator. The recuperator reduces the heat input required to operate a cycle without changing the work output, thereby improving efficiency.

hexane cycle with a maximum temperature of 230°C and a minimum temperature of 40°C with no recuperator. The black curve is the heat requirement per unit mass for the baseline hexane ORC, which includes a recuperator. In the baseline hexane cycle 129.4 kJ/kg of specific heat is recuperated, reducing the required heat input for the cycle by 20%. For the example pictured above, the recuperator negates the cycle heat requirement up to a temperature of 94°C.

3.4.2 Split Stream Recuperator

The standard recuperator described above is an unbalanced heat exchanger in which the heat capacity rate of the hot vapor stream, $\dot{m}_{wf} \cdot c_p$, is much lower than the heat capacity rate of the cold liquid stream. The right side of Figure 3.14 includes a plot of the two streams for a standard recuperator in the T-$\Delta\dot{H}$ plane. The hot stream (red) and the cold stream (blue) have different slopes. The recuperator provides a heat rate for preheating the cold liquid stream. This heat rate cannot be easily altered, but the temperature at which the cold liquid absorbs this heat rate can be changed. If the temperature achieved by preheating the cold liquid in the recuperator is increased, then the temperature requirement for cycle heat source is comparably decreased without affecting the total heat rate required for the cycle heat source.

The maximum possible preheat temperature in the recuperator is achieved by balancing the recuperator heat exchanger. To balance the recuperator, the mass flow is reduced on the cold side of the heat exchanger until the heat capacity rates are the same for the hot and cold streams. This reduction in mass flow is achieved by diverting a fraction of the subcooled liquid stream, as indicated in the schematic on the left side of Figure 3.14. Part of the stream can be routed directly to the heat source, while an appropriate mass flow is passed through the recuperator. The result of this modification is that the hot stream (red) and the split cold stream (green) have the same slope, and the cold stream exit temperature at State 3 is as hot as possible.

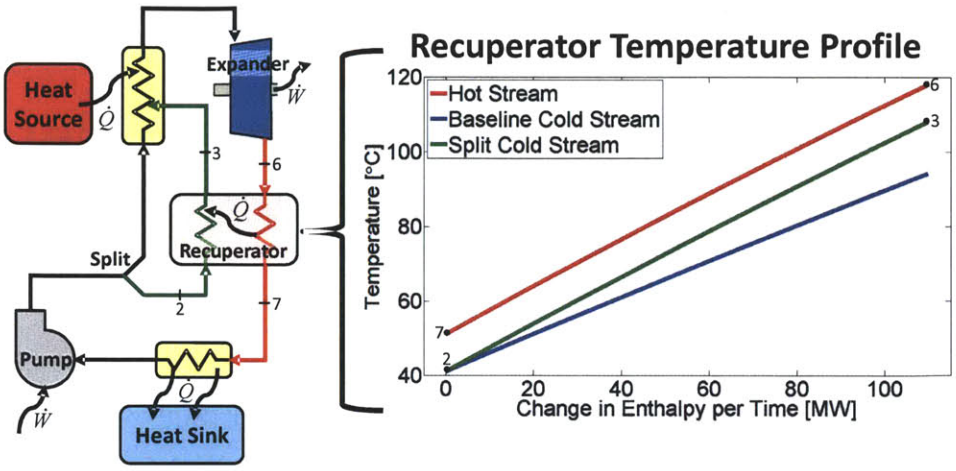

Figure 3.14: Schematic diagram and T-$\Delta\dot{H}$ plot of a split recuperator. The standard straight through recuperator is an unbalanced counter flow heat exchanger (red curve to blue curve on the right). On the cold end of the recuperator, the temperatures approach the pinch temperature potential, ΔT_{pinch}. Towards the hot end of the recuperator, the temperatures diverge. The split recuperator (red curve to green curve) is a balanced heat exchanger that achieves the highest possible preheating temperature as the cold liquid leaves the recuperator at State 3. This high temperature from the recuperator reduces the heat source temperature requirement without affecting the heat rate requirement.

The split cold stream mass flow rate is calculated by first defining the inlet and exit temperatures for both recuperator streams. In an organic Rankine cycle, the hot stream inlet temperature, $T_{hot,in}$, is the expander exit temperature, State 6 in Figure 3.14. The cold stream inlet temperature, $T_{cold,in}$, is the pump exit temperature, State 2 in Figure 3.14. The recuperator exit temperatures are set according to the allowable temperature pinch, ΔT_{pinch}, such that $T_{cold,out} = T_{hot,in} - \Delta T_{pinch}$ (State 3) and $T_{hot,out} = T_{cold,in} + \Delta T_{pinch}$ (State 7). With the inlet and exit states now defined for the hot stream and the cold stream, the pure substance model is used to determine the change in specific enthalpy, Δh, that each stream undergoes in the balanced recuperator. The cold stream mass flow necessary to balance the recuperator can be calculated using an energy balance around the split recuperator, resulting in the relation:

$$\dot{m}_{cold} = \dot{m}_{hot} * \left(\frac{\Delta h_{hot}}{\Delta h_{cold}} \right) \quad . \tag{36}$$

It is important to realize that the second law of thermodynamics must apply not only at the boundary of the recuperator, but at every point inside the recuperator. This can be checked graphically by plotting the recuperator streams on a Temperature vs. Change in Enthalpy per Time graph, as seen above in Figure 3.14. At all values of $\Delta \dot{H}$, the hot stream must locally be at a higher temperature than that of the cold stream. In other words, heat cannot be transferred up the temperature gradient, as that would destroy entropy and be a violation of the second law of thermodynamics. Also, the temperature difference between the two streams must always exceed the predefined pinch temperature difference, ΔT_{pinch}. If the heat exchanger were to pinch internally, the area required to transfer heat from one stream to the other would increase prohibitively. For the hexane split recuperator represented in Figure 3.14, and similarly with most organics at these temperatures, there is no internal first or second law violation in the recuperator.

Figure 3.15 demonstrates the effect of the split recuperator on the working fluid heat requirement. The total heat required to run the organic Rankine cycle remains the same as the baseline case with a straight through recuperator, but the temperature necessary to provide that heat rate is lower at the cold end, making it easier to use low grade heat sources effectively.

The cycle efficiency, η_{cyc}, is identical for a baseline cycle with a straight through recuperator and a cycle with a split recuperator. However, for some heat sources the split recuperator may move the pinch point and increase the heat source utilization, thereby improving the cycle conversion efficiency, η_{conv}. Figure 3.16 illustrates this concept for two examples of cycles with split recuperators. On the left is the FT heat source curve plotted with two hexane cycles: the baseline hexane cycle, and the split recuperator hexane cycle. The baseline cycle already has 99.6% heat source utilization, so splitting the recuperator flow yields

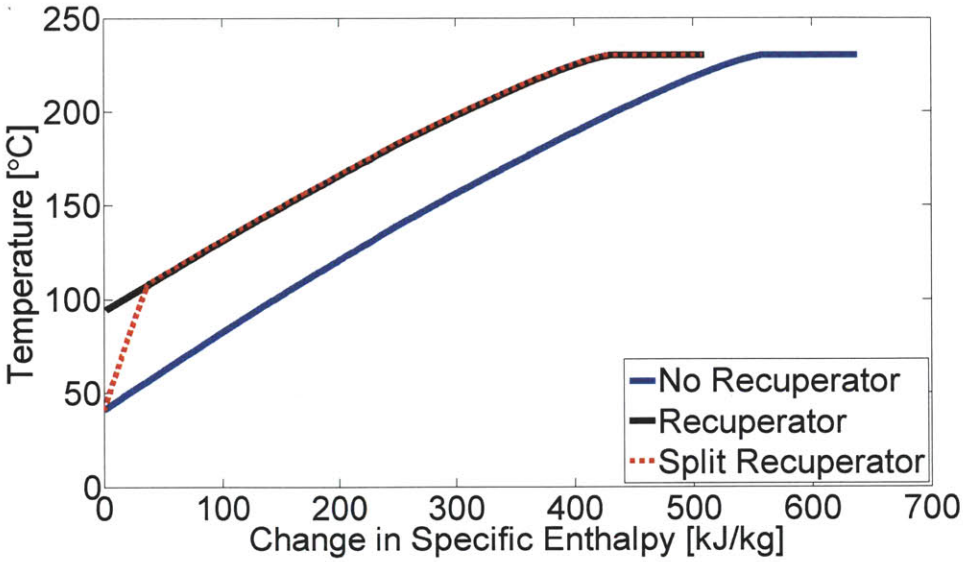

Figure 3.15: Hexane ORC heating profiles with no recuperator, recuperator (baseline case), and split recuperator. The split recuperator heating profile requires the same heat rate as the baseline case, but at lower temperatures.

only a small improvement. On the right side of Figure 3.16 the FT heat source curve is plotted with two decane cycles: the baseline decane cycle and the split recuperator decane cycle. The

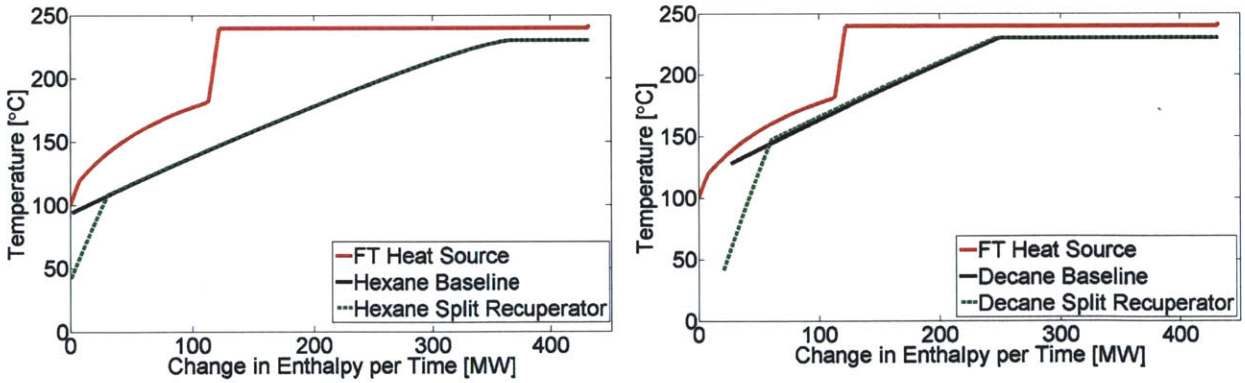

Figure 3.16: ORC heat requirement curves for split recuperator examples using hexane (left) and decane (right) with the Fischer Tropsch heat source, shown in red. The effect of splitting the recuperator is almost imperceptible for hexane compared to the baseline cycle (left) but has a clear advantage for decane (right) where the pinch point moves resulting in increased heat source utilization.

Table 13: Cycle characteristics showing the effect of a split recuperator stream with hexane and decane as working fluids for organic Rankine cycles.

Cycle	Baseline ORC	Split Recuperator	Baseline ORC	Split Recuperator
Working Fluid	Hexane	Hexane	Decane	Decane
T_{pinch} [°C]	104.0	N/A	138.0	157.4
$\dot{m}_{wf}$ [kg/s]	846.4	849.1	771.5	784.2
$\dot{W}_{net}$ [MW]	113.0	113.3	119.4	121.4
η_{cyc}	26.3%	26.3%	29.5%	29.5%
U_{cyc}	99.6%	100%	93.8%	95.3%
η_{conv}	26.2%	26.3%	27.7%	28.1%

baseline decane cycle has only 93.8% heat source utilization due to a pinch point at the cold end of the working fluid heating curve. Splitting the recuperator moves that pinch point and improves the heat source utilization to 95.3%. There is a clear advantage to using a split recuperator for this decane case.

Cycle characteristics for the four cases picture in Figure 3.16 are listed in Table 13. Using the split recuperator, there is no limiting pinch point at the cold end of the hexane cycle, so it achieves 100% heat source utilization. As more complex cycle configurations are introduced, there will be scenarios where a split recuperator has a dramatic effect.

3.4.3 Multiple Pressure Levels

The baseline organic Rankine cycle operates as a single loop with isobaric heating at high pressure and isobaric cooling at low pressure. One means of changing the cycle heat requirement is to include heating at additional pressure levels in the cycle. Figure 3.17 is a schematic of a two pressure configuration with the accompanying fluid states labeled on a T-s diagram. After exiting the condenser at State 1, the working fluid is split into two streams. Stream 1, indicated by the dark green path, is pumped to high pressure. Stream 2, indicated by the light green path, is pumped to low pressure. The high pressure (HP) and low pressure loops (LP) then proceed individually as baseline Rankine cycles through recuperating, preheating,

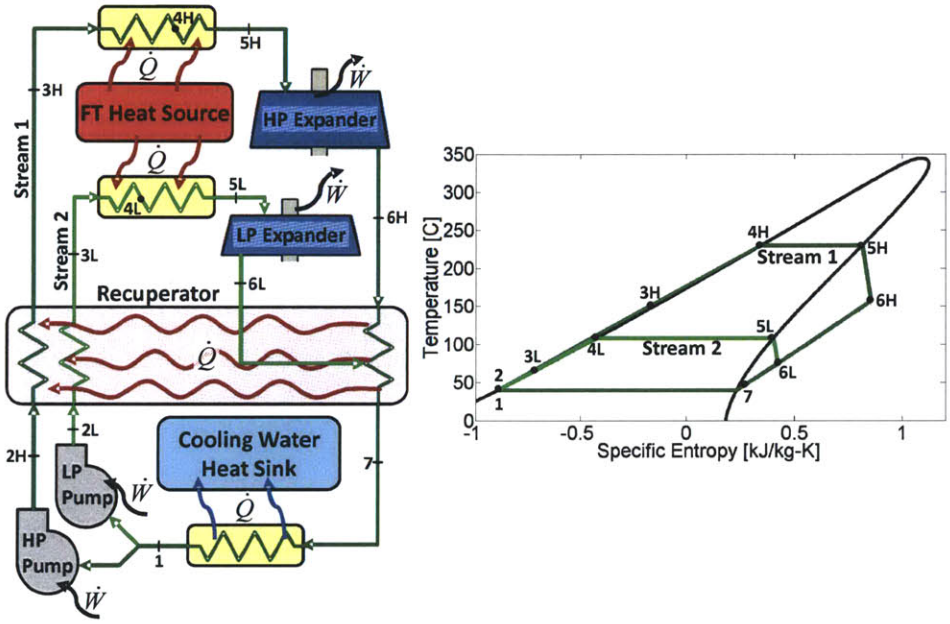

Figure 3.17: Schematic and *T-s* diagram of ORC with additional pressure levels. Heat transfer into the cycle occurs along two isobars in this example: at high pressure from State 3H to State 5H, and at low pressure from State 3L to State 5L. The high pressure loop and the low pressure loop are combined in the recuperator.

boiling, and expanding. The streams are expanded to the same expander exit pressure, $P_{6H} = P_{6L} = P_{low}$. The expander exit temperature for Stream 1, T_{6H}, is greater than the expander exit temperature for Stream 2, T_{6L}. Therefore, Stream 1 passes directly from the expander exit at State 6H into the recuperator. Inside the recuperator, Stream 1 is cooled to the temperature T_{6L}, at which point Stream 2 is introduced and the two streams mix at the same temperature and pressure so as to minimize mixing losses. Finally, the combined stream is cooled and then condensed, and any heat which was not recuperated is rejected to cooling water.

To perform a pinch analysis on the dual pressure level system, a composite curve is formed by combining the heat requirements of the two streams. Figure 3.18 is a plot of the specific heat requirement for each loop, and the result of combining those specific heat requirements into one composite curve. For this example here, the temperature requirements

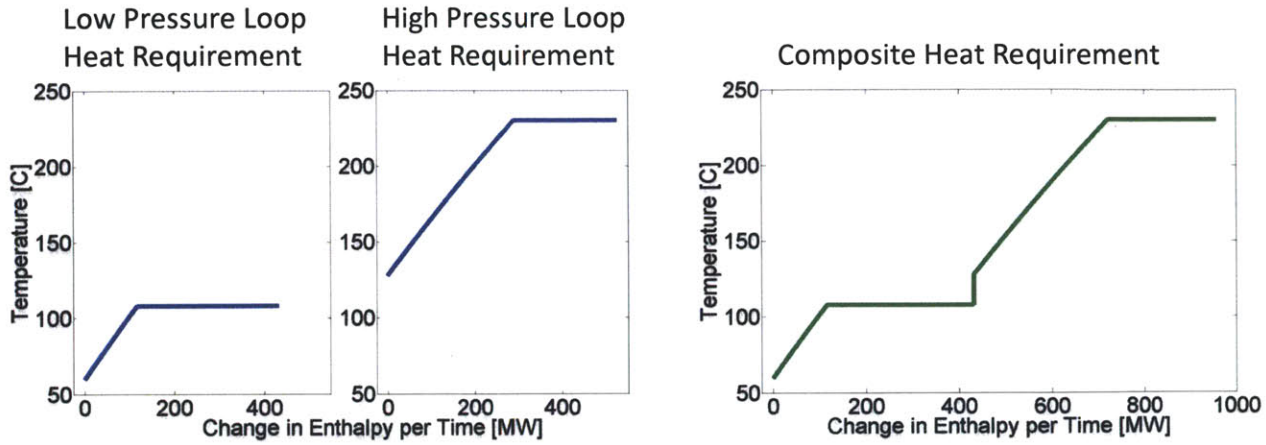

Figure 3.18: The heating profile for the low pressure loop (left) and the high pressure loop (center) are combined into one composite heat requirement profile for the cycle (right).

for the LP loop and the HP loop do not overlap. This results in a temperature gap from 108°C up to 128°C where no heat is absorbed. This gap is a result of the pressure levels that have been chosen for this example, and may not exist in other cases. The mass flow rate for each loop shown in each loop is 1 kg/s in Figure 3.14, but the mass flow rates of the loops will be adjusted individually during the pinch analysis.

As described previously, the baseline ORC has two adjustable parameters available to the designer: pressure level and mass flow rate. These two parameters allow the designer to satisfy two system constraints: a pinch point at the maximum enthalpy per time of the FT heat source curve, and a second pinch point at a lower temperature. It is standard pinch analysis practice to maximize the mass flow of higher pressure streams before considering lower pressure streams, because high pressure streams are generally less expensive than lower pressure streams per unit work output (Shenoy, Sinha, & Bandyopadhyay, 1998).

Each new pressure loop provides two additional degrees of freedom for the cycle designer. The high pressure loop mass flow is maximized first, so that the baseline heat requirement and the two pressure level heat requirement overlap at higher temperatures. The

LP loop pressure level and mass flow are chosen to cause a second pinch point and 100% heat source utilization.

Changing the pressure level of the LP loop moves the saturation temperature for that loop, thus changing the plateau at which boiling occurs. Changing the mass flow of the LP loop stretches the LP heating curve horizontally without changing the HP heating curve. In the two pressure example, the pressure and mass flow of the low pressure loop are chosen achieve full heat source utilization and to reach a second pinch point, matching the heat source profile as closely as possible. The choice of pressure level changes the cycle specific heat requirement thereby changing the mass flow necessary to exhaust the heat source. The choice of mass flow stretches the heating curve horizontally, thereby moving the pinch point. This interdependence of variables makes the pressure level and mass flow selection an iterative process. Figure 3.19

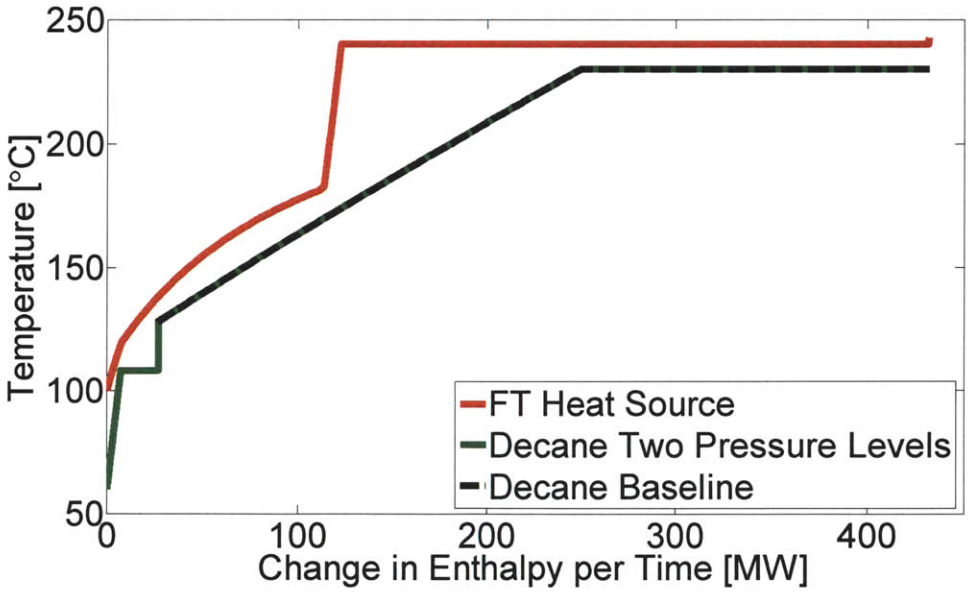

Figure 3.19: Pinch analysis results for a decane ORC with two pressure levels using the FT heat source, with the baseline cycle shown for comparison. The second pressure level allows the cycle to achieve 100% heat source utilization. The high pressure mass flow is maximized first, so the hot end of the cycle heating profile is identical to the baseline cycle heating profile.

Table 14: Cycle characteristics showing the effect of an additional pressure level with decane as the working fluid for organic Rankine cycles.

Cycle	Baseline ORC	Two Pressures
Working Fluid	Decane	Decane
T_{pinch} [°C]	138.0	138.0
$T_{pinch,2}$ [°C]	N/A	118.0
$\dot{m}_{wf,HP}$ [kg/s]	771.5	771.5
$\dot{m}_{wf,LP}$ [kg/s]	N/A	61.9
$\dot{W}_{net}$ [MW]	119.4	123.3
η_{cyc}	29.5%	28.6%
U_{cyc}	93.8%	100%
η_{conv}	27.7%	28.6%

is a plot of the results of a pinch analysis performed on the cycle with two pressure levels. The baseline cycle is also included for comparison.

Table 14 contains cycle characteristic data comparing the cycle with two pressure levels to the baseline cycle with decane. In order to calculate a net work rate, $\dot{W}_{net}$, the work outputs of the high and low pressure turbines as well as the work outputs of the high and low pressure pumps are summed, such that Equation (30) becomes:

$$\dot{W}_{net} = \sum \dot{W}_{exp} + \sum \dot{W}_{pump} \quad . \tag{37}$$

The second pressure level is particularly advantageous in that is allows the cycle to achieve 100% heat source utilization. However, this additional efficiency comes at the cost of significant complexity and equipment.

3.4.4 Reheat Stages

The baseline ORC has isobaric heating before a single stage expander. Another building block that can be employed to alter the cycle heating requirements is the inclusion of reheat stages. Reheat stages are commonly added to thermodynamic cycles as a means of increasing

the average temperature at which heat is transferred into the working fluid, thus making the cycle more efficient.

Figure 3.20 is a schematic of an ORC with one reheat stage, as well as the accompanying fluid states on a T-s diagram. Just as with the baseline cycle, a saturated liquid at State 1 is pumped to a high pressure (State 2) and then heated in the recuperator to State 3b before being preheated and boiled by heat transfer from the heat source. State 3 is included as a reminder of the recuperator exit state in the baseline case. Recall that the baseline cycle has isobaric heating at pressure P_{high} and isobaric cooling at pressure P_{low}. When a reheat stage is added, the saturated liquid at State 5 is expanded to an intermediate pressure, P6a, such that

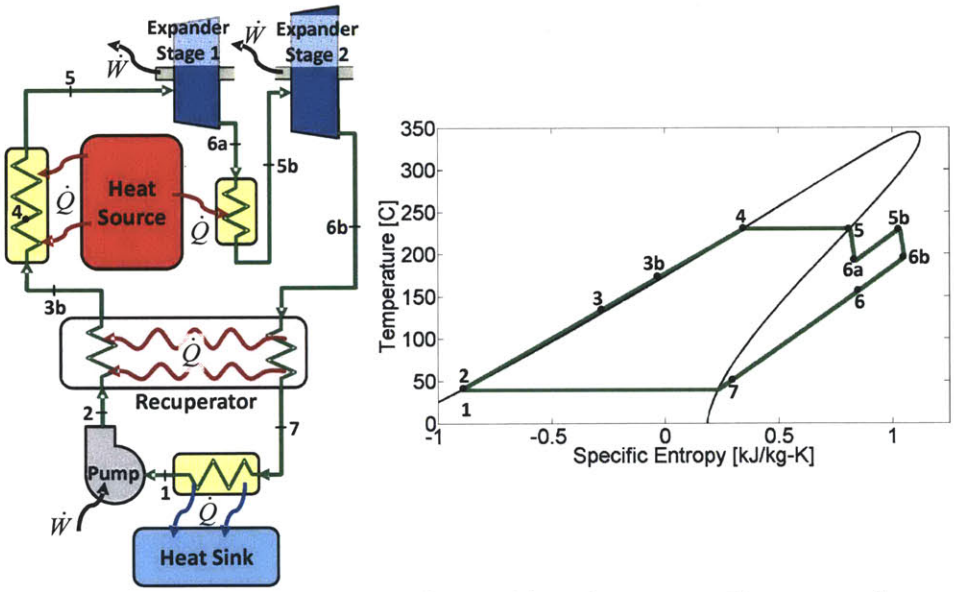

Figure 3.20: Schematic and T-s diagram of ORC with a reheat stage. The saturated vapor at State 5 is expanded to an intermediate pressure at State 6a, then heat is transferred into the working fluid to bring it back up to maximum temperature before expansion is completed. The expander exit state from the baseline ORC (State 6) is at lower temperature than the expander exit state with a reheat stage (State 6b). Thus, the cold stream exits the recuperator at a higher temperature when there is reheat (State 3b) than in the baseline case (State 3).

$P_{high} > P_{6a} > P_{low}$. The stream is then reheated at constant pressure by a heat transfer from the heat source to State 5b, such that $T_{5b} = T_{5a}$ and $P_{5b} = P_{6a}$. Finally, the working fluid is expanded from State 5b to State 6b, where $P_{6b} = P_{low}$. For reference, State 6 is plotted on the T-s diagram. State 6 would be the expander exit state if there were no reheat stages.

A reheat stage changes the cycle heating profile in two ways. Additional heat transfer occurs at the hot end of the cycle from T_{6a} to T_{5b}. Also, additional recuperation is available from T_{6b} down to T_6. To fully define State 6a, the intermediate pressure P6a must be chosen. It is informative to think about the expander stages in terms of their pressure ratios. Across all of the expander stages, the working fluid is expanded from P_{high} to P_{low}. The overall pressure ratio, PR_{tot}, is then defined as:

$$PR_{tot} = \frac{P_{high}}{P_{low}} \quad . \tag{38}$$

In the case with a single reheat stage, the expander is divided into 2 stages. The pressure ratio of the first stage, PR_a, is defined as:

$$PR_a = \frac{P_5}{P_{6a}} = \frac{P_{high}}{P_{6a}} \tag{39}$$

while the pressure ratio of the second stage, PR_b, is similarly defined as:

$$PR_b = \frac{P_{5b}}{P_{6b}} = \frac{P_{5b}}{P_{low}} \quad . \tag{40}$$

Recalling that $P_{6a} = P_{5b}$, Equations (38) through (40) can be combined to yield the relationship between the overall pressure ratio, PR_{tot}, and the pressure ratios of the individual stages:

$$PR_{tot} = PR_a * PR_b \quad . \tag{41}$$

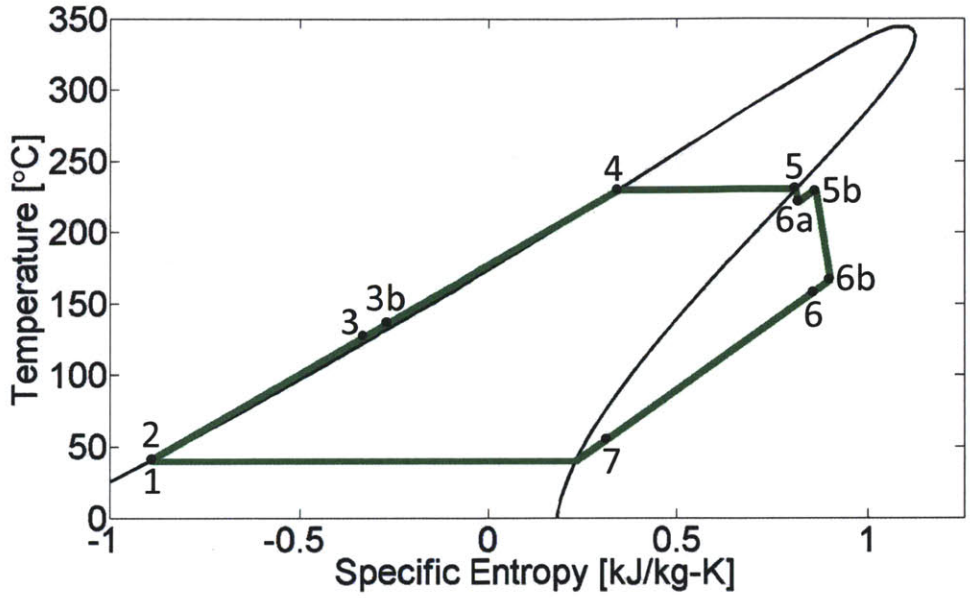

Figure 3.21: *T-s* diagram for an ORC with one reheat stage where most of the expansion occurs after the reheat, from State 5b to State 6b. The second stage expander exit at State 6b is at a much lower temperature than the first stage expander exit at State 6a.

For a cycle with a single reheat stage, choosing the intermediate pressure P_{6a} is effectively equivalent to determining the relationship between the pressure ratios PR_a and PR_b. Figure 3.21 is the T-s diagram for a case where $PR_a << PR_b$. Very little expansion occurs across the first expander stage, and consequently $T_{6a} > T_{6b}$. Again, State 6 is included as the expander exit state if there were no reheat stage. State 3 is the recuperator exit state for the baseline case, while State 3b is the slightly higher temperature recuperator exit state due to the fact that the recuperator hot stream inlet temperature has increases, such that $T_{6b} > T_6$.

Figure 3.22 is a plot of the effect that this reheat cycle has on the working fluid heating profile. On the left side of the figure is the T-Δh plot of the baseline cycle, with additional recuperation due to the reheat stage shown in red and heat input into the reheat stage shown in light blue. On the right side of the figure is the new composite curve made up of the baseline heat requirement with the additional recuperation removed and the reheat added in.

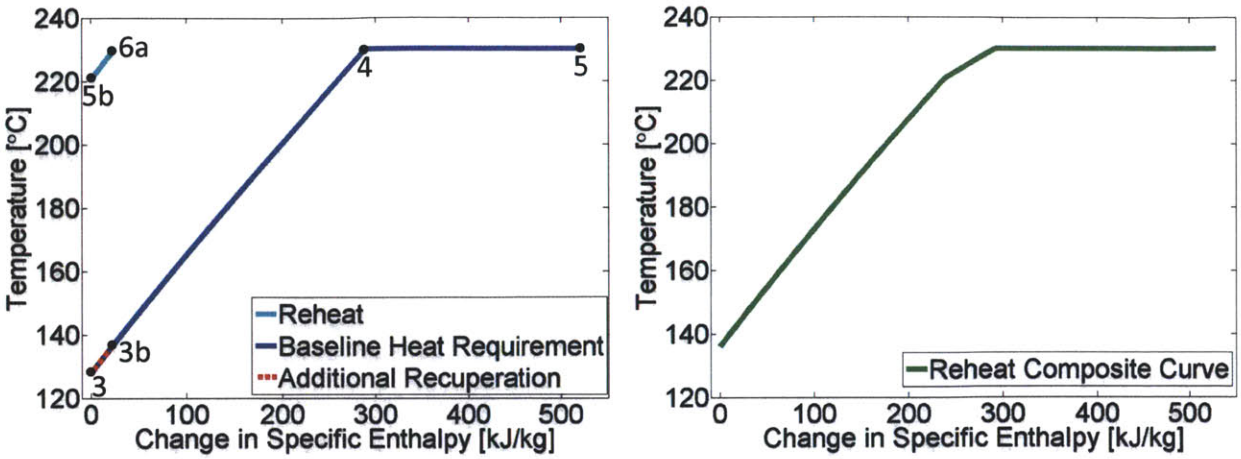

Figure 3.22: Plot of the cycle heat requirement for an ORC with a single reheat stage, in which most of the expansion occurs after the reheat stage. Numbered states match those shown in Figure 3.21. The baseline heat requirement (blue) is plotted on the left. The additional recuperation (dotted red) from State 3 to State 3b due to the reheat stage is removed from the cycle heat requirement. The additional heat (cyan) from State 5b to State 6a due to the reheat stage is then added, yielding the composite curve on the right (green).

For this case where $PR_a << PR_b$, there is minimal temperature drop across the first stage expander, and therefore very little room for reheating and only a small change to the heating profile. Since the goal of a reheat stage is to increase the heat absorbed by the cycle at high temperature, this would be a poor choice of pressure ratios for the reheat stage.

A second option would be to choose the pressure P_{6a} so that $PR_a >> PR_b$. Figure 3.23 shows a T-s diagram with the expander stages sized in this manner. It is clear that $T_{6a} < T_{6b}$, and a significant amount of reheating will take place in this configuration. Again, State 6 is depicted to indicate the baseline cycle expander exit temperature, and State 3 is shown to indicate the baseline cycle recuperator cold stream exit temperature. This scenario simultaneously increases the amount of reheating and the amount of recuperating that occurs.

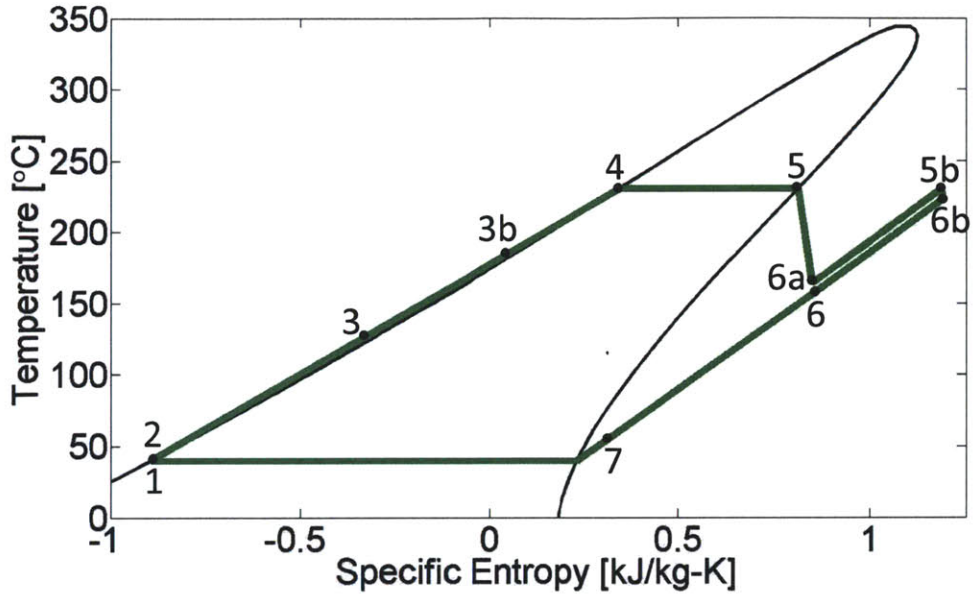

Figure 3.23: *T-s* diagram for an ORC with one reheat stage where most of the expansion occurs before the reheat, from State 5 to State 6a. The second stage expander exit at State 6b is at a much higher temperature than the first stage expander exit at State 6a.

Figure 3.24 shows the T-Δh diagram of the heat requirement in this case where $PR_a >> PR_b$. On the left side are the baseline cycle heating curve with significant additional recuperation shown in red. The heat input from reheating is shown in light blue. On the right side of the figure is the new composite heat requirement curve for the working fluid. The additional recuperation and the reheating for this cycle overlap in temperature, and almost perfectly negate each other in the region of overlap (from T_{5b} to T_{3b}). This limits the influence of the reheating and establishes a limit on the effect that a reheat stage can have on the cycle. Any reheating added to a cycle is only effective up to the point where it begins to overlap in temperature with the additional recuperation.

The most efficacious scenario, then, occurs when the reheat temperature, T_{6a}, is exactly equal to the outlet temperature of the cold side of the recuperator. Finding the pressure that will satisfy this constraint is a time-intense iterative calculation that is dependent on the working fluid, the pinch temperature potential in the recuperator, the number of reheat stages,

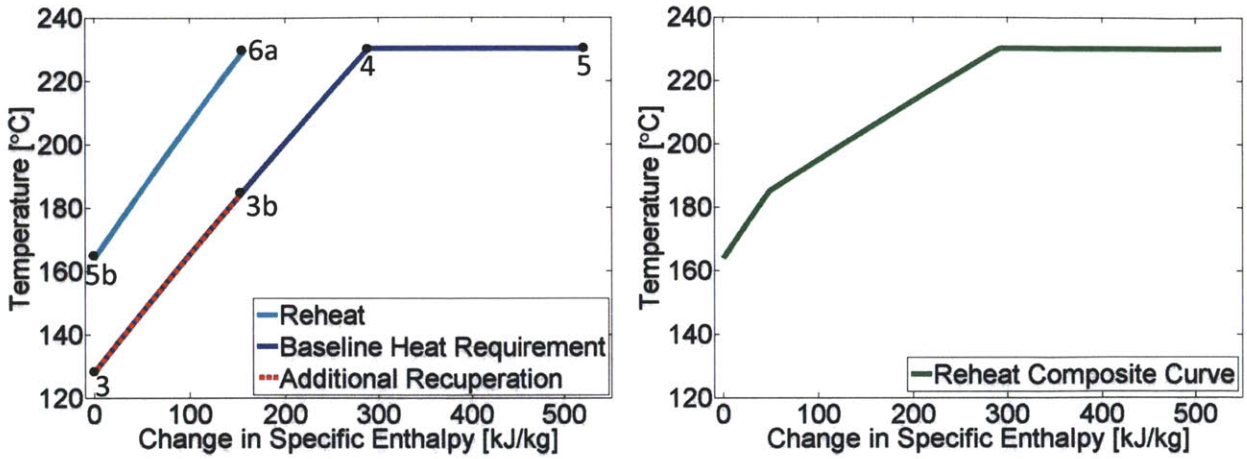

Figure 3.24: Plot of the cycle heat requirement for an ORC with a single reheat stage, in which most of the expansion occurs before the reheat stage. Numbered states match those shown in Figure 3.23. The baseline heat requirement (blue) is plotted on the left. The additional recuperation (dotted red) from State 3 to State 3b due to the reheat stage is removed from the cycle heat requirement. The additional heat (cyan) from State 5b to State 6a due to the reheat stage is then added, yielding the composite curve on the right (green). In this configuration, some of the additional recuperation and the additional reheat overlap between the temperature T_{5b} and T_{3b}, and the two effects negate each other.

and the inclusion of other modifications to the cycle. However, a few reasonable assumptions can greatly simplify this process, leading to a closed form equation for reheat pressure ratios which yield results reasonable close to this ideal case.

The first assumption is that the expander outlet temperature, T_{6b} in the example with a single reheat stage, is a good indication of the recuperator cold stream outlet temperature, T_{3b}. This assumption ignores ΔT in the recuperator, which is generally small. As explained in Section 3.4.2 on split recuperators, this assumption is not entirely accurate for a basic recuperator, because basic recuperators pinch on the cold side and have a larger temperature difference on the hot side. However, it is still a good first order estimate. In any cycle which uses a split recuperator, this assumption will be very accurate, because the recuperator will be a balanced

heat exchanger with consistent ΔT throughout. If T_{6b} is a good representation of recuperator cold stream exit temperature, then the best case scenario will occur when $T_{6a} = T_{6b}$, so that the additional reheat does not overlap in temperature with the additional recuperation.

The second necessary assumption is that the superheated working fluid in the expander acts like an ideal gas. The isentropic efficiency of expanding a gas from a given State A to a new State B is defined as:

$$\eta_{exp} = \frac{h_A - h_B}{h_A - h_{B,rev}} \tag{42}$$

where h is specific enthalpy, the subscript refers to the fluid state, and $h_{B,rev}$ is the enthalpy of State B in the reversible case where there is no entropy generation. For an ideal gas, specific enthalpy found according to the constitutive relation.

$$h_A - h_B = c_p * (T_A - T_B) \quad . \tag{43}$$

Combining Equations (42) and (43) and rearranging, it can be seen that the expander efficiency is related to the temperature ratio across the expander:

$$\eta_{exp} = \frac{1 - \frac{T_B}{T_A}}{1 - \frac{T_{B,rev}}{T_A}} \quad . \tag{44}$$

The temperature ratio across a reversible expander is related to the expander pressure ratio according to the entropy constitutive relation for an ideal gas:

$$\frac{T_{B,rev}}{T_A} = PR_{AB}^{\gamma/\gamma-1} \tag{45}$$

where γ is the specific heat ratio of the gas, and PR_{AB} is the pressure ratio across the expander. Finally, then, combining Equations (42) through (45), it can be seen that the temperature drop across an expander is a function of the pressure ratio and isentropic efficiency:

$$\frac{T_B}{T_A} = 1 - \eta_{exp} * (1 - PR_{AB}^{\gamma/\gamma-1}) \quad . \tag{46}$$

Therefore, for multiple reheat stages with the same expander efficiency, the same expander inlet temperature T_A, and the same pressure ratio, the expander exit temperature should remain constant to the extent that the fluid is similar to an ideal gas. For the organics considered here, this relationship largely holds, so that all reheat stages for a given cycle are chosen to have equal pressure ratios. This relationship is additionally useful, because it sets the pressure requirements for any number of reheat stages. For a cycle with n number of expander stages corresponding to n-1 number of reheat stages and an overall pressure ratio PR_{tot}, the pressure ratio of an individual expander stage, PR_{stage}, is calculated to be

$$PR_{stage} = PR_{tot}^{1/n} \quad . \tag{47}$$

All reheat cycle calculations for this thesis use Equation (47) to set pressures across the expander stages.

The number of reheat stages affects the overall cycle heat requirement. Figure 3.25 shows the Temperature vs. Specific Enthalpy and Temperature vs. Change in Enthalpy per Time graphs for decane cycles with multiple reheat stages. The baseline cycle (magenta), single reheat stage cycle (green), four reheat stage cycle (cyan) and the ten reheat stage cycle (black) follow identical state paths through the T-s plane except during expansion from P_{high} to P_{low}. Each extra reheat stage incrementally increases the specific heat input required to complete one cycle. At the same time, as the number of reheat stages increases, the pressure ratio across each reheat stage becomes smaller, as described by Equation (47). Thus, the temperature drop across each stage becomes smaller, as described by Equation (46). On the T-s graph, it can be seen that the combination of these two trends causes the cycle expansion to approach a limit where isothermal expansion occurs as the number of reheat stages approaches infinity. For the cycle heat input curves on the T-$\Delta\dot{H}$ graph, this trend towards

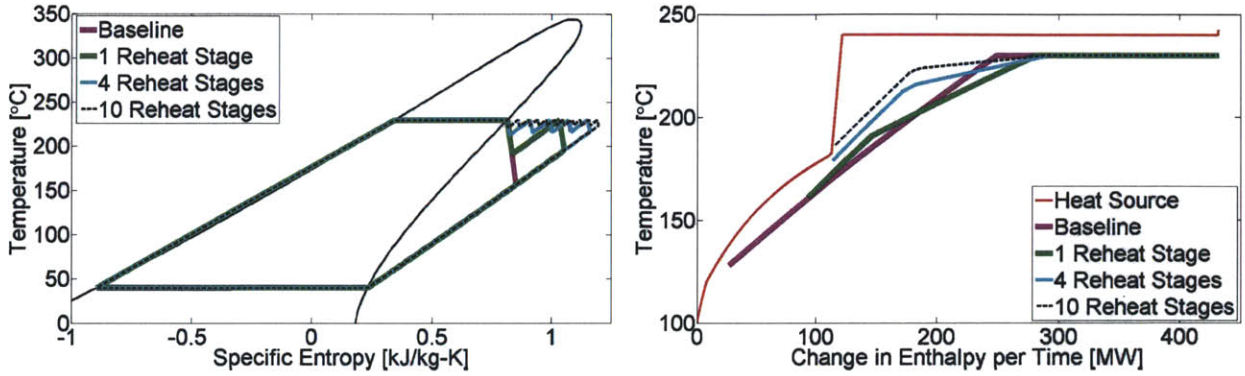

Figure 3.25: T-s diagram and T-$\Delta\dot{H}$ plot showing the effect of multiple reheat stages on the cycle heat requirement for an ORC. As the number of reheat stages increases, the expansion process approaches a limit in which isothermal expansion occurs. Thus, with more reheat stages, the heat rate absorbed by the cycle near the maximum temperature is increased.

isothermal expansion effectively extends the constant temperature plateau due to boiling so that the cycle can more effectively use the large constant temperature heat source available from the FT reactor.

Table 15 contains cycle characteristics for the four cycles plotted in Figure 3.25. As more reheat stages are added, the cycle heat input occurs at progressively higher temperatures and the cycle efficiency, η_{cyc}, increases. However, a significant portion of the FT Heat Source is

Table 15: Cycle characteristics showing the effect of multiple reheat stages with decane as the working fluid for organic Rankine cycles.

Cycle	Baseline ORC	1 Reheat Stage	4 Reheat Stages	10 Reheat Stages
Working Fluid	Decane	Decane	Decane	Decane
T_{pinch} [°C]	138.0	171.1	188.9	195.5
$\dot{m}_{wf}$ [kg/s]	771.5	635.1	591.0	587.3
$\dot{W}_{net}$ [MW]	119.4	103.0	98.5	98.9
η_{cyc}	29.5%	30.5%	31.1%	31.3%
U_{cyc}	93.8%	78.3%	73.5%	73.2%
η_{conv}	27.7%	23.8%	22.8%	22.9%

available at lower temperatures, so the additional heating at high temperatures results in pinching and decreased heat source utilization. Consequently, the cycles shown here with reheat stages all have lower conversion efficiencies, η_{conv}, than the baseline cycle. Reheat stages are shown to be effective at matching the high temperature portion of a heat source, and will prove to be particularly useful when combined with other cycle modifications.

3.4.5 Supercritical Cycle

Up to this point, all of the cycles described in this thesis have been subcritical. That is to say, they have all operated at pressures below the critical pressure of the working fluid so that constant pressure phase change occurs at a constant temperature in the two-phase region. In certain situations, it may be advantageous to have a working fluid heat requirement which does not include a constant temperature plateau. This is achieved by heating the working fluid at a constant pressure P_{high} which is greater than the critical pressure of the fluid.

Figure 3.26 includes a schematic and T-s diagram of the supercritical cycle using

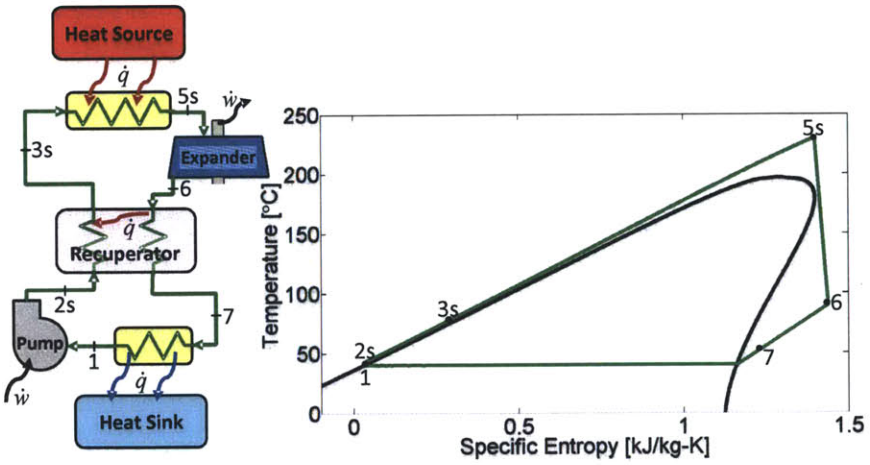

Figure 3.26: Schematic and T-s diagram of a supercritical ORC. From a saturated liquid at State 1, the fluid is pumped to a pressure that exceeds the critical pressure, so that the supercritical fluid absorbs heat without a phase change. The pressure level must be chosen to avoid significant condensation in the expander, because the state path of the fluid may cross into the two phase region between State 5s and State 6.

pentane as a working fluid. Pentane was chosen due to its low critical temperature, $T_{crit} = 196.6°C$, making a supercritical cycle the logical choice for the FT heat source. The necessary equipment for a supercritical cycle is essentially the same as that for the baseline cycle. The fluid path through the T-s states only differs in that States 2 through 5 are at a supercritical pressure, yielding States 2s, 3s, and 5s. There is no saturated liquid state for a supercritical fluid, so state 4 has been omitted. From State 5s, the supercritical pentane is expanded to low pressure, recuperated, and condensed in exactly the same manner as a baseline cycle.

The pinch analysis for this supercritical cycle using the FT heat source is trivial, because the simple shape of the cycle heat requirement does not result in any pinch points at low temperature. Figure 3.27 shows the results of this pinch analysis in the form of a T-$\Delta\dot{H}$ graph. The supercritical pentane cycle heat requirement is shown in green. For comparison, a baseline

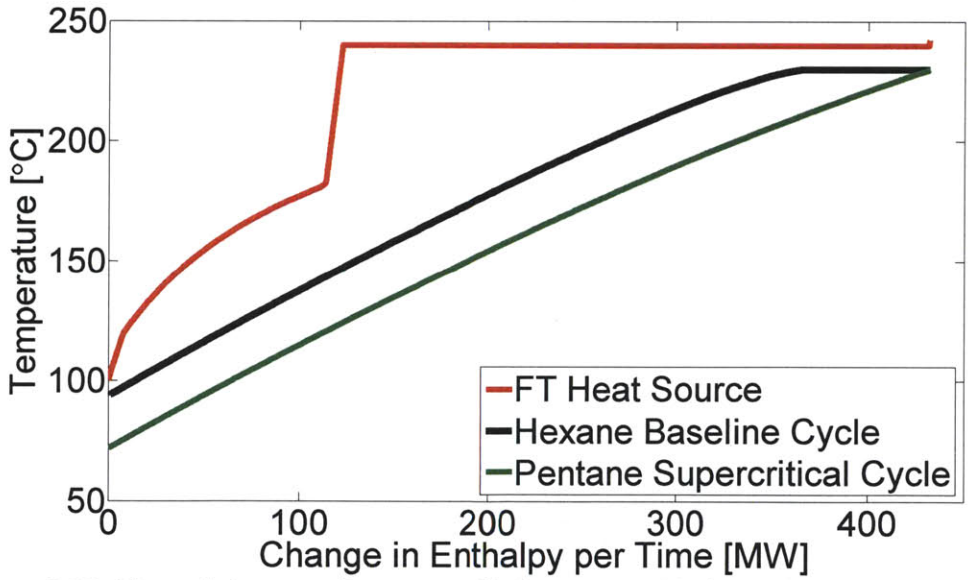

Figure 3.27: The cycle heat requirement profile for a supercritical cycle is plotted with the FT heat source. A hexane baseline cycle is included for comparison. Supercritical cycles are not effective at capturing constant temperature heat sources, because there is no constant temperature boiling in a supercritical cycle.

Table 16: Cycle characteristics comparing a supercritical pentane cycle to the baseline hexane cycle.

Cycle	Baseline ORC	Supercritical ORC
Working Fluid	Hexane	Pentane
T_{pinch} [°C]	104.0	N/A
$\dot{m}_{wf}$ [kg/s]	846.4	880.7
$\dot{W}_{net}$ [MW]	113.0	99.5
η_{cyc}	26.3%	23.0%
U_{cyc}	99.6%	100%
η_{conv}	26.2%	23.0%

hexane cycle is shown in black. The low critical temperature of the pentane makes it impossible to create a "baseline pentane cycle", so hexane is chosen as the next closest alternative. For the FT heat source, it is unlikely that a supercritical cycle would be chosen, because as seen in Figure 3.27, the lack of constant temperature phase change makes the heat curve a poor match. Supercritical cycles are often useful in cases where the heat source is a fluid stream providing only sensible heat, so that the lack of phase change in a supercritical cycle becomes an advantage for matching the shape of the heat source.

Table 16 contains the relevant cycle characteristic data for the pentane supercritical cycle pictured above. As expected, the supercritical cycle achieves full heat source utilization, but has relatively poor cycle efficiency, η_{cyc}, due to poor heat source temperature matching. This results an a conversion efficiency which is less than that of the baseline hexane cycle.

3.4.6 Future Work: Fluid Mixtures

One cycle modification which has not been explored in great detail in this thesis, but could prove useful to an able cycle designer, is that of fluid mixtures. The cycle modifications described in this chapter have all been achieved by manipulating the configurations of cycles which use pure working fluids such as hexane or decane. Pure working fluids boil at constant temperature along an isobar. Fluid mixtures have a characteristic "glide" during boiling such

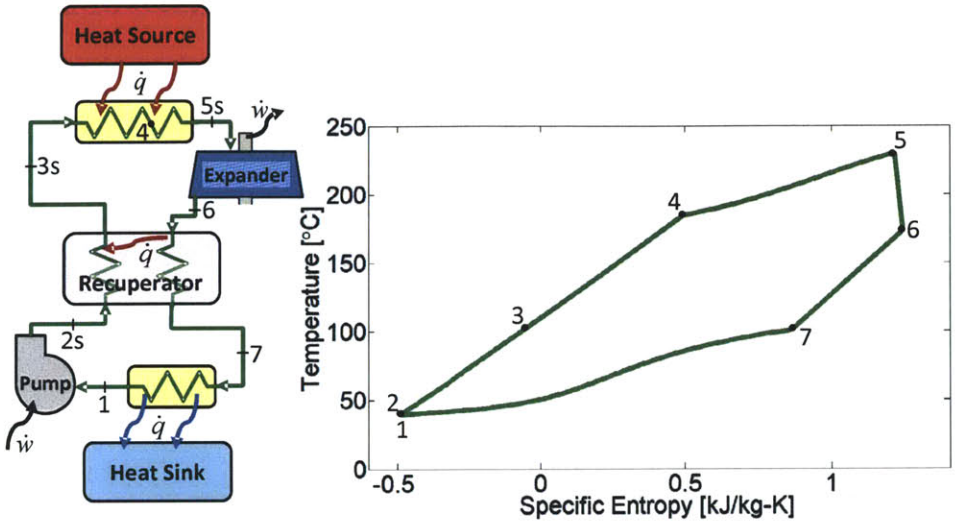

Figure 3.28: Schematic and *T-s* diagram of an ORC using fluid mixtures, to be considered as future work. The mixture shown here is 50% hexane and 50% decane by mass. Boiling from State 4 to State 5 and condensing from State 7 to State 1 occur along a temperature glide rather than at constant temperature. The extend of this temperature glide is determined by the composition of the fluid mixture.

that they experience a change in temperature when boiled along an isobar. Figure 3.28 shows the schematic for a baseline ORC with an accompanying T-s diagram for a working fluid mixture made up of 50% hexane and 50% decane by mass. The there is a temperature glide during boiling from State 4 to State 5, and again during condensation from State 7 to State 1.

The data for this *T-s* diagram was taken from Refprop 8.0, but it's important to note that binary mixing parameters are not available for these fluids, so Refprop estimates the states in Figure 3.28. One of the greatest barriers to calculating the thermodynamic performance of fluid mixtures is finding accurate state equations.

3.5 Customized Cycle

The effect of each cycle building block has been considered individually and its influence on the cycle heat requirement curve has been shown. The building blocks can now be combined with each other to create a customized cycle which affectively targets the Fischer

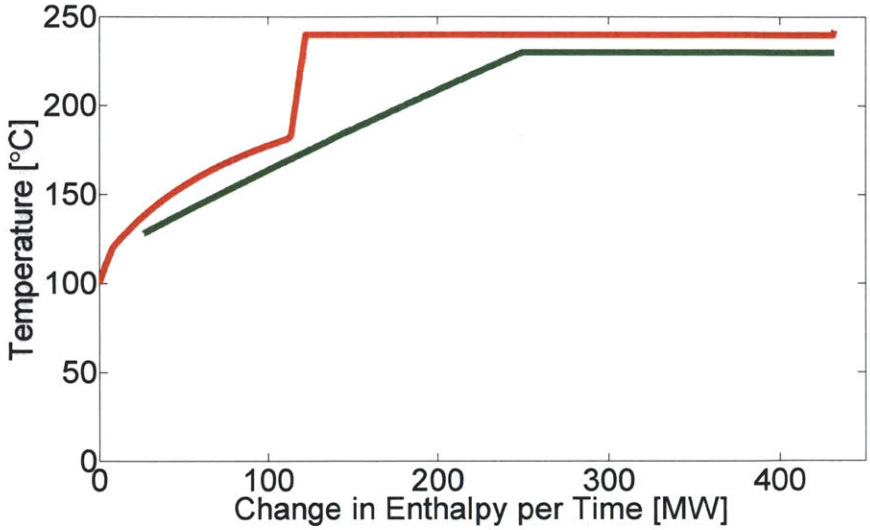

Figure 3.29: The baseline decane cycle heat requirement (green) with the FT heat source curve (red). The cycle fails to achieve full heat source utilization and poorly matches the heat source curve, particularly from 114 MW to 250 MW.

Tropsch heat source. Begin with a baseline decane cycle, with the T-$\Delta\dot{H}$ pictured in Figure 3.29. The hot end of the curve above a value of $\Delta\dot{H} = 250$ MW is matched very well to

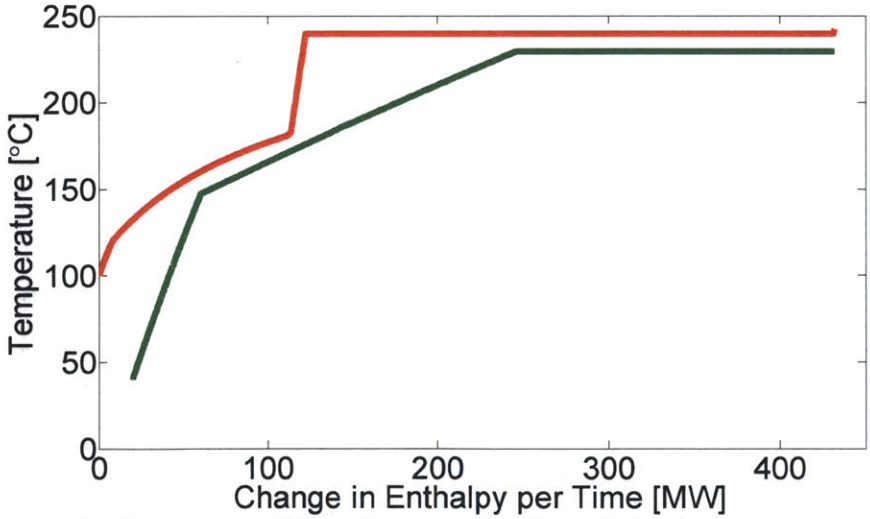

Figure 3.30: The decane ORC with a split recuperator (green) with the FT heat source (red). This cycle has improved heat source utilization of the over the baseline decane cycle because the pinch point is moved. This cycle does not achieve full heat source utilization, and there is poor heat source matching from 114 MW to 250 MW.

the constant temperature heat requirement of the FT heat source. Two obvious sources of inefficiency exist with this baseline cycle: a pinch point at $T_{pinch} = 138°C$ prevents full heat source utilization, and heat transfer across a large temperature gap over the range $120\,\text{MW} < \Delta\dot{H} < 250\,\text{MW}$ generates significant entropy.

The pinch point at the cold end of the curve can be alleviated by splitting the recuperator stream to reduce the temperature requirement of the working fluid curve at the cold end. This effect is shown on the T-$\Delta\dot{H}$ plane in Figure 3.30. Full heat source utilization is not achieved, but there is a significant improvement.

Now the focus shifts to the large temperature gradient caused by the sharp angle in the heat source curve at $\Delta\dot{H} = 122.4\,\text{MW}$. A well matched cycle heating curve would tuck up into this corner and receive heat transfer across a much smaller temperature gradient. It was shown earlier that reheat cycles help to extend constant temperature plateau of the latent

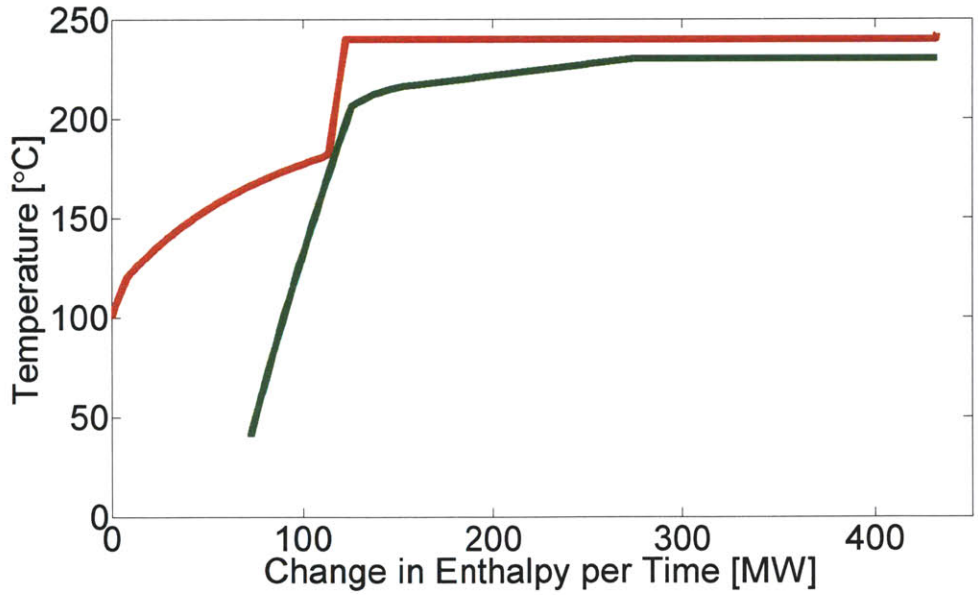

Figure 3.31: The decane ORC heat requirement with a split recuperator and four reheat stages (green) with the FT heat source (red). This cycle is a good match for the FT heat source in the region from 114 MW to 432 MW. The reheat stages cause a pinch point between the cycle heat requirement and the heat source at a pinch temperature of 182°C.

heat, approaching a limit of constant temperature expansion. Four reheat stages will now be added to close this temperature gap. The new working fluid heat requirement curve including four reheat stages and a split recuperator stream is shown on a T-$\Delta\dot{H}$ graph in Figure 3.31.

The large temperature gap caused by the corner in the heat source curve has now been significantly reduced. However, in matching this part of the heat source curve, a new pinch point has been introduced at $T_{pinch} = 182.4°C$. This pinch point drastically limits the heat source utilization of the cycle shown here. One more building block can be implemented to relieve this problem. An additional pressure level will add two more degrees of freedom, allowing a second pinch point and full heat source utilization. Figure 3.32 shows this customized cycle, now including two pressure levels with split stream recuperators, and four reheat stages on the high pressure loop. The baseline heat requirement curve is also included for comparison purposes. It is clear that the customized cycle has significantly improved the heat source matching. In fact, for the decane example shown, the thermal conversion

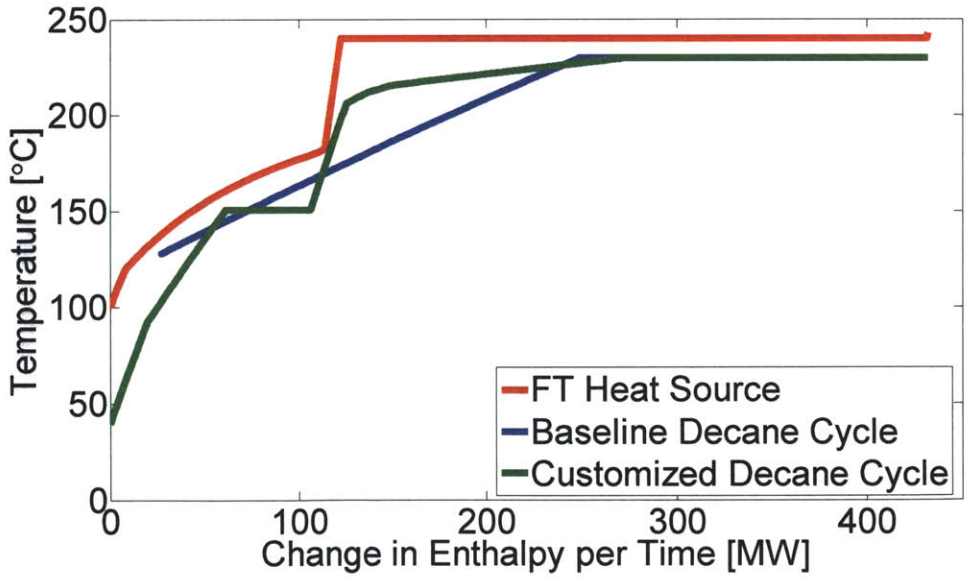

Figure 3.32: The customized decane ORC (green) with two pressure levels, four reheat stages, and two split recuperators, achieves 100% heat source utilization and excellent heat source matching for the FT heat source (red).

efficiency has improved from a baseline efficiency of 27.7% to a customized cycle efficiency of 29.3%. That's 7.2 MW of extra work output from the FT heat source.

It is important to remain cognizant of the equipment requirements that coincide with changes to the ORC. The customized decane cycle working fluid path is shown in schematic form in Figure 3.33. A high pressure loop, shown in dark green, is pumped to high pressure in the HP Pump, and then split around the recuperator. It is heated by the heat source, and expanded through five expander stages with four reheat stages between them. It then transfers heat in the recuperator before rejecting entropy in the condenser. Inside the figure, a low pressure loop is shown in bright green. The low pressure loop is pumped up in the LP Pump and then split around the recuperator. It absorbs heat from the heat source, and is expanded to P_{low} before being introduced back into the HP loop in the recuperator.

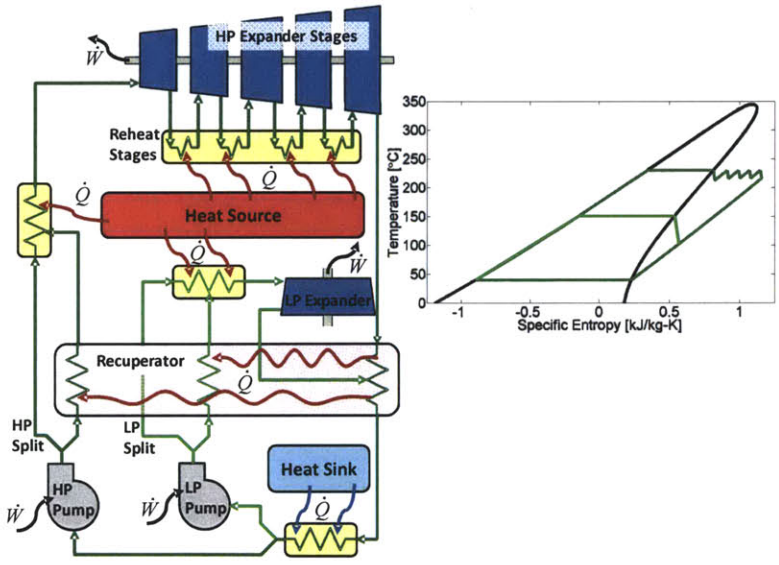

Figure 3.33: Customized ORC schematic diagram with corresponding fluid states in a *T-s* plot. This decane ORC includes a high pressure loop (dark green) with a split recuperator and four reheat stages, as well as a low pressure loop (light green) with a split recuperator. The two loops are combined at low pressure on the hot side of the recuperator.

Table 17: ORC characteristics for customized cycles with split recuperators, 2 pressure levels, and 4 reheat stages on the HP loop. Baseline cycle data is included for comparison.

Cycle	Baseline	Custom	Baseline	Custom	Baseline	Custom	Baseline	Custom	Baseline	Custom
Working Fluid	Hexane	Hexane	Heptane	Heptane	Octane	Octane	Nonane	Nonane	Decane	Decane
T_{pinch} [°C]	104.0	182.4	122.9	182.4	130.6	182.4	135.3	182.4	137.9	182.4
$T_{pinch,2}$ [°C]	N/A	166.9	N/A	164.6	N/A	162.8	N/A	161.5	N/A	160.6
$\dot{m}_{wf,HP}$ [kg/s]	846.4	693.2	808.3	681.5	787.0	673.4	776.9	670.8	771.6	669.2
$\dot{m}_{wf,LP}$ [kg/s]	N/A	130.5	N/A	137.7	N/A	145.1	N/A	150.9	N/A	155.2
$\dot{W}_{net}$ [MW]	113.0	123.0	118.6	125.3	119.4	126.1	119.5	126.4	119.4	126.6
η_{cyc}	26.3%	28.5%	28.2%	29.0%	28.9%	29.2%	29.3%	29.3%	29.5%	29.3%
U_{cyc}	99.6%	100%	97.5%	100%	95.7%	100%	94.5%	100%	93.8%	100%
η_{conv}	26.2%	28.5%	27.5%	29.0%	27.7%	29.2%	27.7%	29.3%	27.7%	29.3%

Table 17 contains the cycle characteristic data for the customized cycle described in this section and depicted in Figure 3.33 above. The hexane cycle shows the greatest improvement, with an increased net work output of 10 MW. The smaller chain hydrocarbons improve primarily by matching the heat source more effectively, thus improving the cycle efficiency. For instance, hexane heat source utilization only improves by 0.4%, but hexane cycle efficiency, η_{cyc}, improves from 26.3% to 28.5%. The larger chain hydrocarbons improve primarily by increasing heat source utilization at low temperatures with small changes to the overall cycle efficiency. For instance, decane heat source utilization improves by 6.2%, but decane cycle efficiency decreases slightly from 29.5% to 29.3% as lower grade heat is incorporated into the cycle.

3.6 Customizable ORC Conclusions

The concept of a customizable organic Rankine cycle has been introduced as a means for matching a particular heat source with an organic Rankine cycle which will efficiently convert the heat into work. The customized cycle is created from a set of building blocks, including a split recuperator, reheat cycles, multiple pressure levels, and supercritical cycles. Fluid mixtures are also a useful building block to be explored as future work. Finally, these cycle

building blocks were used to demonstrate the creation of a customized cycle targeting the FT heat source from the BP Polygeneration Plant Model.

Mathematically, it does not matter greatly what order the building blocks are applied in, as the affects are cumulative. However, it is often requires the least effort to include extra pressure levels last, because calculating pressure levels is an iterative process requiring the designer to assign two parameters (mass flow and pressure level) for each new pressure level. It is reasonable to imagine a situation in which the supercritical working fluid loop would also be included as an extra pressure level in a custom cycle if the situation demanded a heating curve of that shape.

The customized cycles shown in this chapter were created with several "arbitrary" decisions, including the number of reheat cycles, and whether any or all pressure levels should have split recuperator streams. In reality, these choices must be evaluated by balancing additional cost and complexity against the additional work output that each modification introduces to the cycle. These considerations will be discussed in the next chapter.

4 Implementation

Chapter 2 introduced the concept of organic Rankine cycles and demonstrated their efficiency benefits on constant temperature heat sources that are too cold for steam cycles to be practical. Chapter 3 discussed cycle modifications to ORC's that target the maximum conversion efficiency given a particular heat source. In this chapter, the cost of implementing these organic Rankine cycles is assessed and weighed against the performance benefits. Firm recommendations are made for a cycle to fit the Fischer Tropsch reactor heat source, and implementation strategies are discussed.

4.1 Cycle selection and Cost Estimates

The baseline ORC configuration is shown again here in Figure 4.1. The focus is now on the equipment necessary to operate this cycle. There are two primary capital cost drivers for this cycle: expanders, and heat exchangers. Pumps are ignored because they are significantly less expensive than expanders and are relatively insensitive to cycle modifications. The cost

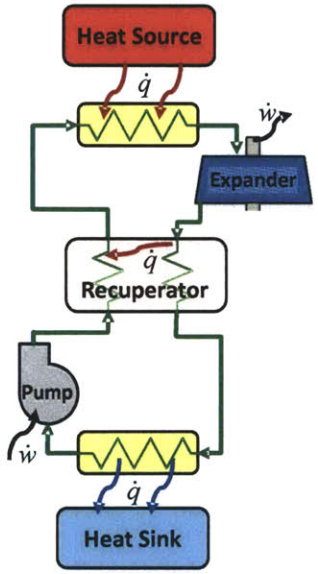

Figure 4.1: Schematic diagram for a baseline ORC. Major sources of equipment cost are the turbine and the heat exchangers.

model developed here relies heavily on the Process Equipment Cost Estimation Final Report published by the National Energy Technology Laboratory, henceforth referred to as the NETL cost report (Loh, Lyons, & White, 2002). The NETL cost report originally quoted costs in 1998 dollars, which have here been converted to 2011 dollars by multiplying by a CPI factor of 1.385 (Bureau of Labor Statistics CPI Inflation Calculator). The NETL report claims an accuracy of +50%/-30% and is recommended for order of magnitude estimates of equipment cost. Therefore, the cost model presented here is intended only as a high level tool to narrow cycle selection. More rigorous cost models are needed for actual plant design.

The purpose of this cost analysis is to compare the use of organic Rankine cycles to a standard low pressure steam cycle to convert the Fischer Tropsch plant heat source into shaft work. Organic Rankine cycles are a niche market relative to steam, and are still a technology that is in development, so cost numbers are not well documented or understood.

4.1.1 Turbine Cost Model

Steam turbines are an established technology with well understood cost drivers.

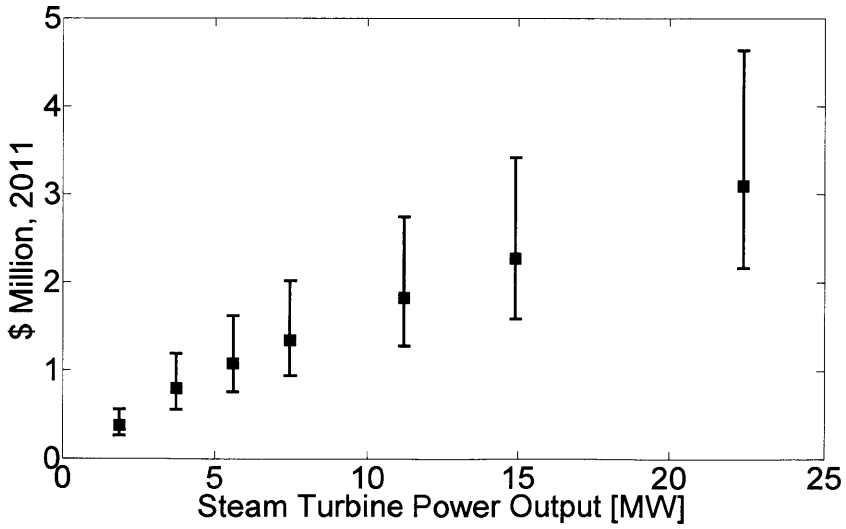

Figure 4.2: Steam Turbine cost curve, converted to 2011 dollars, from the NETL Process Equipment Cost Estimation Final Report. Error bars are included to show the +50%/-30% error cited in the report.

Figure 4.2 shows the NETL cost report data for Purchased Equipment Cost vs. Power Output of steam turbines. The values provided were calculated by assuming steam turbine inlet pressure of 400 psig (2756 kPa), and include the cost of the condenser (Loh, Lyons, & White, 2002).

ORC turbines are a much newer technology than steam turbines, and there is very little publicly available cost data for them. Though there is little published data, a manager of sales at ORMAT discussed the cost competitiveness of organic Rankine cycles over the phone. ORMAT states that an organic turbine is cost competitive with a steam turbine of comparable physical size (Nordquist, 2010). Furthermore, current ORC designs are modular, such that scaling to large power output is achieved by installing multiple units rather than building one larger unit. This means that if the current state of the art in organic turbines is a single unit which outputs 15 MW of power, then any system which outputs more power than 15 MW will have a linearly scaling cost, because to achieve 30 MW it is necessary to install two units, and to achieve 45 MW it is necessary to install three units.

Based on this information from ORMAT, the organic turbine costs in this model are estimated from the steam turbine cost curves by making two assumptions. First, turbine cost is dependent on the discharge volume flow rather than power output. Second, existing organic turbines are cost competitive with steam turbines of comparable physical size. Using these two assumptions, the cost curves for steam turbines are converted into a dollar per volume flow basis, and organic turbine costs can then be estimated based on their volume flows. Then, the size of the current state of the art organic turbine is estimated based on available data, and the organic turbine cost curve is assumed to be linear for all volume flows larger than that of the state of the art system.

The first assumption correlates the cost of the turbines to the physical size of the equipment rather than the power output. This assumption necessitates converting the NETL cost curves into geometric dimensions. The size of a turbine scales with the volume flow of the working fluid through the turbine. For the purpose of this model, the volume flow is taken at

Table 18: State properties used to convert steam turbine power output into steam volume flow. The turbine inlet state matches the IP steam turbine inlet from the BP Polygeneration Plant Model, and the turbine exit pressure matches the LP steam turbine exit pressure from the BP Polygeneration Plant Model.

	specific enthalpy	specific entropy	Temperature	Pressure	Quality	density
State	h (kJ/kg)	s (kJ/kg-K)	T (°C)	P (kPa)	Q (kg/kg)	ρ (kg/m^3)
inlet	3536.9	7.352	535	2900	Superheated	7.923
reversible exit	2281.8	7.352	38.7	6.895	0.880	0.05459
exit	2407.3	7.352	38.7	6.895	0.932	0.05154

the turbine exit state, where it is largest. Taking the volume flow at the turbine exit also allows the model to capture changes to the size of the condenser, which is lumped with the turbine cost in the NETL cost report. The NETL report quotes steam turbine costs for a turbine inlet pressure of 400 psig (2.8 MPa). This is similar to the intermediate pressure (IP) steam turbine in the BP Polygeneration Plant Model. Therefore, the turbine inlet state for this cost model is assumed to match the BP Polygeneration Plant Model IP steam turbine inlet, at a pressure of 2.9 MPa and a temperature of 535°C. The turbine exit state is assumed to be at a pressure 6.895 kPa, matching the low pressure (LP) steam turbine exit state in the BP Polygeneration Plant Model. Expander isentropic efficiency is assumed to be 0.9. Table 18 lists the state properties for steam based on these assumptions at the turbine inlet, reversible exit, and exit.

The turbine power output, $\dot{W}_{turb}$, can be converted to a volume flow at the turbine exit, $\dot{V}_{exit}$, by means of the equation:

$$\dot{V}_{exit} = \frac{\dot{W}_{turb}}{\Delta h_{turbine} \cdot \rho_{exit}} \tag{48}$$

where ρ_{exit} is the density at the turbine exit state, and $\Delta h_{turbine}$ is the change in specific enthalpy from the turbine inlet, h_{inlet}, to the turbine exit, h_{exit}:

$$\Delta h_{turbine} = h_{inlet} - h_{exit} \quad . \tag{49}$$

For the steam turbine cost curve, based on the data in Table 18, $\Delta h_{turbine} = 1129.6\,\text{kJ/kg}$, and the x-axis of the cost curve shown in Figure 4.2 can be converted from power output [MW] to volume flow [m^3/s] using the conversion factor $\dot{V}_{exit} = 17.176 \cdot \dot{W}_{turb}$.

A power law curve is fit to the data so that the cost, C_{turb}, of any volume flow can be interpolated:

$$C_{turb} = 0.05867 \cdot \dot{V}_{exit}^{\ 0.6768} - 0.2169 \tag{50}$$

where C_{turb} is in units of millions of dollars, 2011. Figure 4.3 shows the cost data from the NETL cost report with volume flow of the working fluid as the independent variable. The power law fit given by Equation (50) is plotted in red.

The second assumption, that *existing* organic turbines are cost competitive with steam turbines of comparable size, is now applied. This means that the organic turbine cost will fit the

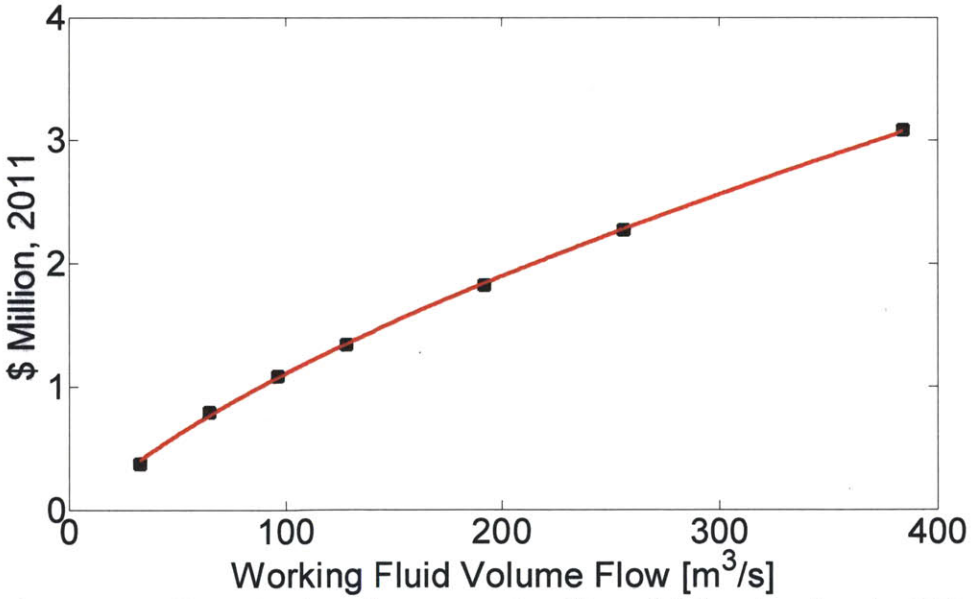

Figure 4.3: Turbine exit volume flow vs. cost, in millions of dollars, based on the NETL Process Equipment Cost Estimation Final Report. A fitted power law curve is shown in red.

cost curve shown above in Figure 4.3 up to the size of the largest existing ORC turbine. Any application larger than that is met by using modular ORC's with a cost that scales linearly. Thus, the size of a current state of the art organic turbine must be determined and located on the turbine cost curve.

The current published state of the art in organic turbines is taken to be the 15 MW organic Rankine cycle operating on pentane made by Ormat (Bronicki & Schochet, 2005). The Ormat system is used for geothermal and waste heat applications with heat source temperatures ranging from 100°C up to 300°C. Heat is carried from the source to the working fluid by a thermal oil in these applications, so the temperature drop from the source to the working fluid is greater than if there were direct heating. The maximum working fluid temperature is assumed to be 250°C for this analysis. Pentane has a critical temperature of 196.55°C, so this is a supercritical ORC (see Section 3.4.5). Figure 4.4 is a T-s plot of the supercritical pentane ORC described here. The maximum specific entropy at which

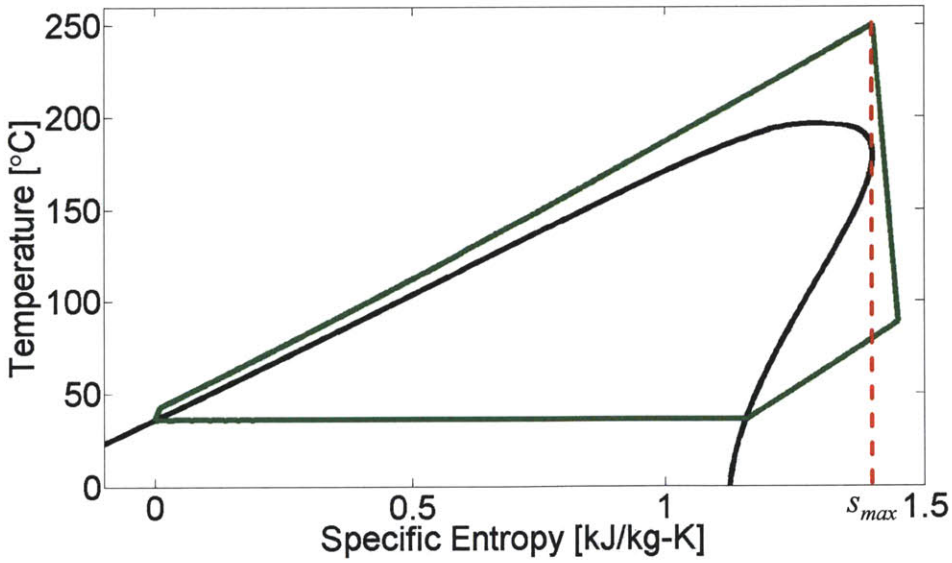

Figure 4.4: T-s diagram of a supercritical pentane ORC matching specifications for a state of the art ORMAT system. The maximum specific entropy at which condensation can occur for pentane is indicated by the red dashed line. The expander inlet is set to this value to assure that no condensation occurs during expansion.

condensation can occur for pentane is s_{max} = 1.40 kJ/kg-K, so the expander inlet state is set to this value. This maximum specific entropy is identified by the red dashed line in Figure 4.4, and setting the expander inlet to this value assures that no condensation occurs inside the expander.

The turbine exit pressure is assumed to be 1 atm (101.325 kPa) to prevent oxygen from leaking into the closed loop system. (The saturation temperature of pentane at 101.325 kPa is 36.1°C, so that this assumption is very similar to the minimum cycle temperature of 40°C used earlier in this thesis for other organic Rankine cycles. If a cycle minimum temperature of 40°C is assumed, the state of the art volume flow calculated is 10% lower.) The expander is assumed to have an isentropic efficiency of 0.9, resulting in the expander inlet and exit states shown in Table 19.

The turbine exit volume flow for a state of the art 15 MW Ormat ORC turbine is calculated using Equation (48), where the specific enthalpy drop across the turbine is $\Delta h_{turbine} = 155.0\,\text{kJ/kg}$, the density at the turbine exit is $\rho_{exit} = 2.494\text{kg/m}^3$, and the cycle power output is $\dot{W}_{exit} = 15\,\text{MW}$. This results in a maximum organic turbine volume flow rate of $\dot{V}_{exit} = 38.8\text{m}^3/\text{s}$. Up to a volume flow of 38.8 m^3/s, ORC turbines match the steam turbine cost

Table 19: State properties used to determine the size of current state of the art organic turbines. Ormat makes a 15 MW turbine with pentane as the working fluid that uses heat sources as hot as 300°C and ambient air as the heat sink. Turbine isentropic efficiency is assumed to be 0.9.

	specific enthalpy	specific entropy	Temperature	Pressure	Quality	density
State	h (kJ/kg)	s (kJ/kg-K)	T (°C)	P (kPa)	Q (kg/kg)	ρ (kg/m^3)
inlet	610.38	1.40	250	17345	supercritical	420.04
reversible exit	438.18	1.40	79.7	101.325	superheated	2.563
exit	455.4	1.448	88.5	101.325	superheated	2.494

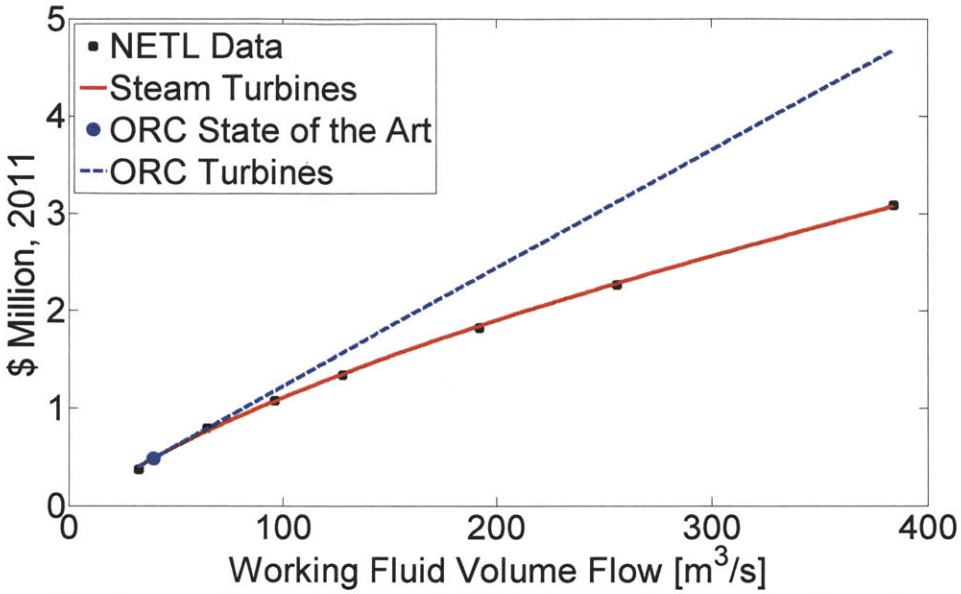

Figure 4.5: Steam turbine cost curve and ORC turbine cost curve as functions of volume flow at the turbine exit. The two curves are identical up to the size of a state of the art ORC turbine. At larger sizes, the steam turbines continue to realize economies of scale, while the modular ORC units have a linear cost curve.

curve. At higher volume flows, ORC turbine costs scale linearly. Therefore, the ORC cost, C_{ORC} in millions of dollars, can be estimated using the following equation:

$$\begin{aligned} C_{ORC} &= 0.05867 \cdot \dot{V}_{exit}^{\ 0.6768} - 0.2169 \quad \text{for} \dot{V}_{exit} \leq 38.8 \text{m}^3/\text{s} \\ C_{ORC} &= 0.01217 \cdot \dot{V}_{exit} + 8.636 \times 10^{-3} \quad \text{for} \dot{V}_{exit} > 38.8 \text{m}^3/\text{s}. \end{aligned} \tag{51}$$

The steam turbine cost curve described in Equation (50) and the ORC turbine cost curve described in Equation (51) are plotted here in Figure 4.5. The two curves overlap up to a volume flow of 38.8 m^3/s, which is the size calculated for a state of the art ORC turbine with pentane working fluid. These two curves will be used to calculate all turbo-machinery costs.

4.1.2 Heat Exchanger Cost Model

The NETL cost report estimates heat exchanger cost as a function of total area required for the heat exchanger. The report data is plotted in Figure 4.6, along with a cost curve fit. The

data show that the cost of the heat exchanger grows linearly with the total surface area required for the heat transfer.

The curve fit shown in red in Figure 4.6 relates the total area of a heat exchanger network, A_{tot} [m^2], to the cost of the heat exchanger network in millions of dollars, C_{HX}, using the following relationship:

$$C_{HX} = 1.743 \times 10^{-4} \cdot A_{tot} + 1.327 \times 10^{-2} \quad . \tag{52}$$

A thorough heat exchanger cost model requires an in depth heat exchanger network design, an understanding of the heat exchanger geometries which will be used, and an iterative calculation to find an appropriate compromise between pressure drop and heat transfer. The cost model presented here uses broad assumptions about the overall heat transfer coefficient, U, for the entire heat exchanger network represented in the composite curves on the $T - \Delta\dot{H}$ diagrams which were presented in Chapter 3. This method of estimating heat exchanger costs

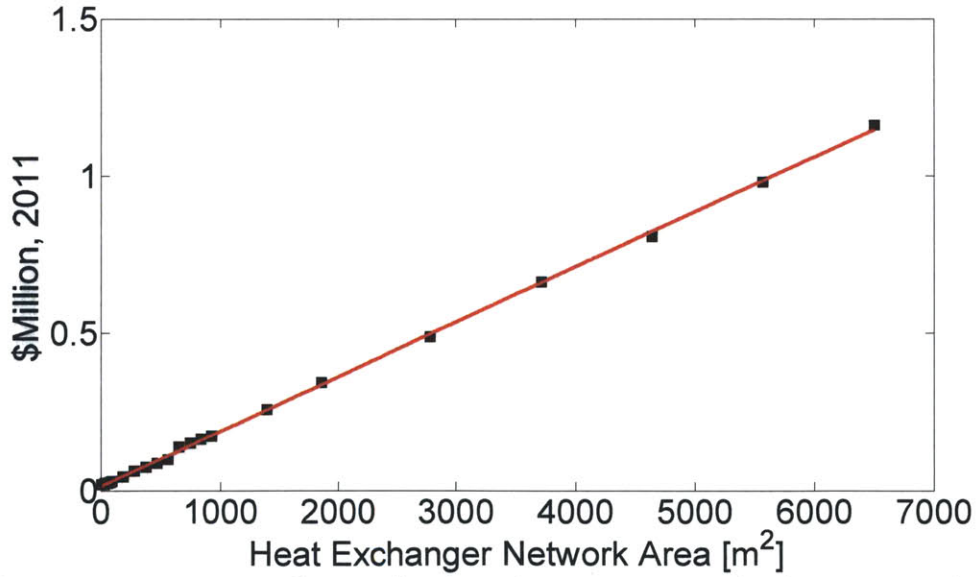

Figure 4.6: Heat cost curve base on data from the NETL cost report has been converted to 2011 dollars.

is considerably faster than designing heat exchanger networks, and provides useful order of magnitude information about the relative costs of different cycles.

The total heat exchanger area, Atot, is related to the total heat rate in the heat exchanger, $\dot{Q}$, by:

$$A_{tot} = \frac{\dot{Q}}{U \cdot \Delta T_{LM}} \tag{53}$$

where U is the overall heat transfer coefficient, and ΔT_{LM} is the log mean temperature difference from the hot stream to the cold stream. The heat rate and the temperature difference across the heat exchanger can be determined using pinch analysis, so all that remains is to choose an appropriate overall heat transfer coefficient.

The Fischer Tropsch system composite heating curve is composed mostly of hydrocarbon streams with some other byproducts such as water and carbon dioxide. This composite heating curve was discussed in detail in Section 3.2. Some streams include liquid or condensing phases, but for the purpose of determining an overall heat transfer coefficient here, the heat source will be treated as a gaseous hydrocarbon mixture.

The working fluids considered are either steam or organics. Figure 4.7 shows the $T - \Delta\dot{H}$ graph resulting from a pinch analysis with the FT Heat Source and two different baseline Rankine cycles, one ORC using hexane as the working fluid (left) and the other cycle using steam (right). The overall heat transfer coefficient for the ORC heat exchanger network will be divided into two increments for an ORC, with one overall heat transfer coefficient for the sensible heat region, U_{sens}, and one overall heat transfer coefficient for the latent heat region, U_{lat}. The latent heat transfer coefficient will naturally be the larger, because boiling flow generally has higher convection coefficients. The recuperator, which is not represented in Figure 4.7, will also use U_{sens}, because it is a gaseous hydrocarbon to liquid hydrocarbon heat exchanger. Similarly, the steam cycle that uses water as a working fluid is assigned different

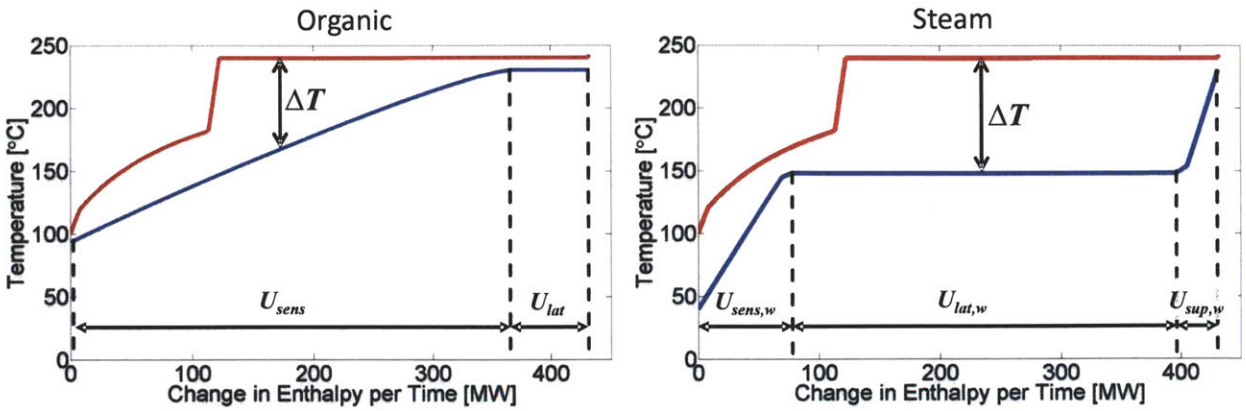

Figure 4.7: Pinch analysis results for a baseline hexane ORC (left) and a baseline steam cycle (right) with the FT Plant Heat Source. For the organic cycle, sensible heat will be assumed to have an overall heat transfer coefficient U_{sens}, and the latent heat will be assumed to have a (higher) overall heat transfer coefficient U_{lat}. For the water cycle, there is an overall heat transfer coefficient for the sensible heat region, $U_{sens,w}$, one for the latent heat region, $U_{lat,w}$, and one for the superheat region, $U_{sup,w}$.

heat transfer coefficients for the sensible heat region, $U_{sens,w}$, the latent heat region, $U_{lat,w}$, and the superheat region, $U_{sup,w}$.

The overall heat transfer coefficient, U, and the temperature difference across the heat exchanger network, ΔT, are both functions of $\Delta \dot{H}$, as shown in Figure 4.7. For this isobaric heating, the heat transfer rate across the heat exchanger network is equal to the change in enthalpy per time of the streams. This relationship was defined previously in Equation (25), which is repeated here:

$$\dot{Q} = \Delta \dot{H} \quad . \tag{25}$$

The total area for the heat exchanger network is calculated by using an integral form of Equation (53) along with the ΔT values defined by the pinch analysis and the appropriate overall heat transfer coefficients:

$$A_{tot} = \int dA = \int \frac{d\dot{Q}}{U \cdot \Delta T} \tag{54}$$

where dA is an incremental heat exchanger area, $d\dot{Q}$ is an incremental heat transfer rate, and U and ΔT are both functions of $\dot{Q}$.

The selection of appropriate overall heat transfer coefficients is important for estimating heat exchanger areas accurately. The overall heat transfer coefficients used in this model borrow from two sources: *Systematic Methods of Chemical Process Design* by Biegler, Grossman, and Westerberg (Biegler, Grossmann, & Westerberg, 1997), and *Heat and Mass Transfer* by A. F. Mills (Mills, 1995). Table 20 includes a list of the overall heat transfer coefficients provided by these sources which were taken into account in this model.

The overall heat transfer coefficient values in Table 20 are used to estimate the five overall heat transfer coefficient values needed for the heat exchanger cost model. Case #4 and Case #5 in Table 20 show that liquid light organics typically have lower heat transfer coefficients than water. The overall heat transfer coefficients used for the heat exchanger cost model are given in Table 21, along with a brief explanation of how they were selected.

The overall heat transfer coefficients contained in Table 21 are inserted into Equation (53) to calculate the total area of the heat exchanger network for any given organic Rankine cycle configuration. This total area can then be plugged into Equation (52) to yield a total cost.

Table 20: Relevant overall heat transfer coefficients for organics and steam.

Case #	Fluid 1	Fluid 2	U [W/m^2-K]	Source
1	liquid water	gaseous hydrogen containing natural gas mixtures	450-710	Biegler
2	boiling propane, butane, etc.	condensing steam	1140-1700	Biegler
3	boiling water	condensing steam	1420-2270	Biegler
4	liquid water	liquid water	800-2500	Mills
5	liquid light organics	liquid light organics	200-450	Mills

Table 21: Overall heat transfer coefficients used to estimate the heat exchanger sizes for the ORC and steam Rankine cycle cost model.

	U [W/m^2-K]	Description (Case # refers to Table 20)
U_{sens}	450	Case #1, with organic liquid instead of water – use the low end estimate
U_{lat}	1140	Case #2, with FT Reactor instead of condensing steam – use the low end estimate
$U_{sens,w}$	710	Case #1, use the high end estimate
$U_{lat,w}$	1420	Case #3, with FT Reactor instead of condensing steam – use the low end estimate
$U_{sup,w}$	450	Case #1, with steam instead of liquid water – use the low end estimate

of the heat exchanger network

4.2 Cost Model Results

4.2.1 Steam Rankine Cycle Costs

The steam Rankine cycle costs are calculated to understand any cost savings that may be realized when the FT Heat Source is no longer used to generate steam. These savings on the steam side will be used to offset the cost of implementing an organic Rankine cycle in the Fischer Tropsch plant.

First, it is important to appreciate how steam is used in the BP Polygeneration Plant Model. Heat sources throughout the plant are used to generate steam. Depending on the

Table 22: LP steam turbine inlet and exit fluid states, taken from the BP Polygeneration Plant Model.

	specific enthalpy	specific entropy	Temperature	Pressure	Quality	density
State	h (kJ/kg)	s (kJ/kg-K)	T (°C)	P (kPa)	Q (kg/kg)	ρ (kg/m^3)
inlet	2917.1	7.235	228.0	450	supercritical	1.982
exit	2407.3	7.352	38.7	6.895	0.932	0.05154

Table 23: Cost estimation for removing the FT Heat Source from the BP Polygeneration Plant Model steam island. A net reduction in power output of 93.6 MW saves $7.2 million.

Case	$\dot{W}_{turb}$ [MW]	$\dot{V}_{exit}$ [m^3/s]	Turbine Cost [million]	A_{tot} [m^3]	Heat Exchanger Cost [million]	Total Cost [million]
Basic BP Polygeneration Plant Model	483	18400	$43.4	N/A	N/A	$43.4
No FT Heat Source	394.2	15000	$39.1	-7469	-$1.3	$37.8
Net	-88.8	-3673	-$4.3	-7469	-$1.3	-$5.6

temperature at which the heat is available, it is used for low pressure (LP) steam, intermediate pressure (IP) steam, or high pressure (HP) steam. The steam is then transported in constant pressure steam headers to a "steam island", where it provides heat for process streams or is passed through turbines to generate power. In the baseline BP Polygeneration Plant model, the LP steam turbine has a work output of 483 MW. When the low pressure steam generated by the FT Heat Source is no longer available to the steam island, the size of the LP steam turbine will shrink, and this will result in cost savings. The LP turbine inlet and exit states, taken from the BP Polygeneration Plant Model, are given in Table 22.

A pinch analysis for a steam Rankine cycle using the FT heat source was presented in Chapter 3. The total work output of this steam cycle is 88.8 MW, and the inlet state (240°C, 450kPa) and exit state (40°C, 7.385kPa, 0.896 Quality) are very similar to the LP steam turbine in the Polygeneration Plant Model. Therefore, by removing the steam associated with the FT Heat Source from the steam plant, the LP turbine output will be reduced by 88.8 MW. The cost model results for the steam Rankine cycle are presented in Table 23.

4.2.2 ORC Costs

The removal of the FT Plant Heat Source from the BP Polygeneration Plant steam island has resulted in a decreased power output of 88.8 MW at a cost savings of $5.6 million. This low pressure steam will now be replaced with a stand alone organic Rankine cycle, local to the

Table 24: Cost model results for baseline organic Rankine cycles using the FT plant heat source. The value "net power output" includes the loss of power from the steam island due to removal of the FT plant heat source, and includes cycle pump work. The value "net cost" includes savings from the reduced size of the LP steam turbine. Cycle state points for all baseline cycles are included in Appendix I.

Working Fluid	$\dot{W}_{turb}$ [MW]	$\dot{V}_{exit}$ [m^3/s]	Turbine Cost [million]	A_{tot} [m^3]	Heat Exchanger Cost [million]	Cycle Cost [million]	Net Power Output [MW]	Net Cost [million]
Hexane	117.0	847.0	$10.3	54300	$9.5	$19.8	24.2	$14.2
Heptane	120.8	2242.8	$27.3	72100	$12.6	$39.9	29.8	$34.3
Octane	120.6	5855.1	$71.3	78100	$13.6	$84.9	30.6	$79.3
Nonane	120.1	15225.4	$185.3	81700	$14.3	$199.6	30.7	$194.0
Decane	119.8	39849.5	$485.0	83500	$14.6	$499.5	30.6	$493.9

Fischer Tropsch plant. Baseline cycles using the alkanes of hexane up to decane have been considered for their efficiency. Those same baseline cycles are plugged into the cost model, and the results are shown in Table 24. Hexane is predicted to have an total installed cost for the turbine and the

The cost model provides great clarity to the fluid selection process. For the FT heat source, with over 300 MW of heat rate available to an ORC, the volume flow through the turbine grows quickly as the size of the hydrocarbon chain increases from hexane up through decane. This causes the cost of turbo-machinery to increase prohibitively. Hexane is the clear winner for fluid choice, due to its small volume flow while still converting the heat source more efficiently than steam.

As a final step in the cost examination, the cost model is applied to estimate the cost of a customized cycle using hexane as the working fluid. This is the same customized cycle targeting the FT heat source that was analyzed previously in Section 3.5. The cycle schematic is reproduced here in Figure 4.8. This cycle includes two pressure loops, one high pressure (HP)

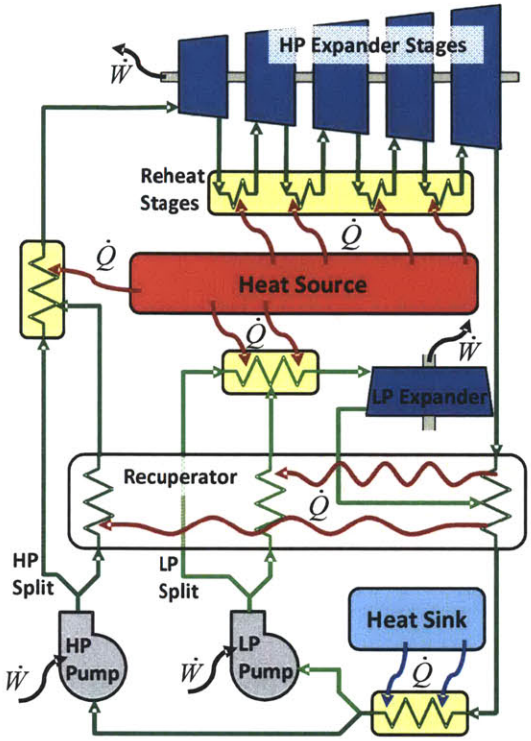

Figure 4.8: Custom cycle schematic for an ORC targeting the FT plant heat source. A high pressure loop and low pressure loop each pass through split recuperators. The high pressure loop also includes four reheat stages.

loop and one low pressure (LP) loop. Both loops have split recuperators, and there are four reheat stages on the HP loop, resulting in five HP turbine stages and one LP turbine stage.

The cost model is applied to the turbine stages by treating each individual stage as a separate turbine. This is a conservative estimate, because each turbine stage does not have its own condenser, but this is a simple way to reflect the additional complexity of reheat stages in the total equipment cost. Table 25 shows the cost results for the turbine stages in this customized hexane cycle.

Table 25: Turbine stage costs for the customized ORC using hexane as a working fluid.

Turbine Stage	$\dot{W}_{turb}$ [MW]	$\dot{V}_{exit}$ [m^3/s]	Turbine Stage Cost [million]
HP 1	15.1	19.6	$0.25
HP 2	22.9	59.8	$0.74
HP 3	24.7	149.8	$1.83
HP 4	25.4	363.3	$4.43
HP 5	25.6	871.0	$10.61
LP	13.0	122.7	$1.50
Turbine Total	126.7	N/A	$19.4

A total cost evaluation of the cycle customized cycle is included in Table 26. The baseline hexane cycle is also included for comparison.

The customized cycle cost with hexane as a working fluid validates the earlier choice to forego longer chain hydrocarbons in favor of hexane. The customized hexane cycle is estimated to cost slightly less than a baseline heptane cycle, while providing a larger improvement in power output. Using a rough assumption that electricity is valued at $0.10/kW-hr, a continuously operating baseline hexane ORC increases the polygeneration plant electricity revenue by $16.9 million/year. The custom hexane cycle, meanwhile, increases the polygeneration plant electricity revenue by $25.8 million/year. Based on this cost analysis,

Table 26: Overall cost results for the customized cycle using hexane as a working fluid. The capital expenditure for building a customized ORC to target the Fischer Tropsch heat source comes out to almost exactly $1000/kW.

cycle	$\dot{W}_{turb}$ [MW]	$\dot{V}_{exit}$ [m^3/s]	Turbine Cost [million]	A_{tot} [m^3]	Heat Exchanger Cost [million]	Cycle Cost [million]	Net Power Output [MW]	Net Cost [million]
Baseline	117.0	847.0	$10.3	54300	$9.5	$19.8	24.1	$14.2
Custom	126.7	Table 25	$19.4	98700	$17.2	$36.6	34.2	$31.0

either system is paid off in the first year and leads to increased revenues for the remaining life of the plant. It is highly worth considering a more advanced cost model to explore the details of replacing the low pressure steam in the FT plant with a customized hexane ORC.

4.2.3 Cost Model Future Work

The cost model presented in this thesis demonstrates the practical viability of organic Rankine cycles for replacing low pressure steam in the conversion of low grade heat sources into shaft work. Many of the assumptions which contributed to the cost model are subject to change over time. The assumption that a 15 MW organic turbine is current "state of the art" is likely already incorrect, and should be revisited as companies publish details of their newest technologies. Cost curves should be updated with some regularity to assure that modern manufacturing techniques and material costs are accounted for.

The current cost model can be used in greater depth to predict the effect of incremental design changes. The cost-benefit analysis has been presented here for a baseline hexane cycle and one configuration of a customized hexane cycle. It would be informative to explore more customized cycle configurations to understand the trade-off between cost and efficiency as the complexity of the cycle is increased or reduced. What if a third pressure level is included? What if only two reheat stages are used? These are questions which could be answered in the future.

Finally, the cost model may help the designer to choose appropriate parameters for the cycle. For all of the analysis presented here, the minimum allowable temperature difference has been set to 10°C. This assumption can be relaxed, allowing for a better understanding of the trade-off between performance and cost as the temperature difference between the heat sources and the heat exchanger network is varied.

4.3 Integrated Fischer Tropsch ORC System

The Fischer Tropsch reactor has thus far been considered for its usefulness as a source of low grade heat. Thorough analysis has shown hexane to be an efficient and cost effective working fluid for an organic Rankine cycle that operates off the heat of reaction from the FT reactor. But the FT reactor is useful as more than just a source of heat: it is also a source of hexane.

The FT reactor takes in a feed stream of syngas, composed primarily of CO and H_2, and in a catalyzed reaction it synthesizes the feed stream into a mixture of longer chain hydrocarbons ranging from methane (C_1) up as high as C_{64}. The product stream is passed to a distiller where various cuts of hydrocarbon size are separated out. It is possible to take a hexane cut off the distiller and feed it into an ORC.

There are myriad benefits to using a cut of the FT product stream to pick up heat in the FT reactor. The efficiency improvements have been discussed in detail. Furthermore, leaks between the shell side and the tube side of the reactor have little consequence, because the coolant (or working fluid) is one of the reactor products. More importantly, the FT plant provides an immediate source of working fluid such that the organic fluid can be continuously refreshed to maintain the integrity of the cycle as degradation occurs over time. The problems of fluid degradation were discussed in Section 2.3.2. Most organic Rankine cycles must operate in a limited temperature range to assure chemical stability, with maximum temperature usually ranging from 100°C to 300°C. By constantly refreshing the fluid, the upper temperature limit can be increased, because products of degradation are removed. Higher input temperatures lead to even more efficient cycles.

One possible manifestation of this integrated FT-ORC system is shown here in Figure 4.9. This example shows a fixed bed reactor, which is one of several options for the Fischer Tropsch reaction. A distillate taken from the Fischer Tropsch reactor product stream, in this case a hexane cut, is used as the working fluid for an organic Rankine cycle which has the Fischer

Tropsch reactor as its primary heat source. This working fluid can be recycled into the product stream after being used for the organic Rankine cycle. As seen in Figure 4.9, syngas enters the reactor at (1) and passes through catalyst packed tubes at (2) where the reaction occurs. Products flow out of the reactor at (3) and are separated by distillation downstream.

Constant reactor temperature is maintained, by boiling coolant at constant pressure on the shell side of the reactor. The heat transfer coefficient inside the reactor is kept high by maintaining a considerable coolant velocity across the tubes. Figure 4.9 shows a coolant recirculation loop at (4) which maintains high coolant velocity across the tubes even if the overall mass flow of coolant through the reactor is small. To avoid temperature gradients as coolant is injected into the reactor, the liquid coolant is introduced into the coolant recirculation stream at (5). The mass flow rate of the recirculation stream is significantly greater than that of the coolant inlet stream. This causes the heat capacity rate of the

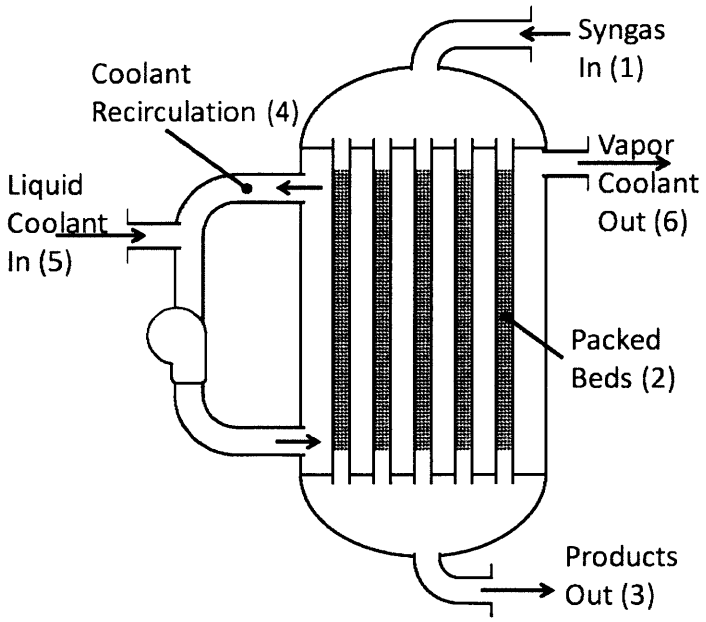

Figure 4.9: Fixed bed Fischer Tropsch reactor showing the path of the coolant (working fluid) for the integrated Fischer Tropsch – ORC System. Coolant recirculation maintains high fluid velocity across reactor tubes for maximum heat transfer, and allows colder fluid to enter the reactor without causing temperature gradients.

recirculation stream to be greater than the heat capacity rate of the liquid coolant inlet stream so that the reactor tubes will not be exposed to colder temperatures. It is important to maintain a constant temperature inside the reactor, because the catalyst (and therefore the product mix) is temperature sensitive.

Saturated vapor is drawn off the top of the reactor and used as the working fluid for an organic Rankine cycle, depicted in Figure 4.10 below. The numbering scheme has been maintained from previous chapters. The high pressure vapor at State 5 is passed through an expander to generate shaft work. The expander exit stream is superheated vapor at State 6 which can be passed through a recuperator. The low pressure vapor exits the recuperator at State 7 and is cooled to the saturation temperature at State 8 before being condensed to a saturated liquid at State 1 and then pumped to high pressure at State 2. The high pressure

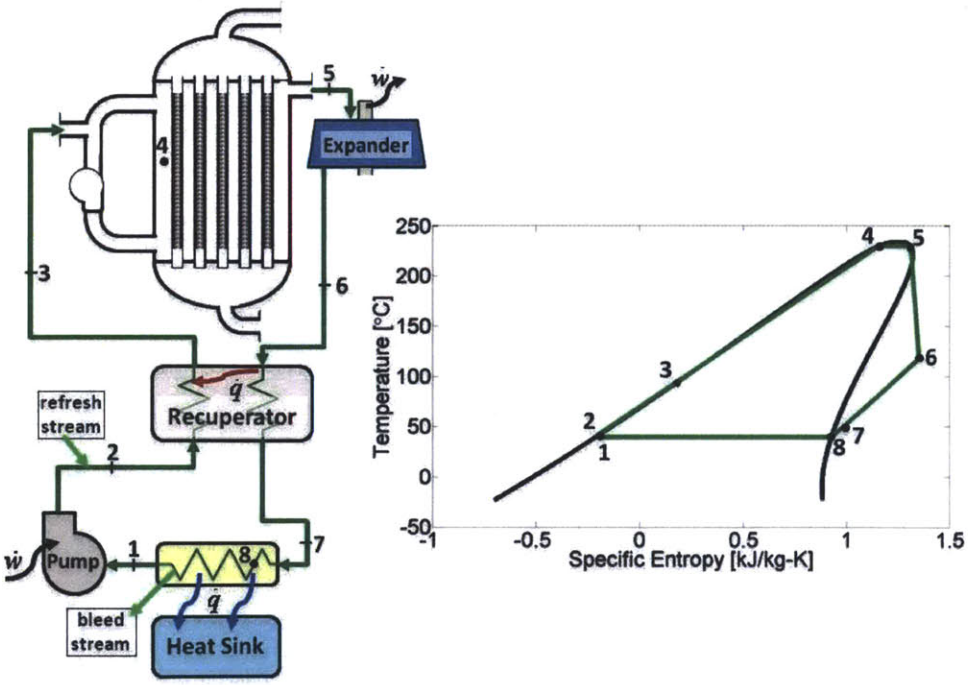

Figure 4.10: Integrated FT-ORC system schematic diagram with related states depicted on a *T-s* diagram. The cycle working fluid is constantly recycled by bleeding off non-condensable gases and some liquid from the condenser and introducing a refresh stream from the distiller into the pressurized liquid at State 2.

liquid stream is preheated in the recuperator before being returned to the reactor as a coolant at State 3. Non-condensable gases and other degraded fluid components are bled off the condenser, and additional working fluid from the distiller is fed into the cycle at State 2.

The hexane cycles explored in this thesis have assumed pure hexane as a working fluid. In reality, the purity of the hexane is determined by the degree of distillation. The cost of distillation increases non-linearly with the required purity. Table 27 contains fluid states for a baseline hexane cycle, using the numbering scheme in Figure 4.10. The working fluid states in Table 27 were not calculated using pure hexane, but were calculated with a hypothetical cut off the distiller comprised of 90% hexane, 5% pentane, and 5% heptane by mass. As discussed earlier in Section 3.4.6, constant pressure phase changes do not happen at constant temperature for a fluid mixture. In this case, there is a small 0.6°C temperature glide during

Table 27: Organic Rankine cycle states for a baseline ORC with heat source and sink of 240°C and 30°C respectively. Expander and pump efficiencies assumed to be 0.9. The working fluid is a hexane mixture, consisting of 90% hexane, 5% pentane, and 5% heptane by mass.

State	h (kJ/kg)	s (kJ/kg-K)	T (°C)	P (kPa)	Q	ρ (kg/m^3)
1	-62.664	-0.1918	40	41.127	0	639.91
2rev	-58.252	-0.1918	40.9	2870.0	subcooled	642.73
2	-57.762	-0.1902	41.1	2870.0	subcooled	642.53
3	74.579	-0.1978	95.3	2870.0	subcooled	590.33
4	499.56	1.1672	229.4	2870.0	0	327.39
5	580.01	1.3272	230	2870.0	1	147.30
6rev	429.19	1.3272	112.1	41.127	superheated	1.117
6	444.19	1.3658	119.4	41.127	superheated	1.096
7	311.85	0.9963	51.1	41.127	superheated	1.343
8	298.33	0.9540	43.5	41.127	1	1.378

Table 28: Organic Rankine cycle characteristics for a baseline ORC with heat source and sink of 240°C and 30°C respectively. Expander and pump efficiencies assumed to be 0.9. The hexane mixture working fluid is of 90% hexane, 5% pentane, and 5% heptane by mass.

Fluid	w_{exp} [kJ/kg]	w_{pump} [kJ/kg]	w_{net} [kJ/kg]	q_{rec} [kJ/kg]	q_{in} [kJ/kg]	η_{cyc}	η_{Carnot}	η_{opt}
Hexane	138.3	-4.9	133.5	129.4	508.5	26.3%	40.9%	64.2%
Hexane Mixture	135.8	-4.9	130.9	132.3	505.5	25.9%	40.9%	63.3%

isobaric boiling from State 4 to State 5, and a temperature glide of 3.5°C during isobaric condensation from State 8 to State 1. Given constant temperature heat source and heat sink, this glide will reduce cycle efficiency.

The cycle characteristics for the ORC using the hexane mixture are shown in Table 28, along with the cycle characteristics for the pure hexane cycle. The impurities in the hexane have decreased the cycle efficiency from 26.3% efficient to 25.9% efficient. This is not a significant concern. Verily, distillation costs do not pose a significant barrier to implementation of an integrated FT-ORC system.

4.4 Conclusions

The BP-MIT Conversion Project has undertaken the study of a coal-fed polygeneration plant as part of a larger effort to improve the efficiency of natural resource consumption. This polygeneration plant has been analyzed for heat integration opportunities which might yield efficiency improvements. The plant's abundant supply of low-grade heat, primarily used to generate low pressure steam, is a source of inefficiency which was targeted in this thesis.

The largest source of low grade heat in the polygeneration plant is the Fischer Tropsch reactor, which converts syngas into liquids and waxes. The FT reactor produces 309 MW of heat rate at a constant temperature of 240°C. Including the processes surrounding the reactor, the Fischer Tropsch plant outputs a heat rate of 431 MW. The polygeneration plant has an HHV input rate for coal of 8014 MW, meaning that the FT plant represents 5.4% of the overall plant

heat source. Small improvements to conversion of the heat supplied by the FT plant yield significant gains.

Various organic materials were analyzed as potential working fluids to operate a Rankine cycle integrated into the FT plant. Alkanes ranging in size from hexane up to decane show great promise for efficiency improvements, but an equipment cost analysis clearly indicates that hexane is the best choice of working fluid out of those considered. Longer chain alkanes are slightly more efficient than hexane, but significantly more expensive. For instance, if the working fluid is changed from hexane to heptane, the efficiency of a baseline ORC using the FT heat source will improve from 26.2% to 27.5%, but the equipment cost more than doubles.

An organic Rankine cycle using hexane as the working fluid can be integrated into the Fischer Tropsch plant, using the available heat rate more efficiently than steam. The baseline hexane cycle achieves a 26.2% conversion efficiency of the FT heat source, while a low pressure steam cycle only achieves 20.6% efficiency. Thus, the hexane ORC improves overall plant power output by 24.2 MW. This represents an improvement of 0.3 points if considered against the HHV input rate of coal to the plant, but is an improvement of 1.3% on the overall electricity output of the polygeneration plant, which is a significant gain.

The hexane ORC can be further integrated into the Fischer Tropsch plant by constructing a customized cycle that targets the temperature profile available from the FT heat source. The heat requirement profile of the ORC is manipulated to match the heat source by routing the working fluid through the cycle to achieve the best possible recuperation, reheating the working fluid between multiple expander stages to absorb more heat at the FT reactor temperature, and including an extra pressure level to use all of the heat available to temperatures as low as 100°C. These changes yield a customized cycle which converts the FT heat source with an efficiency of 28.5%, yielding an increase in the overall electricity output of

34.2 MW. That is 0.4 points improvement on the conversion of the HHV input rate of coal into the plant, and a 1.8% increase of electricity output for the polygeneration plant.

Furthermore, the building blocks used to create the customized hexane ORC have utility beyond this isolated example. This work has presented a set of building blocks, including reheat stages, pressure levels, split flow recuperators, and supercritical cycles, and has demonstrated that these building blocks can be combined to target the Fischer Tropsch plant heat source profile with great success. Using these same building blocks, an ORC can be designed to match an arbitrary heat source profile, so that a skilled designer can quickly configure a cycle to fully and efficiently utilize a complex heat source.

The final contribution of this work was to identify the complimentary nature of organic Rankine cycles and the Fischer Tropsch process. Hexane is one of the products of the Fischer Tropsch reaction, and therefore is readily available from the distiller in the FT plant. Leaks between the reactor and coolant are of little consequence if hexane is the coolant, and there are not additional safety and environmental concerns introduced when the working fluid chosen is already handled by the plant. Constantly refreshing the hexane working fluid in the ORC can prevent degradation of the working fluid, and improve the reliability of the ORC operation.

In conclusion, this thesis has considered the BP Polygeneration Plant and identified the Fischer Tropsch reactor as a prime candidate for integrating an organic Rankine cycle to increase overall plant efficiency. Various fluids and cycle configurations were analyzed, and it has been shown that an organic Rankine cycle using hexane as the working fluid results in significant efficiency gains, and is uniquely suited to integration into the Fischer Tropsch plant.

Works Cited

Andersen, W. C., & Bruno, T. J. (2005). Rapid Screening of Fluids for Chemical Stability in Organic Rankine Cycle Applications. *Industrial Engineering and Chemistry Research* , 5560-5566.

Biegler, L. T., Grossmann, I. E., & Westerberg, A. W. (1997). *Systematic Methods of Chemical Process Design.* Prentice Hall.

Bronicki, L. Y., & Schochet, D. N. (2005). Bottoming Organic Cycle for Gas Turbines. *ASME Turbo Expo 2005: Power for Land, Sea, and Air.* Reno-Tahoe, Nevada: ASME.

Bureau of Labor Statistics CPI Inflation Calculator. (n.d.). Retrieved August 18, 2011, from United States Department of Labor: http://www.bls.gov/data/inflation_calculator.htm

Calderazzi, L., & di Paliano, P. C. (1997). Thermal stability of R-134a, R-141b, R-13I1, R-7146, R-125 associated with stainless steel as a containing material. *International Journal of Refrigeration , 20* (6), 381-389.

Doty, F. D., & Siddarth, S. (2009). A Dual-Source Organic Rankine Cycle (DORC) for Improved Efficiency in Conversion of Dual Low- and Mid-Grade Heat Sources. *Proceedings of the ASME 2009 3rd International Conference of Energy Sustainability.* San Francisco, CA.

Forster, P., Ramaswamy, V., Artaxo, P., Berntsen, T., Betts, R., Fahey, D. W., et al. (2007). Changes in Atmospheric Constituents and in Radiative Forcing. In S. Solomon, D. Qin, M. Manning, Z. Chen, M. Marquis, K. B. Averyt, et al., *Climate Change 2007: The Physical Science Basis. Contribution of Working Group I to the Fourth Assessment*

Report of the Intergovernmental Panel on Climate Change. Cambridge, United Kingdom and New York, NY, USA: Cambridge University Press.

International Energy Agency. (2010). *World Energy Outlook 2010 Executive Summary.* Paris, France.

Jain, M. L., Demirgian, J., Krazinski, J. L., Bushby, H., & Mattes, H. (1984). *Determination of Thermal-Degradation Rates of Some Candidate Rankine-Cycle Organic Working Fluids for Conversion of Industrial Waste Heat into Power.* Argonne, IL: Argonne National Lab.

Lemmon, E. W., Huber, M. L., & McLinden, M. O. (2007). NIST Standard Reference Database 23: Reference Fluid Thermodynamic and Transport Properties-REFPROP, Version 8.0. Gaithersburg, MD: National Institute of Standards and Technology.

Leyzerovich, A. S. (2005). *Wet-steam Turbines for Nuclear Power Plants.* Tulsa, OK: Pennwell.

Linnhoff, B., Townsend, D. W., Boland, D., Hewitt, G. F., Thomas, B. A., Guy, A. R., et al. (1994). *A User Guide on Process Integration for the Efficient Use of Energy.* Warwick, UK: Warwick Printing Company Ltd.

Loh, H. P., Lyons, J., & White, C. W. (2002). *Process Equipment Cost Estimation Final Report.* Pittsburgh, PA: DOE/NETL.

Mills, A. F. (1995). *Heat and Mass Transfer.* Chicago: Richard D. Irwin, Inc.

Morgan, D., Mills, K., Zakak, A., Reinhold, V., & Carr, S. (1982). *Determination of the Thermal Stability of Organic Working Fluids Used in Rankine-Cycle Power Systems for Solar Cooling.* Waltham, MA: Thermo Electron Corp.

National Institute for Occupational Safety and Health. (2005). *NIOSH Pocket Guide to Chemical Hazards.* Cincinnati, Ohio: Dept. of Health and Human Services, Centers for Disease Control and Prevention.

Nordquist, J. (2010, 12 16). Manager of Sales, Geothermal Development, ORMAT. (K. J. DiGenova, Interviewer)

Quoilin, S., & Lemort, V. (2009). Technological and Economical Survey of Organic Rankine Cycle Systems. *5th European Conference on Economics and Management of Energy in Industry.* Vilamoura, Algarve, Portugal.

Serra, L. M., Lozano, M.-A., Ramos, J., Ensinas, A. V., & Silvia, N. A. (2009). Polygeneration and efficient use of natural resources. *Energy* , 575-586.

Shenoy, U. V., Sinha, A., & Bandyopadhyay, S. (1998). Multiple Utilities Targeting for Heat Exchanger Networks. *Chemical Engineering Research and Design* , 259-272.

Tabor, H. Z., & Bronicki, L. (1962). *Patent No. 3,040,528.* Jerusalem, Israel.

Van Bibber, L., Shuster, E., Haslbeck, J., Rutkowski, M., Olson, S., & Kramer, S. (2007). *Baseline Technical and Economic Assessment of a Commercial Scale Fischer-Tropsch Liquids Facility.* DOE/NETL.

Woods, M. C., Capicotto, P. J., Haslbeck, J. L., Kuehn, N. J., Matuszewski, M., Pinkerton, L. L., et al. (Revision 2, 2010). *Cost and Performance Baseline for Fossil Energy Plants. Volume 1: Bituminous Coal and Natural Gas to Electricity Final Report.* U.S. Department of Energy, National Energy Technology Laboratory. National Energy Technology Laboratory.

Appendices

Appendix I: Baseline Cycle States

Table 29: Organic Rankine cycle states for a baseline hexane cycle with heat source and sink of 240°C and 30°C respectively. Expander and pump efficiencies assumed to be 0.9.

State	h (kJ/kg)	s (kJ/kg-K)	T (°C)	P (kPa)	Q	ρ (kg/m^3)
1	-68.50	-0.209	40	37.29	0	640.74
2rev	-64.13	-0.209	40.9	2843	Subcooled	643.53
2	-63.64	-0.207	41.1	2843	Subcooled	643.34
3	57.87	0.151	91.1	2843	Subcooled	595.43
4	495.50	1.153	230	2843	0	326.95
5	574.20	1.310	230	2843	1	147.14
6rev	420.54	1.310	110.5	37.29	Superheated	1.019
6	435.89	1.350	118.0	37.29	Superheated	0.9988
7	306.53	0.988	51.1	37.29	Superheated	1.2182

Table 30: Organic Rankine cycle states for a baseline heptane cycle with heat source and sink of 240°C and 30°C respectively. Expander and pump efficiencies assumed to be 0.9.

State	h (kJ/kg)	s (kJ/kg-K)	T (°C)	P (kPa)	Q	ρ (kg/m^3)
1	-141.64	-0.414	40	12.33	0	666.72
2rev	-139.27	-0.414	40.4	1595	Subcooled	668.10
2	-139.00	-0.413	40.5	1595	Subcooled	668.00
3	38.61	0.095	112.9	1595	Subcooled	603.02
4	387.75	0.880	230	1595	0	441.37
5	559.54	1.222	230	1595	1	61.706
6rev	393.56	1.222	133.0	12.33	Superheated	0.3674
6	410.15	1.262	140.7	12.33	Superheated	0.3604
7	232.54	0.780	50.5	12.33	Superheated	0.4638

Table 31: Organic Rankine cycle states for a baseline octane cycle with heat source and sink of 240°C and 30°C respectively. Expander and pump efficiencies assumed to be 0.9.

State	h (kJ/kg)	s (kJ/kg-K)	T (°C)	P (kPa)	Q	ρ (kg/m^3)
1	-210.66	-0.593	40	4.126	0	686.04
2rev	-209.31	-0.593	40.2	935.9	Subcooled	686.82
2	-209.15	-0.592	40.3	935.9	Subcooled	686.77
3	-12.56	-0.035	120.7	935.9	Subcooled	618.46
4	305.00	0.673	230	935.9	0	491.82
5	512.69	1.086	230	935.9	1	34.770
6rev	342.42	1.086	141.73	4.126	Superheated	0.1369
6	359.46	1.127	149.5	4.126	Superheated	0.1344
7	162.86	0.599	50.3	4.126	Superheated	0.1761

Table 32: Organic Rankine cycle states for a baseline nonane cycle with heat source and sink of 240°C and 30°C respectively. Expander and pump efficiencies assumed to be 0.9.

State	h (kJ/kg)	s (kJ/kg-K)	T (°C)	P (kPa)	Q	ρ (kg/m^3)
1	-276.12	-0.751	40	1.414	0	702.14
2rev	-275.33	-0.751	40.1	564.2	Subcooled	702.57
2	-275.23	-0.751	40.2	564.2	Subcooled	702.54
3	-67.71	-0.167	125.3	564.2	Subcooled	632.62
4	231.77	0.499	230	564.2	0	525.63
5	457.72	0.948	230	564.2	1	21.489
6rev	285.87	0.948	146.8	1.414	Superheated	0.05197
6	303.05	0.988	154.6	1.414	Superheated	0.05102
7	95.52	0.435	50.2	1.414	Superheated	0.06759

Table 33: Organic Rankine cycle states for a baseline decane cycle with heat source and sink of 240°C and 30°C respectively. Expander and pump efficiencies assumed to be 0.9.

State	h (kJ/kg)	s (kJ/kg-K)	T (°C)	P (kPa)	Q	ρ (kg/m^3)
1	-338.74	-0.894	40	0.4867	0	714.78
2rev	-338.26	-0.894	40.1	348.6	Subcooled	715.03
2	-338.19	-0.894	40.1	348.6	Subcooled	715.01
3	-124.85	-0.295	128.0	348.6	Subcooled	644.82
4	164.30	0.345	230	348.6	0	547.75
5	400.13	0.814	230	348.6	1	13.965
6rev	227.54	0.814	149.5	0.4867	Superheated	0.01972
6	244.82	0.854	157.3	0.4867	Superheated	0.01936
7	31.45	0.287	51.0	0.4867	Superheated	0.02579

Table 34: Steam Rankine cycle states for a baseline cycle with heat source and sink of 240°C and 30°C respectively. Expander and pump efficiencies assumed to be 0.9.

State	h [kJ/kg]	s [kJ/kg-K]	T [°C]	P [kPa]	Q [kg/kg]	ρ [kg/m^3]
1	167.5	0.572	40	7.39	0	992.2
2rev	168.0	0.572	40.01	450	subcooled	992.4
2	168.0	0.573	40.03	450	subcooled	992.4
3	623.1	1.821	147.9	450	0	919.0
4	2743.4	6.856	147.9	450	1	2.416
5	2921.3	7.243	230	450	superheated	1.974
6rev	2256.4	7.243	40	7.39	0.868	0.05902
6	2322.8	7.455	40	7.39	0.896	0.05720

Table 35: Cycle characteristics for baseline Rankine cycles with wet working fluids (water and ethanol) and various dry organic working fluids. Assumes constant temperature heat source and sink at 240°C and 30°C respectively. Expander and pump efficiencies assumed to be 0.9. The Baumann Rule is applied for wet fluids.

Fluid	Y_{avg} [kg/kg]	w_{exp} [kJ/kg]	w_{pump} [kJ/kg]	w_{net} [kJ/kg]	q_{rec} [kJ/kg]	q_{in} [kJ/kg]	η_{cyc}	η_{Carnot}	η_{opt}
Water	0.0521	567.3	-0.5	566.8	N/A	2753.3	20.6%	40.9%	50.3%
Ethanol	0.05	283.6	-6.7	276.9	N/A	1091.4	25.4%	40.9%	62.0%
Hexane	N/A	138.3	-4.9	133.5	129.4	508.5	26.3%	40.9%	64.2%
Heptane	N/A	149.4	-2.6	146.8	177.6	520.9	28.2%	40.9%	68.6%
Octane	N/A	153.2	-1.5	151.7	196.6	525.2	28.9%	40.9%	70.6%
Nonane	N/A	154.7	-0.9	153.8	207.5	525.4	29.3%	40.9%	71.5%
Decane	N/A	155.3	-0.5	154.8	213.4	525.0	29.5%	40.9%	72.0%
Dodecane	N/A	156.4	-0.2	156.2	220.8	526.4	29.7%	40.9%	72.5%
Cyclohexane	N/A	157.0	-3.0	154.0	108.4	551.9	27.9%	40.9%	68.2%
Toluene	N/A	166.9	-1.6	165.3	76.9	581.9	28.4%	40.9%	69.4%

Appendix II: Fischer Tropsch Plant Stream Data

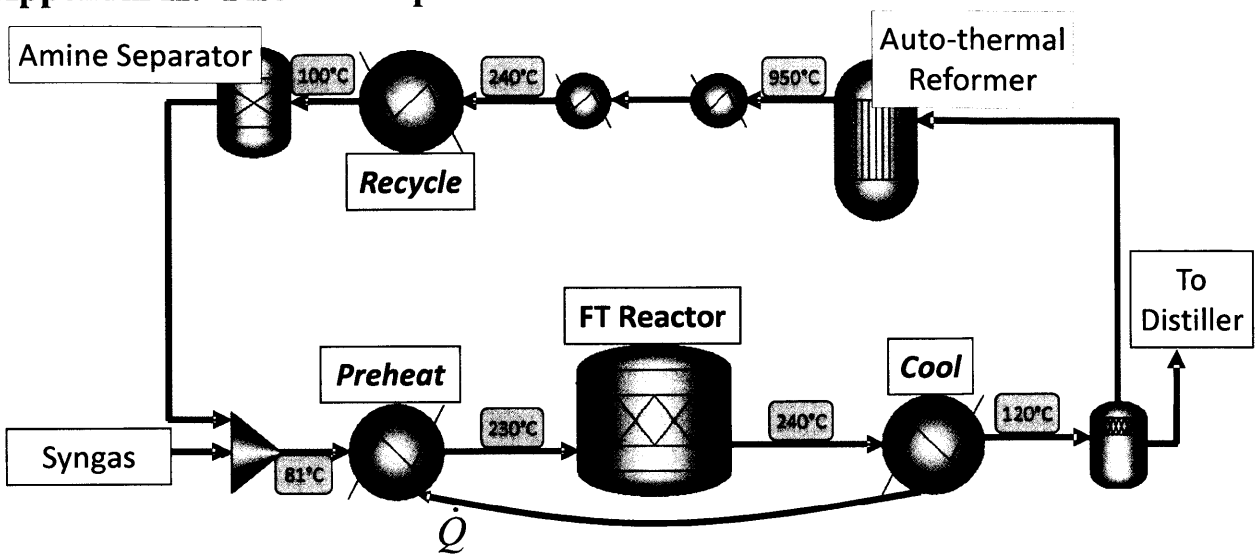

Figure A.1: Fischer Tropsch plant schematic showing relevant stream mass flows. Syngas entering the plant is preheated from 81°C to 230°C before entering the reactor, "Stream Preheat". Hydrocarbon products exiting the reactor are cooled from 240°C to 120°C, "Stream Cool". Light gases are recycles, and heat is used for the ORC as they cool from 240°C to 100°C, "Stream Recycle".

Stream data in the tables below were calculated in Aspen Plus® using the Peng-Robinson equation of state with the Boston-Mathias alpha function (PR-BM).

Table 36: Temperature vs. Change in Enthalpy per Time data for "Stream Recycle" as it cools from 240°C down to 100°C. The composition of "Stream Recycle" is, by mole fraction: 0.179 CO; 0.0978 CO_2; 0.361 H_2; 0.288 H_2O; 0.0634 N_2; 0.0110 AR; and trace amounts of HCl;

T	$\Delta\dot{H}$	T	$\Delta\dot{H}$	T	$\Delta\dot{H}$	T	$\Delta\dot{H}$	T	$\Delta\dot{H}$	T	$\Delta\dot{H}$	T	$\Delta\dot{H}$
[°C]	[MW]	[°C]	[MW]	[°C]	[MW]	[°C]	[MW]	[°C]	[MW]	[°C]	[MW]	[°C]	[MW]
100.0	0.00	126.1	10.99	143.8	21.54	157.0	32.08	167.2	42.63	175.4	53.18	191.2	63.29
101.2	0.44	126.9	11.43	144.4	21.98	157.5	32.52	167.6	43.07	175.7	53.62	194.1	63.73
102.5	0.88	127.8	11.87	145.0	22.42	157.9	32.96	168.0	43.51	176.0	54.06	196.9	64.17
104.9	1.76	128.6	12.31	145.6	22.85	158.4	33.40	168.3	43.95	176.3	54.50	199.8	64.61
106.0	2.20	129.4	12.75	146.2	23.29	158.9	33.84	168.7	44.39	176.6	54.94	202.6	65.05
107.2	2.64	130.2	13.19	146.8	23.73	159.3	34.28	169.1	44.83	176.9	55.38	205.5	65.49
108.3	3.08	131.0	13.62	147.4	24.17	159.8	34.72	169.4	45.27	177.2	55.82	208.3	65.93
109.4	3.52	131.8	14.06	148.0	24.61	160.2	35.16	169.8	45.71	177.5	56.26	211.1	66.37
110.5	3.96	132.6	14.50	148.6	25.05	160.7	35.60	170.1	46.15	177.8	56.70	214.0	66.80
111.6	4.39	133.4	14.94	149.2	25.49	161.1	36.04	170.5	46.59	178.1	57.14	216.8	67.24
112.7	4.83	134.1	15.38	149.7	25.93	161.5	36.48	170.8	47.03	178.3	57.57	219.7	67.68
113.7	5.27	134.9	15.82	150.3	26.37	162.0	36.92	171.2	47.47	178.6	58.01	222.5	68.12
114.8	5.71	135.6	16.26	150.8	26.81	162.4	37.36	171.5	47.91	178.9	58.45	225.4	68.56
115.8	6.15	136.4	16.70	151.4	27.25	162.8	37.80	171.9	48.35	179.2	58.89	228.2	69.00
116.8	6.59	137.1	17.14	151.9	27.69	163.2	38.24	172.2	48.79	179.4	59.33	231.0	69.44
117.8	7.03	137.8	17.58	152.4	28.13	163.7	38.68	172.5	49.22	179.7	59.77	233.9	69.88
118.8	7.47	138.5	18.02	153.0	28.57	164.1	39.12	172.9	49.66	180.0	60.21	236.7	70.32
119.7	7.91	139.2	18.46	153.5	29.01	164.5	39.56	173.2	50.10	180.3	60.65	239.6	70.76
120.7	8.35	139.9	18.90	154.0	29.45	164.9	40.00	173.5	50.54	180.5	61.09	242.4	71.20
121.6	8.79	140.5	19.34	154.5	29.89	165.3	40.43	173.8	50.98	180.8	61.53		
122.5	9.23	141.2	19.78	155.0	30.33	165.7	40.87	174.1	51.42	180.9	61.69		
123.4	9.67	141.9	20.22	155.5	30.77	166.1	41.31	174.5	51.86	182.7	61.97		
124.3	10.11	142.5	20.66	156.0	31.20	166.4	41.75	174.8	52.30	185.6	62.41		
125.2	10.55	143.1	21.10	156.5	31.64	166.8	42.19	175.1	52.74	188.4	62.85		

Table 37: Temperature vs. Change in Enthalpy per Time data for "Stream Cool" as it cools from 240°C down to 120°C. The composition of "Stream Cool" is, by mole fraction: 0.178 CO; 0.049 CO_2; 0.333 H_2; 0.324 H_2O; 0.063 N_2; 0.011 Ar; and hydrocarbons, 0.025 (C_1-C_4); 0.008 (C_5-C_{11}), 0.005 (C_{12}-C_{22}), 0.004 (C_{23}-C_{64}).

T	$\Delta\dot{H}$	T	$\Delta\dot{H}$	T	$\Delta\dot{H}$	T	$\Delta\dot{H}$	T	$\Delta\dot{H}$	T	$\Delta\dot{H}$	T	$\Delta\dot{H}$
[°C]	[MW]	[°C]	[MW]	[°C]	[MW]	[°C]	[MW]	[°C]	[MW]	[°C]	[MW]	[°C]	[MW]
120.0	0.00	138.0	13.50	151.7	27.01	162.5	40.52	171.0	54.02	178.0	67.53	195.4	81.03
120.7	0.47	138.6	13.97	152.2	27.48	162.8	40.98	171.3	54.49	178.3	67.99	197.1	81.50
121.4	0.93	139.1	14.44	152.6	27.94	163.1	41.45	171.6	54.95	178.5	68.46	198.9	81.96
122.1	1.40	139.6	14.90	153.0	28.41	163.4	41.91	171.8	55.42	178.7	68.92	200.6	82.43
122.8	1.86	140.1	15.37	153.4	28.87	163.8	42.38	172.1	55.88	178.9	69.39	202.3	82.89
123.5	2.33	140.7	15.83	153.8	29.34	164.1	42.84	172.3	56.35	179.1	69.85	204.0	83.36
124.2	2.79	141.2	16.30	154.2	29.80	164.4	43.31	172.6	56.82	179.3	70.32	205.7	83.83
124.8	3.26	141.7	16.76	154.6	30.27	164.7	43.78	172.9	57.28	179.5	70.79	207.4	84.29
125.5	3.73	142.2	17.23	155.0	30.74	165.0	44.24	173.1	57.75	179.8	71.25	209.2	84.76
126.2	4.19	142.7	17.70	155.3	31.20	165.3	44.71	173.4	58.21	180.0	71.72	210.9	85.22
126.8	4.66	143.2	18.16	155.7	31.67	165.6	45.17	173.6	58.68	180.2	72.18	212.6	85.69
127.5	5.12	143.7	18.63	156.1	32.13	165.9	45.64	173.9	59.14	180.4	72.65	214.3	86.15
128.1	5.59	144.1	19.09	156.5	32.60	166.2	46.10	174.1	59.61	180.6	73.11	216.0	86.62
128.7	6.05	144.6	19.56	156.9	33.06	166.5	46.57	174.3	60.08	180.8	73.58	217.7	87.08
129.3	6.52	145.1	20.02	157.2	33.53	166.8	47.04	174.6	60.54	181.0	74.05	219.5	87.55
130.0	6.99	145.6	20.49	157.6	34.00	167.1	47.50	174.8	61.01	181.2	74.51	221.2	88.02
130.6	7.45	146.0	20.96	158.0	34.46	167.4	47.97	175.1	61.47	181.4	74.98	222.9	88.48
131.2	7.92	146.5	21.42	158.3	34.93	167.7	48.43	175.3	61.94	181.6	75.44	224.6	88.95
131.8	8.38	147.0	21.89	158.7	35.39	168.0	48.90	175.5	62.40	181.8	75.91	226.3	89.41
132.4	8.85	147.4	22.35	159.0	35.86	168.3	49.36	175.8	62.87	182.0	76.37	228.0	89.88
133.0	9.31	147.9	22.82	159.4	36.32	168.6	49.83	176.0	63.33	182.2	76.84	229.7	90.34
133.6	9.78	148.3	23.28	159.7	36.79	168.9	50.30	176.2	63.80	182.4	77.31	231.5	90.81
134.1	10.25	148.7	23.75	160.1	37.26	169.1	50.76	176.5	64.27	183.4	77.77	233.2	91.28
134.7	10.71	149.2	24.22	160.4	37.72	169.4	51.23	176.7	64.73	185.1	78.24	234.9	91.74
135.3	11.18	149.6	24.68	160.8	38.19	169.7	51.69	176.9	65.20	186.9	78.70	236.6	92.21
135.8	11.64	150.1	25.15	161.1	38.65	170.0	52.16	177.2	65.66	188.6	79.17	238.3	92.67
136.4	12.11	150.5	25.61	161.5	39.12	170.2	52.62	177.4	66.13	190.3	79.63	240.0	93.14
136.9	12.57	150.9	26.08	161.8	39.58	170.5	53.09	177.6	66.59	192.0	80.10		
137.5	13.04	151.3	26.54	162.1	40.05	170.8	53.56	177.8	67.06	193.7	80.57		

Table 38: Temperature vs. Change in Enthalpy per Time data for "Stream Preheat" as it heats from 81°C down to 240°C. The composition of "Stream Preheat" is, by mole fraction: 0.308 CO; 0.028 CO_2; 0.619 H_2; 0.001 H_2O; 0.038 N_2; 0.007 Ar; and trace amounts of O_2, HCl, CH_4.

T	$\Delta\dot{H}$	T	$\Delta\dot{H}$	T	$\Delta\dot{H}$	T	$\Delta\dot{H}$	T	$\Delta\dot{H}$	T	$\Delta\dot{H}$	T	$\Delta\dot{H}$
[°C]	[MW]	[°C]	[MW]	[°C]	[MW]	[°C]	[MW]	[°C]	[MW]	[°C]	[MW]	[°C]	[MW]
81.0	0.00	104.1	6.53	127.2	13.06	150.3	19.60	173.4	26.13	196.4	32.66	219.4	39.19
81.8	0.23	104.9	6.76	128.0	13.29	151.1	19.82	174.2	26.35	197.2	32.88	220.2	39.42
82.6	0.45	105.7	6.98	128.8	13.51	151.9	20.05	174.9	26.58	198.0	33.11	221.0	39.64
83.4	0.68	106.5	7.21	129.6	13.74	152.7	20.27	175.7	26.80	198.8	33.33	221.8	39.87
84.2	0.90	107.3	7.43	130.4	13.96	153.5	20.50	176.5	27.03	199.6	33.56	222.6	40.09
85.0	1.13	108.1	7.66	131.2	14.19	154.3	20.72	177.3	27.25	200.4	33.79	223.4	40.32
85.8	1.35	108.9	7.88	132.0	14.42	155.1	20.95	178.1	27.48	201.2	34.01	224.2	40.54
86.6	1.58	109.7	8.11	132.8	14.64	155.9	21.17	178.9	27.70	201.9	34.24	224.9	40.77
87.4	1.80	110.5	8.33	133.6	14.87	156.7	21.40	179.7	27.93	202.7	34.46	225.7	40.99
88.2	2.03	111.3	8.56	134.4	15.09	157.5	21.62	180.5	28.15	203.5	34.69	226.5	41.22
89.0	2.25	112.1	8.78	135.2	15.32	158.3	21.85	181.3	28.38	204.3	34.91	227.3	41.44
89.8	2.48	112.9	9.01	136.0	15.54	159.0	22.07	182.1	28.61	205.1	35.14	228.1	41.67
90.6	2.70	113.7	9.23	136.8	15.77	159.8	22.30	182.9	28.83	205.9	35.36	228.9	41.89
91.4	2.93	114.5	9.46	137.6	15.99	160.6	22.52	183.7	29.05	206.7	35.59	229.7	42.12
92.2	3.15	115.3	9.68	138.4	16.22	161.4	22.75	184.5	29.28	207.5	35.81	230.5	42.34
93.0	3.38	116.1	9.91	139.2	16.44	162.2	22.97	185.3	29.51	208.3	36.04	231.3	42.57
93.8	3.60	116.9	10.14	140.0	16.67	163.0	23.20	186.1	29.73	209.1	36.26	232.1	42.79
94.6	3.83	117.7	10.36	140.8	16.89	163.8	23.42	186.9	29.96	209.9	36.49	232.9	43.02
95.4	4.05	118.5	10.59	141.5	17.12	164.6	23.65	187.7	30.18	210.7	36.71	233.7	43.24
96.2	4.28	119.3	10.81	142.3	17.34	165.4	23.87	188.4	30.41	211.5	36.94	234.5	43.47
96.9	4.51	120.1	11.04	143.1	17.57	166.2	24.10	189.2	30.63	212.3	37.16	235.3	43.70
97.7	4.73	120.9	11.26	143.9	17.79	167.0	24.33	190.0	30.86	213.1	37.39	236.0	43.92
98.5	4.96	121.6	11.49	144.7	18.02	167.8	24.55	190.8	31.08	213.8	37.61	236.8	44.15
99.3	5.18	122.4	11.71	145.5	18.24	168.6	24.78	191.6	31.31	214.6	37.84	237.6	44.37
100.1	5.41	123.2	11.94	146.3	18.47	169.4	25.00	192.4	31.53	215.4	38.06	238.4	44.60
100.9	5.63	124.0	12.16	147.1	18.69	170.2	25.23	193.2	31.76	216.2	38.29	239.2	44.82
101.7	5.86	124.8	12.39	147.9	18.92	171.0	25.45	194.0	31.98	217.0	38.52	240.0	45.05
102.5	6.08	125.6	12.61	148.7	19.14	171.8	25.68	194.8	32.21	217.8	38.74		
103.3	6.31	126.4	12.84	149.5	19.37	172.6	25.90	195.6	32.43	218.6	38.97		